Addis Ababa University
School of Graduate Studies

Finite Element Based Surface Fatigue Estimation in Involute Spur Gear under Rolling Sliding Contact Conditions

A thesis submitted to the school of Graduate studies of Addis Ababa University in partial fulfillment of the Degree of Masters of Science in Mechanical Engineering (Mechanical Design Stream)

By
Solomon Tekeste

Advisor
Dr. Daniel Tilahun

October 2011
Addis Ababa

Acknowledgements

The completion of this project has required the help and support of numerous people. I could never have done any of this thesis, without the support and encouragement of a lot of people. It is my pleasure to extend my sincere thanks and appreciations to those individuals who have spent their own contribution for successful completion of this research. Specially, I would like to extend sincere gratitude to my advisor Dr. Daniel Tilahun, for all of his help and guidance throughout this thesis work. I have learned so much from him. He was the one who inspire and encourage me to work on this project. I also appreciate not only for his professional, timely and valuable advices, but also for his continuous scheduled follow up and valuable comments during my thesis work.

I am also grateful to thank all staff of Bahir Dar Agricultural Mechanization Research Center for their impressive collaboration during study period. Their unlimited cooperation in all matters as well as readiness and open mind for any enquiries, have made me to extend my appreciations from the bottom of my heart. My sincere thanks go to Ato Wolelaw Endalew for his valuable information and assistances which have been counted since the first day of my study.

My special gratefulness goes to my families and friends for their support, encouragement, patience and understanding. I feel a deep sense of appreciation for my father and mother who formed my vision, and taught me the good morals, starting from childhood to now, that truly matter in life.

Abstract

There are two main factors that affect the service life of gears: surface durability and tooth bending strength. Pitting and scoring is a phenomenon in which small particles are removed from the surface of the tooth due to the high contact stresses that are present between mating teeth. After the investigation of shot pinning to increase the tooth bending strength in gears, surface durability, in the form of macro and micropitting, is now considered the dominant restriction on gear life and performance. The main objective of this thesis is to develop a method for the investigation of surface fatigue in involute spur gears using finite element analysis. In achieving this two-dimensional & three- dimensional equivalent contacting cylinders to model involute spur gear in contact and three- dimensional model of involute spur gear is used. Modeling of involutes spur gear to study contact stress under different working conditions using CATIA & ANSYS software is done. In addition parametric study to investigate the effect of loading condition and material types in contact stress in gears, estimation of surface fatigue in rolling-sliding contact condition in spur gear by finite element method using ANSYS Workbench software, effect of initial surface roughness on surface fatigue is studied. The results obtained are compared with analytical method. Results from FEA using ANSYS show that, a 2D model, estimates accurately contact pressure and stresses bellow the contacting surface, where as the 3D Model estimate contact pressure with reasonable accuracy and failed to estimate stresses bellow the contacting surface. Results from ANSYS Workbench, for a 3D model of involute spur gear, shows that contact stress and shear stress results, correlated with theoretical formulation, with tolerable accuracy but, failed to estimate von-Mises stress with acceptable accuracy. Results from ANSYS Workbench, for a 3D model of equivalent contacting cylinders, show that contact stress, von-Mises stress and shear stress results, correlated with theoretical formulation, with tolerable accuracy. Finally, in estimating surface fatigue, this paper verified that, as the surface roughness increases the minimum fatigue life and the load caring capacity for a specific design life decreases.

Contents

List of Figures

List of Tables

Nomenclature

b	Half of contact width
C_a	Application factor for pitting resistance
C_f	Surface condition factor
C_H	Hardness ratio factors for pitting resistance
C_m	Load distribution factor for pitting resistance
C_p	Elastic coefficient
C_s	Size factor for pitting resistance
C_v	Dynamic factor for pitting resistance
D_g	Gear pitch diameters
D_p	Pinion pitch diameters,
E_e	Equivalent modulus of material,
E_1	Youngus Modulus for material i
F	Force acting over contact length L
I	Geometry factor for pitting resistance
K_A	Application factor
K_g	Buckinghum load stress factor
K_R	Reliability factors
K_T	Temperature factors
K_V	Dynamic factor
$K_{H\beta}$	Face load distribution factor for contact stress
$K_{H\alpha}$	Transverse load distribution factor
L	Contact length
m	Module
m_c	Contact ratio
P_{max}	Maximum contact pressure
$P(x)$	Pressure distribution
r_{ag}	Addendum circle radius of gear

r_{ap}	Addendum circle radius of pinion
r_{bg}	Base radius of gear
r_{bp}	Base radius of pinion
R_g	Radius of gear
R_p	Radius of pinion
R_e	Equivalent radius of curvature
R_1	Radius of cylinder 1
R_2	Radius of cylinder 2
s_c	Contact stress number
S_c	Allowable contact stress
S_H	AGMA factor of safety, a stress ratio
S_{Hmin}	Minimum required safety factor
T_p	Torque on pinion
u	Gear ratio
W_n	Normal force applied on pinion
W_t	Tangential component of force
Z_B	Tooth contact factor
Z_E	Elasticity factor
Z_H	Zone factor
Z_L	Lubricant factor.
Z_N	Stress cycle life factor
Z_{NT}	Life factor for contact stress.
Z_R	Roughness factor
Z_V	Speed factor.
Z_W	Work hardening factor.
Z_X	Size factor.
Z_ϵ	Contact ratio factor
Z_β	Helix angle factor
ϕ	Pressure angle.
μ	Coefficient of friction,

$\boldsymbol{v_i}$	Poison ratio for material i
$\boldsymbol{\sigma_c}$	Contact stress.
$\boldsymbol{\sigma_{HG}}$	Pitting stress limit.
$\boldsymbol{\sigma_{HO}}$	Nominal contact stress at pitch point
$\boldsymbol{\sigma_{HP}}$	Permissible contact stress
$\boldsymbol{\sigma_{ort}}$	Maximum orthogonal shear stress,
$\boldsymbol{\sigma_{von}}$	Maximum vonMiss stress,
$\boldsymbol{\sigma_x}$	Shear stress along x
$\boldsymbol{\sigma_y}$	Shear stress along y
$\boldsymbol{\sigma_z}$	Shear stress along z
$\boldsymbol{\tau_{max}}$	Maximum shear stress
Δ	Approach of center distance of the rollers
$\boldsymbol{\Lambda}$	Parameter characterizing the ratio of the minimum film thickness to the composite surface roughness

Chapter One

1. Introduction

1.1. Background of the Project

There are two main factors that affect the service life of gears: surface durability, tooth bending strength. Pitting and scoring is a phenomenon in which small particles are removed from the surface of the tooth due to the high contact stresses that are present between mating teeth. Pitting is actually the fatigue failure of the tooth surface. In other words, pitting is a surface fatigue failure due to many repetitions of high contact stress, which occurs on gear tooth surfaces when a pair of teeth is transmitting power.

In a gear the entire interacting tooth flanks roll and slip simultaneously over each other except at the pitch diameter, where the contact is only obtained by pure rolling. Traction between the tooth flanks is undesirable because it causes an opposing torque, generates heat, and encourages rolling contact fatigue which can lead to surface fatigue, Van Beek [1]. Surface fatigue is a process by which the surface of a material is weakened by cyclic loading, which is one type of general material fatigue.

In spite of this facts, gear design currently relies on design standards, BS ISO 6336-1 [2], derived from a combination of analytical and empirical analysis, to estimate the surface and subsurface stresses in the gear teeth. Such methodology requires significant approximation, and as such is not typically suitable for highly stressed, non-critical applications. After the investigation of shot peening to increase the tooth bending strength in gears, surface durability, in the form of macro and micropitting, is now considered the dominant restriction on gear life and performance. Suzuki [3], has shown this , as it is depicted in figure 1. In addition, a broken tooth tends to be catastrophic to a gear unit, so the designer usually makes the teeth large enough so that they are definitely less appropriate to fail in breakage mode than in a pitting mode. This makes the design life of a gear unit primarily dependent on its surface fatigue capacity (pitting resistance) rather than on its cantilever beam capacity (capacity to resist tooth breakage).

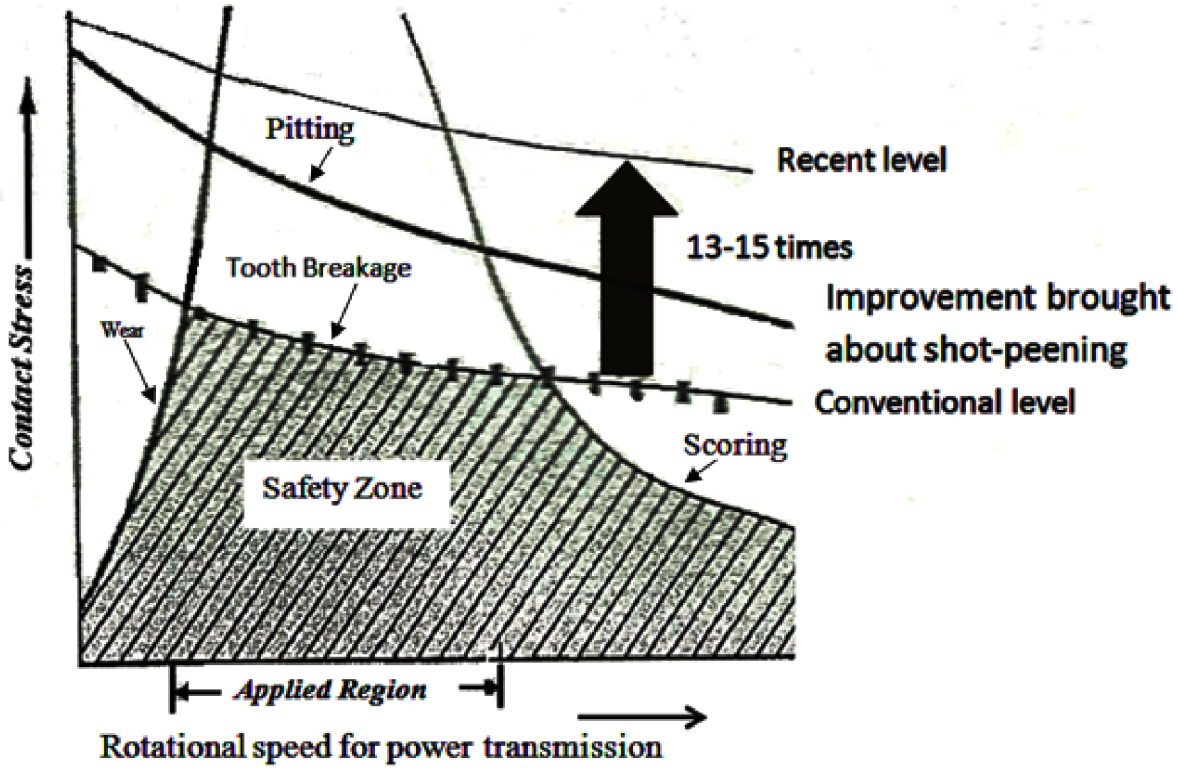

Figure 1.1: Failure of gears with respect to contact stress and rotational speed, Suzuki [3].

As shown in the figure the vertical axis represents the contact stress and the horizontal axis represents the rotational speed of the gear. The applied region in the rotational speed range refers the rotational speed of the gears commonly used in power transmission gears.

While the standards incorporate calculation of surface durability with regard to pitting, they are based primarily on the Hertzian pressure, Hertz [4]. Other contributing factors including friction, direction and magnitude of sliding, the influence of lubricant, temperature and surface roughness are not directly considered; rather allowance is made for their influence with empirical derating factors. Therefore, accurate calculation of contact stresses is vital to the analysis and prediction of surface fatigue and wear.

Although gears have been used by human for many years for various applications still a large number of unsolved problems exist. One of these problems is the assessment of the stress and strain status of the gear under rolling-sliding contact conditions for the investigation of the mechanically originated tooth surface damage of gears, prediction of wear and fatigue as well as

change of material properties and different working conditions. Since the mechanical problem is of high complexity because of the contact condition and the material behavior, only a numerical approach seems to be appropriate.

1.2. Objectives of this Thesis

The objectives of this thesis work are

- 3D Modeling of involute spur gear to study contact using CATIA & ANSYS software and comparing results with theoretical formulation.
- Perform parametric study to investigate the effect of loading condition and material types in contact stress in gears.
- To estimate of surface fatigue in rolling-sliding contact condition in spur gear by finite element method using ANSYS Workbench software.
- Study the effect of initial surface roughness on surface fatigue.

1.3. Organization of the thesis

This thesis is organized in to six chapters. In the first chapter, background and justification of this thesis work and the objectives to be achieved are discussed. In chapter two, a review of literature relevant to this thesis work, which has been investigated by different researchers, is given. Chapter three is about analytical method in contact stress analysis and surface fatigue estimation in gears. In chapter four, finite element method (FEM) is used, to develop involutes spur gear using CATIA, and 3D finite element analysis is done in ANSYS workbench. In addition numerical and analytical model using cylinders in contact is developed and contact stress analysis is done. It also illustrates variation in stress results under different loading condition and material types. This chapter also presents detailed information about the analysis of surface fatigue in gears, under different working condition. In chapter five results of the analysis are summarized and discussions are made based on the outputs of the FEM. In addition, comparison of analytical and numerical solutions is made. Finally, chapter six gives conclusion achieved from this thesis work and propose future work in this field of study.

Chapter Two

2. Literature Review

Contact stresses between curved bodies in compression are often termed "Hertzian" contact stresses after the work on the subject by Hertz [4] in 1881. This work was concerned primarily with the evaluation of the maximum compressive stresses set up at the mating surfaces for various geometries of contacting body but it formed the basis for subsequent extension of consideration by other workers of stress conditions within the whole contact zone both at the surface and beneath it. It has now been shown that the strength and load-carrying capacity of engineering components subjected to contact conditions is not completely explained by the Hertz equations by themselves, but that further consideration of the working conditions is an essential additional requirement. Therefore many researchers are interested on the subject.

Many of these researchers used the finite element analysis techniques for the analysis of the gear tooth. Much work has been done to model the contact between mating teeth as parallel contacting cylinders. Buckingham [5] shows that two contacting parallel cylinders can be used to fair accuracy to study contact stresses of spur gears. Abersek and Flasker [6] represented the contact between two gear teeth with two cylinders. Their analysis also addressed the sliding of gear teeth flanks and included coulomb friction. They performed a finite element analysis of two cylinders to determine their accuracy compared to Hertz theory.

Dudley [7] said that Hertz theory can be applied to gears quite easily. He recognized that this is a good approximation near the pitch circle. However, when contact is near the base circle the change in radius is rapid and is not a very good approximation. Pottinger et al [8] verified that the contact stress in gear teeth could be approximated with Hertz theory through photoelastic studies.

Wei [9], investigates the characteristics of an involute gear system including contact stresses, bending stresses, and the transmission errors of gears in mesh. To estimate transmission error in a gear system, the characteristics of involute spur gears were analyzed by using the finite element

method. The contact stresses were examined using 2-D FEM models. The bending stresses in the tooth root were examined using a 3-D FEM model. The results of the two dimensional FEM analyses from ANSYS are presented. These stresses were compared with the theoretical values.

Ali [10], studied contact stress between two spur gear teeth using ANSYS in different contact positions, representing a pair of mating gears during rotation. A programme has been developed to plot a pair of teeth in contact. The programme gives graphic results for the profiles of teeth in each position and location of contact during rotation. Finite element 2D models were made and stress analysis was done and finite element analysis results were compared with theoretical calculations.

Pottinger et al [8] verified the results for the stresses in a single gear tooth. He utilized an experimental model to validate his analytical model. He assumed that there are no stress gradients in the tooth parallel to the tooth axis. This assumption allowed him to simplify the model to 2-D, utilizing plane stress. Chen and Tsai [11] developed a finite element model applied to an involutes gear considering friction effects. The loss of Torque transmission due to friction and effective friction coefficient were evaluated and computed.

Moriwaki [12] developed a technique named Global Local Finite Element Analysis (GLFEM) and applied it to a gear tooth for its stress analysis. He realized that for doing the stress analysis of the gear using the finite element analysis, a load acts at a point on the tooth profile and for that a fine subdivision is required at the applied load point. In GLFEM, no fine subdivision is required for the analysis. This method also guarantees an easy determination of the critical section. In fact, GLFEM is a numerical analysis technique that combines finite element solutions and the classical analytical ones on the basis of the energy principle.

Chen and Tsay [13] investigated the contact stress and bending stress of a helical gear set with localized bearing contact, by means of finite element analysis (FEA). They proposed a helical gear set comprised of an involute pinion and double crowned gear. Mathematical models of the complete tooth geometry of the pinion and the gear had been derived based on the theory of gearing. A mesh generation program was also developed for finite element analysis.

Negash [14] investigates the characteristics of an involute helical gear system mainly focused on bending and contact stresses using analytical and finite element analysis. To estimate the bending stress, three-dimensional solid models for different number of teeth are generated by Pro/Engineer and the numerical solution is done by ANSYS. The analytical investigation is based on Lewis stress formula. This thesis also considers the study of contact stresses induced between two gears using 2D model and the analysis is carried out on the equivalent contacting cylinders. The results obtained from ANSYS are presented and compared with theoretical values. In this work a parametric study is conducted by varying the face width and helix angle to study their effect on the bending stress of helical gear.

Chien-Hsing Li et al [15] established a batch module called, ”integration of finite element analysis and optimum design” by taking gear systems as testing examples. This batch module consisted of I-DEAS, ABAQUS/Standard and MOST software, which serve as the preprocessor, the numerical solver and the optimizer, respectively. A simple and practical method was developed, through which this module was enabled which would search for contact nodes and elements and also it would automatically define the contact surfaces for contact analysis. For the testing example, a simple gear-pair system and a complete planetary gear system were used for this integrated module. The module would automatically construct the geometrical model, analyze the contact stress and solve for the optimal solutions when gearing parameters are input.

Hinojosa et al [16], develops mathematical model to determine the surface stress acting on the tooth of gear tooth. The new expression is obtained by using the maximum-shear-stress distribution and the Tresca failure criteria in order to know the maximum-shear-stress value and its location beneath the contact surface.

Ruben et al [17], investigate the stresses in the contact zone among a couple of spur gears using the finite element method in Autoslip. The analysis is done by using a plane model involving the contact between two teeth. The results obtained are compared with the Hertz theory and AGMA procedure for calculating contact stresses in spur gear.

The development of spalls in cylindrical or spherical surfaces in rolling contact under heavy contact loads have been observed and investigated for decades. An early problem definition and explanation attempt of the spalling process was completed in 1935 by Way [18]. Since then numerous attempts have been made to develop models for initiation of surface contact fatigue cracks and their evolution to spalls. In spite of all these attempts, as is concluded by Blake and Draper [19], Bower [20] and Tallian [21], the mechanism causing rolling contact fatigue to initiate and propagate is still not fully understood. A spalling model should be able to explain a number of experimentally found observations.

Based on experiments, Way [18] pointed out that in order to produce spalling damage it is necessary that; oil is present, the oil viscosity is below a critical value and the surface roughness is above a critical value. It was also noticed that a hardened surface has higher resistance towards spalling than an unhardened surface.

Bower [20] concluded that apart from explaining the effect of oil presence, the spalling model should also explain that, the forward direction of crack propagation and the life dependence on presence and direction of frictional forces.

Alfredsson [22] develops a mechanism for surface initiated contact fatigue is based on tensile surface stresses from local asperity contacts. It is also realized that sub-surface initiated contact fatigue is the result of tensile residual stresses that emanate from plastic deformation below the surface. These mechanisms clearly show that contact fatigue cracks follow the same rules as ordinary fatigue cracks in hardened steel.

Dimitrov and Kovatchev [23], developed a computer model for determination of gear teeth fatigue life. The model is based on a net of micro cracks and their mutual interaction and growth. In this research, it is considered that the gear tooth contacting surface is failed due to pitting when the size of pits increases to 40 μm. The model is developed by the use of Mechanical Desktop and Matlab computer packages.

Hassan et al [24] studied fatigue in gears of the hydraulic pump in JD 955 harvester combine through the finite element method and using contact analysis for precise determination of the contact region of the engaged teeth so that their lifespan was estimated using ANSYS software. In their research, they have found that, in fully reverse loading, one can estimate longevity of a gear as well as find the critical points that more possibly the crack growth initiate from. For the investigated gears, the most critical points were detected. Furthermore, the allowable number of load cycles and using fully reverse loading was gained.

Lin & Kuang [25], used dynamic model of an engaging spur gear pair to study the bending and surface fatigues. In this study, a computational algorithm is developed to simulate the bending and tooth surface stresses. In addition, they have studied how the parameters, such as tooth number, profile shifted factor, and tooth surface hardness, influence the break and surface failures of a spur gear pair.

Ferreira [26], developed a model for the analysis of tooth flank surface fatigue damage in spur gears, in particular micropitting contact fatigue initiation and mild wear. The prominent features of the model are a mixed film lubrication model and the application of the Dang Van high-cycle multi-axial fatigue criterion. By taking into account the roughness of the contacting gear teeth, the non-Newtonian behavior of the lubricating oil, the temperature variations within the contact and the elastic and fatigue properties of the gear material, it allows for a realistic, if approximate, modeling of the physical phenomena behind the onset of micropitting.

Batista & Dias [27], studied the contact fatigue of carbonitrided and shot-peened gears, and effects of residual stresses.The X-ray diffraction technique was used to characterise the evolution of residual stresses, during contact fatigue tests of carbo-nitrided and shot-peened gears from an automotive gearbox. A numerical model was developed to predict residual stress relaxation and to estimate the most probable site of contact fatigue crack initiation, using multiaxial fatigue criteria. An experimental method combining the X-ray diffraction stress analysis and the electric resistance strain gauge technique was used to determine the mechanical characteristics of the surface-treated layers. The Dang Van multiaxial fatigue criterion was used to estimate the most probable depth of contact fatigue crack initiation,

taking in to account the influence of residual stresses, roughness and friction.

Johansson et al [28] studied RCF-testing of selectively densified rollers of power metallurgy materials for gear applications. In this study pre–alloyed power metallurgy materials were tested using the ZF-RCF test. Reference material was low-alloyed case hardened steel DIN 16MnCr5 (AISI 5115) commonly used for gear applications. Test samples, rollers Ø30X30 mm, were pressed from different test materials as cylinders, machined to an oversize compared to the finished roller, selectively densified on a rolling machine and finally heat treated in different ways. The tested rollers were characterized with respect to microstructure, mechanical properties, and surface characteristics. Damage mechanisms were examined and failure analyses were performed on the rollers in order to trace crack initiation and propagation.

Gang Deng and Tsutomu Nakanishi [29], evaluated surface fatigue strength of rollers based on surface temperature. In this research, surface temperatures of rollers under different rolling and sliding conditions are measured using a thermocouple. The effects of load P, mean velocity V_m and sliding velocity V_s on surface temperature are clarified. An experimental formula, which expresses the linear relationship between surface temperature and the $p^{O.86}$; V_m^{-31}; $V_s^{O.83}$ value, is used to determine surface temperature. By comparing calculated and measured temperature on the tooth surface of a gear, this formula is confirmed to be applicable for gear tooth surface temperature calculation.

Tsutomu et al [30] studied the influences of surface texture and lubricating oil temperature on surface failure of rolling-sliding contact in the case of case-carburized alloy steels. In this paper influence of initial surface roughness on surface fatigue and influence of initial surface roughness on wear were studied experimentally.

Rolling-contact fatigue pits are frequently seen in the contact end of rolling contact surfaces of gears. It is supposed that it is the cause the partial contact pressure produced at the end. But, Susumu et al [31] studied experimentally that fatigue pits produced not exactly at the end rather at some distance to the inside from the end. This means that the critical position for rolling fatigue moves from contact end to inside of contact area. This might be because of contact pressure distribution at contact end under the condition of plastic contact. Pitting positions are

distributed widely in contact area for the reason that there are many factors influenced the probability in the rolling fatigue mechanism. The reproducibility of generative chance at some position in contact is not so strong. But, experimental results show that a tendency to generate a fatigue pit. So it is necessary to conduct more fatigue test for prediction of pitting probability.

To investigate experimentally, the plastic contact condition at contact end, Susumu et al [31] have used maximum partial contact pressure at the end that can produce plastic deformation or test rollers with different tapper angle. In addition in this study the longest fatigue durability was obtained by the smallest tapper angle roller. It was easily estimated that the partial contact pressure at contact end of the smaller tapered roller was lower than contact pressure of the larger tapered roller. In the case of tapered shape roller, changing data of contact width are of use to prevent pitting failure. So it is necessary to develop the simple method for prediction of contact width under plastic deformation.

Although there has been some progress on this particular subject of rolling contact fatigue, there are still a number of questions to be answered. Most of previous work, on contact stress analysis is done using 2D model, in this thesis it is tried to extend to 3D model. Furthermore surface fatigue studies in gears requires experimental setup in most previous studies but, experimental contact fatigue test is time-consuming and subject to variability, artificially produced surface defects (accelerated fatigue test) have been used to study defect-related contact fatigue. In addition this test requires sophisticated laboratory setup. Therefore, to increase computational efficiency, reduce cost and time required for analysis, computational methods that uses computer to analyze surface fatigue should be used, this thesis work focuses towards that end.

Chapter Three

3. Analytical Method in Surface Fatigue Estimation

Elements that roll and/or slide against each other under high contact pressure, developing concentrated subsurface and surface contact stresses that can cause surface pitting or spalling after many cycles of the load. *Pitting* is a surface fatigue failure due to many repetitions of high contact stresses. Obvious examples of rolling and/or sliding machine element are the mating teeth of a pair of gears, a cam and follower, a wheel and rail, and a chain and sprocket. Knowledge of the surface strength of materials is necessary if the designer is to create machines having a long and satisfactory life.

Contact fatigue differs from classic structural fatigue (bending or torsional) in that it results from a contact or Hertzian stress state. This localized stress state results when curved surfaces are in contact under a normal load. In a rolling motion, generally one surface moves over the other. Rolling contact components have a fatigue life (number of cycles to develop a noticeable fatigue spall).The endurance limit obtained by the rotating-beam test is frequently called the *flexural endurance limit,* because it is a test of a rotating beam. However, unlike structural fatigue, contact fatigue has no endurance limit, Shigley [32], instead it has surface endurance shear. If one compares the fatigue lives of cyclic torsion with rolling contact, the latter are seven orders of magnitude greater, Bhargava [33]. Rolling contact life involves ten to hundreds of millions of cycles.

Contact fatigue produces a surface damage that is unique and well recognized. Contact fatigue occurs in gears along the pitch line. The geometry of tooth mesh is such that rolling occurs at the pitch line while sliding occurs at the addendum as the gears come out of mesh. An example of pitch line contact fatigue is shown in figure 3.1 Tallian [34]. The pits seen on the teeth will grow in size and depth, ultimately resulting in tooth fracture.

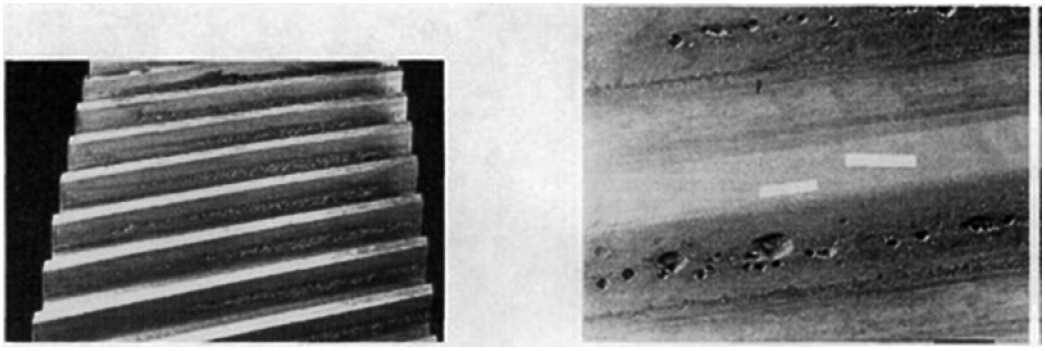

Figure 3.1: Pitch Line Spalling Of Medium-Hardened Gears, Tallian [34]

3.1. Mechanisms of Contact Fatigue

The surface fatigue mechanism is not definitively understood. The contact-affected zone, in the absence of surface shearing tractions, entertains compressive principal stresses. Rotary fatigue has its cracks grown at or near the surface in the presence of tensile stresses that are associated with crack propagation, to catastrophic failure. There are shear stresses in the zone, which are largest just below the surface. Cracks seem to grow from this stratum until small pieces of material are expelled, leaving pits on the surface.

The contact geometry and the motion of the rolling elements produce an alternating subsurface shear stress. Subsurface plastic strain builds up with increasing cycles until a crack is generated. The crack then propagates until a pit is formed. Once surface pitting has initiated, the operation becomes noisy and rough running. If allowed to continue, fracture of the rolling element and catastrophic failure occurs.

Contact fatigue is also surface generated. In fact, surface-originating spalls are more prevalent than subsurface-generated cracks. Proving subsurface fracture origin is difficult because a metallographic section only shows a profile of the crack which, in three dimensions, may have a surface origin. The higher the tangential force or traction, the more likely will be surface-generated contact fatigue. With shear stresses higher and closer to the surface, surface defects (dents, scratches, etc.) all contribute to higher incidence of surface-originating fatigue. As the

developing spall matures, a surface layer loosens and eventually breaks out, leaving a pit. While the pit develops, the loose layer batters the fracture surface, obliterating the surface features. [35]

3.2. Contact Stress Analysis

In many engineering applications, such as rolling bearings, gears, cams, etc., machine components whose functioning depends upon rolling and sliding motion in contact along surfaces while under load. In this case, the contacting surfaces are non-conformal, hence the resulting contact areas are very small and the pressures are very high. From the point of view of machine design it is essential to know the values of stresses acting in such contacts. These stresses can be determined, from the analytical formulae, based on the theory of elasticity, developed by Hertz in1881 [1, 36].

Most machine components are designed on the basis of stress in the main body of the member, that is, in portions of the body not affected by the localized stresses. In other words, damage to most mechanical components is associated with stresses and strains in portions of the component far removed from the points of application of the loads. However, in certain situations the contact stresses between the surfaces of two externally loaded bodies (e.g., meshing gear teeth) can be the significant stresses; that is, the stresses on or somewhat below the surface of the contact are the major causes of damage to one or both of the bodies. Therefore, analysis Hertzian stresses provide important information about surface and subsurface stresses for static loading of concentrated contacts.

3.3. Hertz Theory of Contact

The contact between two surfaces gives rise to an area of contact, and a pressure distribution over this contact area. If the surfaces have a simple geometry, the contact theory of Hertz (1881) can be used for calculating the contact area and the pressure distribution. The shape of the contact area depends on the shape (curvature) of the contacting bodies. For example, point contacts occur between two balls, line contacts occur between two parallel cylinders and elliptical contacts, which are the most frequently found in many practical engineering

applications, occur when two cylinders are crossed, or a moving ball is in contact with the inner ring of a bearing, or two gear teeth are in contact. To illustrate the contact between two elastic bodies, the simpler contact of two parallel cylinders (Figure 3.2) is presented based on the Hertz theory. This type of contact is used to derive contact pressure distribution, stresses and displacements for the two dimensional line contacts, Manuel [37]

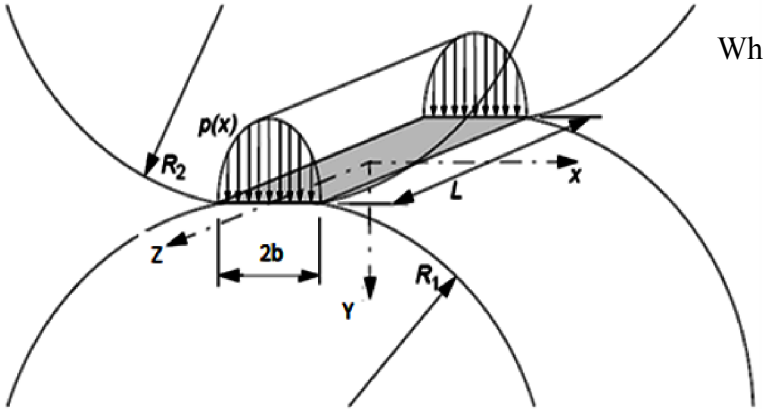

Where

- R_1 is the radius of cylinder 1
- R_2 is the radius of cylinder 1
- P(x) is the pressure distribution
- b is half of the contact width
- L is the contact length

Figure 3.2: The Hertz pressure distribution of a two dimensional contact, Alfredsson [22].

When cylinders are in line contact, sustained by a force F, a flattened rectangular zone exists in which the pressure distribution is elliptical.

$$P(x) = \frac{2F}{\pi b^2 l}\sqrt{b^2 - x^2} \quad \text{..... (3.1)}$$

Where F is the force acting over the contact length L and $2b$ is the contact width. The maximum contact pressure at $x = 0$ is

$$P_{max} = \frac{2F}{\pi b l} \quad \text{..... (3.2)}$$

The half width of the contact zone b is

$$b = \sqrt{\frac{4F}{\pi l}\frac{[1-\nu_1^2]/E_1 + [1-\nu_2^2]/E_2}{1/R_1 + 1/R_2}} \quad \text{..... (3.3)}$$

The analytic model for surface contact stress proposed by Smith [38] is, used. Let x, y, and z be the tangential, radial and axial directions at the contact point. Assuming the plane strain case at the contact point, the stresses at xy plane can be written as,

$$\sigma_x = -\frac{p_{max}}{\pi}\left\{(b^2 + 2x^2 + 2y^2)\frac{y}{b}\bar{\varphi} - 2\pi\frac{y}{b} - 3xy\varphi + \mu\left[(2x^2 - b^2 - 3y^2)\varphi + 2\pi\frac{x}{b} + 2(b^2 - x2{-}y2)xb\varphi\right.\right. \quad \text{(3.4)}$$

$$\sigma_y = -\frac{P_0}{\pi}y(b\bar{\varphi} + x\varphi + \mu y\varphi) \quad \text{(3.5)}$$

$$\sigma_z = -\frac{2\upsilon}{\pi}p_{max}\left\{\left[(b^2 + x^2 + y^2)\frac{z}{b}\bar{\varphi} - \frac{\pi y}{b} - 2xy\varphi\right] + \mu\left[(x^2 - b^2 - y^2)\varphi + \frac{\pi x}{b} + (b^2 - x^2 - y2)xb\varphi\right.\right. \quad \text{(3.6)}$$

$$\tau_{xy} = -\frac{p_{max}}{\pi}\left\{y^2\varphi + \mu\left[(b^2 + 2x^2 + 2y^2)\frac{y}{b}\bar{\varphi}\right] - 2\pi\frac{y}{b} - 3xy\varphi\right\} \quad \text{(3.7)}$$

where p_{max} the maximum surface pressure, μ is the coefficient of friction, and b is the contact width φ and $\bar{\varphi}$ can be written as

$$\varphi = \frac{\pi}{\lambda_1}\frac{1-\lambda_3}{\lambda_3\sqrt{2\lambda_3+\lambda_4}} \quad \text{(3.8)}$$

$$\bar{\varphi} = \frac{\pi}{\lambda_1}\frac{1+\lambda_3}{\lambda_3\sqrt{2\lambda_3+\lambda_4}} \quad \text{(3.9)}$$

$$\lambda_1 = (b + x)^2 + y^2 \quad \text{(3.10)}$$

$$\lambda_2 = (b - x)^2 + y^2 \quad \text{(3.11)}$$

$$\lambda_3 = \left(\frac{\lambda_2}{\lambda_1}\right)^{1/2} \quad \text{(3.12)}$$

$$\lambda_4 = (\lambda_1 + \lambda_2 - 4b^2)/\lambda_1 \quad \text{(3.13)}$$

Using Eqs. (3.4)-(3.13), the principal stresses and the maximum shear stress at $y = 0$ can be calculated. Along the y axis, the orthogonal stresses are,

$$\sigma_y = \frac{-p_{max}}{\sqrt{1+(\frac{y}{b})^2}} \quad \text{(3.14)}$$

$$\sigma_x = -p_{max}\left\{\left[2 - \frac{1}{1+(\frac{y}{b})^2}\right]\sqrt{1+(\frac{y}{b})^2} - 2\frac{y}{b}\right\} \quad \text{(3.15)}$$

$$\sigma_z = -2p_{max}\left[\sqrt{1+(\frac{y}{b})^2}\right] - \frac{y}{b} \quad \text{(3.16)}$$

These equations can be useful where rolling contact exists, such as in cams, roller bearings, and gear teeth. The approach of the center of the rollers, Δ is:

$$\Delta = \frac{2F}{\pi l}\left(\frac{1-\nu_1^2}{E_1} + \frac{1-\nu_2^2}{E_2}\right)\left(ln\frac{d_1}{b} + ln\frac{d_2}{b} + \frac{2}{3}\right) \quad \text{(3.17)}$$

The largest principal stress is compressive and located at the center of the rectangular flat and is $-p_{max}$ in magnitude. The largest shear stress is approximately 0.30 P_{max} and is located at about 0.78b below the surface. The maximum compressive stress is repeatedly applied in rolling cylinders. At a position of y = 0.4b, z = 0.915b the shear stress has a magnitude of 0.242 P_{max} but is completely reversed in rolling cylinders. The peak values of the equivalent stress using the Von Mises criterion, the maximum shear stress, and the maximum orthogonal shear stress can be calculated from the maximum Hertz stress as follows[39]:

Maximum shear stress, $\tau_{max} = 0.30\ p_{max}$ ..... (3.18)

Maximum VonMiss stress, $\sigma_{von} = 0.57p_{max}$ ..... (3.19)

Maximum orthogonal shear stress, $\sigma_{ort} = 0.242p_{max}$ ..... (3.20)

Hertz's model of contact stresses are based on the following simplifying assumptions [40]

- The materials in contact are homogeneous and the yield stress is not exceeded,
- Contact stress is caused by the load which is normal to the contact tangent plane which effectively means that there are no tangential forces acting between the solids,
- The contact area is very small compared with the dimensions of the contacting solids,

- The contacting solids are at rest and in equilibrium,
- The effect of surface roughness is negligible.

Lots of contact problems do not fit the assumptions listed.

3.4. Non-Hertzian contact

Even though, Hertz's theory forms the basis for classical contact mechanics, most of the assumptions have been removed by different authors, to take in to account the real working conditions. These conditions are, when there is friction, non linear material properties, complex geometries, when there is a lubricant, etc. Now a days, numerical methods has got attention to solve these types of nonlinear problems. Generally nonlinear structural behavior arises for a number of reasons, as cited in Wei [9] which can be categorized as:

1. Geometric Nonlinearities (Large Strains, Large Deflections)
2. Material Nonlinearities (Plasticity)
3. Change in Status (boundary) Nonlinearities (Contact).

Contact is considered as a "changing status" type of non-linearity. Depending on whether the contact is open or closed, and if closed, sticking or sliding, the system's stiffness changes accordingly. In addition, the area over which contact occurs is typically not known at the beginning of analysis. Hence the contact between two bodies categorized to the third group. Therefore, in this thesis contact non-linearity will be examined closely, because the gear teeth in mesh are behaving in this fashion.

The contact is highly non-linear because one or both of the following are present, Stachowiak [40]

- The actual regions of contact are unknown until the problem has been solved. Depending on the load, material, boundary conditions and other factors, and surfaces can come into and go out of contact with each other in a largely unpredictable and abrupt manner.
- Most contact problems need to account for friction. Contact and friction between solids is a complex problem which involves the mechanical properties of the materials, the

geometrical characteristics of the rough surfaces, the properties of any lubricant that might be present in the motion, and the temperature of the contacting surfaces. There are several friction laws and models to choose from, and all are nonlinear. Frictional response can be chaotic, making solution convergence difficult.

In addition to those difficulties, many contact problems must also address multi-field effects, such as the conductance of heat and electrical currents in the areas of contact. However with the rapid development of computational mechanics, great progress has been made in numerical analysis nonlinear problem. Using the finite element method, many contact problems, ranging from relatively simple ones to quite complicated ones, can be solved with high accuracy.

3.5. Application of Hertz Contact Stress Equations in Spur Gear

The way in which tooth surfaces of properly aligned gears make contact with each other is responsible for the heavy loads that gears are able to carry. In theory, gear teeth make contact along lines or at points; in service, however, because of elastic deformation of the surfaces of loaded gear teeth, contact occurs along narrow bands or in small areas. The radius of curvature of the tooth profile has an effect on the amount of deformation and on the width of the resulting contact bands.

As it is discussed in the pervious, meshed spur gears can be modeled by two parallel cylinders in contact. From equation (3.3), half of the contact width b, can be rewritten as,

$$b = \sqrt{\frac{4FR_e}{\pi l E_e}} \quad \text{..... (3.21)}$$

Where R_e is the equivalent radius of curvature, given by,

$$R_e = \frac{1}{\left({}^{1}/_{R_1} + {}^{1}/_{R_2}\right)} \quad \text{..... (3.22)}$$

Where R_1 and R_2 are the instantaneous values of the radii of curvature on the pinion- and gear-tooth profiles, respectively, at the point of contact.

At the pitch point $R_1 = R_p$ & $R_2 = R_g$ and given by

$$R_p = \frac{D_p \sin\phi}{2} \quad \& \quad R_g = \frac{D_g \sin\phi}{2} \quad \text{..... (3.23)}$$

where D_p & D_g are the pitch diameters, and D_p is for Pinion and D_g for gear and ϕ is the pressure angle. Therefore, at the pitch point R_e becomes

$$R_e = \frac{1}{\left(\frac{2}{sin\phi}\left(1/D_p + 1/D_g\right)\right)} \quad \text{..... (3.24)}$$

and E_e is the equivalent modulus of the material, given by,

$$E_e = \frac{1}{[1-\nu_1^2]/E_1 + [1-\nu_2^2]/E_2} \quad \text{..... (3.25)}$$

Substitute the value of b from equation (3.21) into (3.2), to find the maximum contact pressure, P_{max} results in

$$P_{max} = -\left[\frac{FE_e}{\pi l R_e}\right]^{1/2} \quad \text{..... (3.26)}$$

For the driver pinion, and gear follower,

$$F = W_n = \frac{W_t}{cos\phi} = \frac{T_p}{R_p cos\phi} \quad \text{..... (3.27)}$$

Where

- R_p is the radius of the pinion and
- T_p is the torque on the pinion
- W_n the normal force applied on the pinion
- W_t tangential component of the force

Substitute the value of F from equation (3.27) into (3.26) results in

$$P_{max} = \sigma_c = -\left[\frac{T_p E_e}{\pi l R_p cos\phi R_e}\right]^{1/2} \quad \ldots\ldots\ldots\ldots\ldots\ldots (3.28)$$

where σ_c is the contact stress.

By accounting for load sharing in the value of *Wt* used, equation (3.27) can be solved for the Hertzian stress for any or all points from the beginning to the end of tooth contact. Of course, pure rolling exists only at the pitch point. Elsewhere the motion is a mixture of rolling and sliding. Equation (3.28) does not account for any sliding action in the evaluation of stress.

3.6. Contact Ratio

The zone of action of meshing gear teeth is shown in Figure 3.3. Tooth contact begins and ends at the intersections of the two addendum circles with the pressure line. In figure 3.3, initial contact occurs at *a* and final contact at *b*. Tooth profiles drawn through these points intersect the pitch circle at *A* and *B*, respectively. As shown, the distance *AP* is called the *arc of approach* q_a , and the distance *P B*, the *arc of recess* q_r . The sum of these is the *arc of action* q_t .

Now, consider a situation in which the arc of action is exactly equal to the circular pitch, that is, $q_t = p$. This means that one tooth and its space will occupy the entire arc *AB*. In other words, when a tooth is just beginning contact at *a*, the previous tooth is simultaneously ending its contact at *b*. Therefore, during the tooth action from *a* to *b*, there will be exactly one pair of teeth in contact.

Next, consider a situation in which the arc of action is greater than the circular pitch, but not very much greater, say, $q_t = 1.2p$. This means that when one pair of teeth is just entering contact at *a*, another pair, already in contact, will not yet have reached *b*.

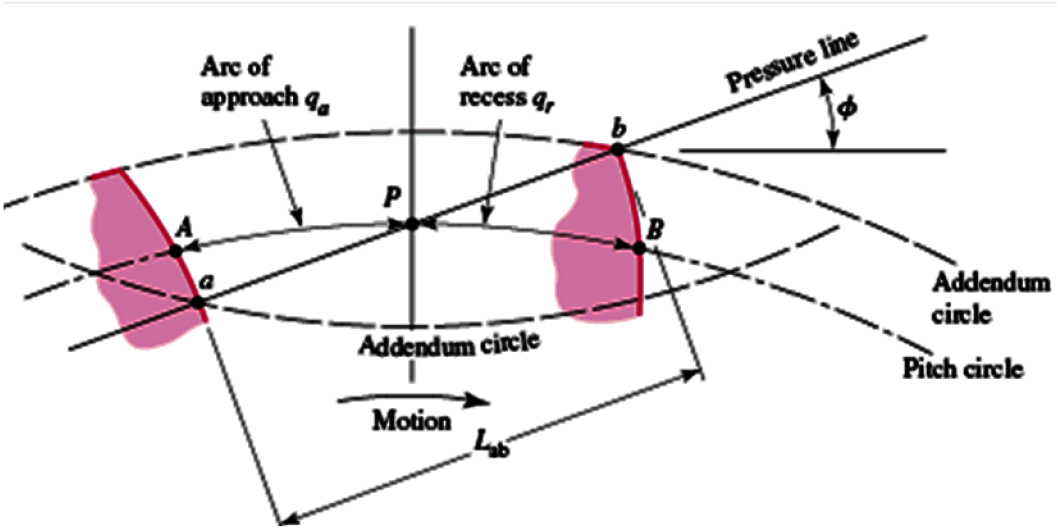

Figure 3.3: Definition of Contact Ratio, Shigley [32].

Thus, for a short period of time, there will be two teeth in contact, one in the vicinity of *A* and another near *B*. As the meshing proceeds, the pair near *B* must cease contact, leaving only a single pair of contacting teeth, until the procedure repeats itself. Because of the nature of this tooth action, either one or two pairs of teeth in contact, it is convenient to define the term *contact ratio* m_c as

$$m_c = \frac{q_t}{p} \quad \text{..... (3.29)}$$

Where p is the circular pitch

Contact ratio is a number that indicates the average number of pairs of teeth in contact. Note that this ratio is also equal to the length of the path of contact divided by the base pitch. Gears should not generally be designed having contact ratios less than about 1.20, because inaccuracies in mounting might reduce the contact ratio even more, increasing the possibility of impact between the teeth as well as an increase in the noise level.

An easier way to obtain the contact ratio is to measure the line of action *ab* instead of the arc distance *AB*. Since *ab* in figure 3.3 is tangent to the base circle when extended, the base pitch p_b

must be used to calculate m_c instead of the circular pitch as in Eq. (3.29). If the length of the line of action is L_{ab}, the contact ratio is

$$m_c = \frac{L_{ab}}{p_b} = \frac{L_{ab}}{pcos\varphi} \quad \text{..... (3.30)}$$

Where p_b, is the base pitch, and the circular pitch is given by

$$p = \pi m \quad \text{..... (3.31)}$$

Where m is the module and L_{ab} is given by

$$L_{ab} = \sqrt{(r_{ap})^2 + (r_{bp})^2} + \sqrt{(r_{ag})^2 + (r_{bg})^2} + (r_p + r_g)sin\varphi \text{..... (3.32)}$$

Where

- r_{ap} is addendum circle radius of the pinion
- r_{ag} is addendum circle radius of the gear
- r_{bp} base radius of the pinion
- r_{bg} base radius of the gear
- r_p&r_g pitch radius of the pinion and the gear respectively

r_{ap}, r_{ag}, r_{bp} & r_{bg} for standard involute spur gear given by,

$$\left.\begin{array}{l} r_{ap} = r_p + m \\ r_{ag} = r_g + m \\ r_{bp} = r_p cos\varphi \\ r_{bg} = r_g cos\varphi \end{array}\right\} \quad \text{..... (3.33)}$$

In this study spur gear used as model have properties as seen in table (4.2), therefore, substitute these values, ($r_p = 28.75$, $r_g = 56.25$, $m = 2.5$ and $\varphi = 20°$) in equation (3.32) results in L_{ab} =5.443686 and the solve for contact ratio, m_c

$$m_c = \frac{L_{ab}}{pcos\varphi} = \frac{5.443686}{\pi * 2.5 * \cos(20°)} = 1.699 \cong 1.7$$

Contact ratio of (1.7) means two pairs of teeth are in contact (70%) of the time and one pair carries the load (30%) of the time. In this thesis work, for purposes of a realistic analysis of the performance characteristics of a pair of gears, the most severe load condition is considered. This is when a single pair of teeth assumes the full burden. At contact ratio CR of (1.0) it would mean that one tooth is in contact (100%) of the time.

3.7. Gear Tooth Surface Durability and Breakage

Pitting is a fatigue failure where small cracks form in the tooth surface and then grow to the point where small, round bits of metal break out of the tooth surface. Traditionally, the gear designer first determines a pitch diameter and a face width for the pinion that are large enough for the pinion to last for the required service life with a probability of failure less than 1%. This determination is based on a possible pitting fatigue failure. It is assumed in the beginning that the surface finish, the tooth accuracy, the lubrication, and the needed profile and helix modifications will all be carried out well enough to avoid any serious risk of scuffing. Normally, the pinion is more appropriate to fail in pitting than the gear, so the sizing of the pinion tends to determine the needed size of the gear.

After the pitch diameter of the pinion has been determined, the size of the teeth is determined by calculations regarding a possible failure in tooth breakage.

3.8. AGMA Contact Stress Equations

Two fundamental stress equations are used in the American Gear Manufacturer Association (AGMA) methodology, one for bending stress and another for pitting resistance (contact stress). In AGMA terminology, these are called *stress numbers,* as contrasted with actual applied stresses, and are designated by a lowercase letter *s* instead of the Greek lower case σ. According to Shigley [32], the fundamental equation for pitting resistance (contact stress) is

$$s_c = C_p \left(\frac{W_t C_a}{C_v} \frac{C_s}{dF} \frac{C_m C_f}{I} \right)^{1/2} \quad \text{..... (3.34)}$$

$$C_p = \left[\frac{1}{\pi\left(\frac{(1-\nu_1^2)}{E_1}+\frac{(1-\nu_2^2)}{E_2}\right)}\right]^{1/2} \quad \text{..... (3.35)}$$

Where

- s_c = contact stress number
- C_p = elastic coefficient
- W_t = transmitted tangential load
- C_a = application factor for pitting resistance
- C_s = size factor for pitting resistance; use 1.0 or more until values are established
- C_m = load distribution factor for pitting resistance use
- C_f = surface condition factor use 1.0 or more until values are established
- C_v = dynamic factor for pitting resistance
- d = operating pitch diameter of pinion, in (mm)
- F = net face width of narrowest member
- I = geometry factor for pitting resistance

3.9. Factors Influencing Contact Fatigue Life

Factors influencing contact fatigue life of hardened steel bearings and gears can be roughly classified into four categories: material, lubrication and surface finish, dimensional precision, and environmental conditions. Most factors discussed in this section are dependent upon and different for the type of material in question, through hardened or carburized. Therefore, material usage should be a function of manufacturing capabilities, operating environments, and more often that not, cost.

I. Hardness

Contact fatigue is influenced more by highly localized conditions than by the general properties of the bulk material. Early research on contact fatigue utilized mechanical engineering and elastic stress analysis with little emphasis on materials, until an understanding of how material hardness influences contact fatigue life [42]. Contact fatigue measurements on hardened steels indicate an increasing life with increasing component hardness, although there is an optimal hardness range that is application dependent to ensure maximum contact fatigue life [43, 44].

II. Residual Stresses

Favorable compressive residual stress profiles, like those found in carburized components, increase the contact fatigue life of bearings and gears, Hogbin [45]. Residual stresses can be formed during heat treatment, subsequent peening processes, and/or cyclic loading. Residual stress can either increase or decrease the maximum Hertzian shear stress according to the following equation, Scott [44]:

$$\tau_{oct}^{r} = -\tau_{oct} - \frac{1}{2}(\pm s_r) \quad \ldots\ldots\ldots\ldots\ldots\ldots\ldots\ldots\ldots\ldots (3.36)$$

where τ_{oct} is the maximum shearing stress, τ_{oct}^{r} is the maximum shearing stress modified by the residual stress, and S_r is the residual stress. The positive/negative sign (±) indicates that the residual stress may be tensile or compressive, respectively. For the case of compressive residual stresses, fatigue crack initiation and propagation rates are decreased due to a decrease in the effective applied stress and results in longer life.

III. Lubrication and Surface roughness

Lubrication and surface roughness also play important roles in contact fatigue life. Most of surface initiated contact fatigue is influenced by lubrication and surface finish condition of the contacting surface. Therefore, it is important to have a basic understanding of lubrication and surface roughness, to better comprehend the phenomenon of contact fatigue.

The influence of the surface roughness on EHL:-

In the evaluation of EHL film thickness it has been assumed that the contacting surfaces lubricated by EHL films are flat. In practice however, the surfaces are never flat, they are rough, covered by features of various shapes, sizes and distribution. The question arises of how the surface roughness affects the mechanism of elastohydrodynamic film generation, Stachowiak [40].

Commonly, the roughness of two contacting surfaces are added to form the so-called composite root mean square roughness, RMS or σ_q.

$$\sigma_q = \sqrt{\frac{1}{l}\int_0^l r^2(x)dx} \quad \text{..... (3.37)}$$

Where r is the combined deviation from the mean surface height. The surface roughness should be investigated in combination with the lubricant film thickness by calculating the film thickness ratio λ. Some combinations of load, slip, lubrication and surface topology may lead to wear. Fan et al. [46] noted that the initial contact fatigue crack under some conditions might be halted or removed by wear.

Local film variation as a function of local surfaces roughness is perhaps best characterized by a parameter proposed by Tallian [34]. The ratio of the minimum film thickness to the composite surface roughness of two surfaces in contact is defined as, Δ:

$$\Lambda = \frac{\Phi_T h_0}{(\sigma_A^2+\sigma_B^2)^{0.5}} \quad \text{..... (3.38)}$$

Where:

- h_0 is the minimum film thickness [m];
- σ_A is the RMS surface roughness of body 'A' [m];
- σ_B is the RMS surface roughness of body 'B' [m];
- Λ is the parameter characterizing the ratio of the minimum film thickness to the composite surface roughness;

- Φ_T is the thermal effects correction factor given by:

$$\Phi_T = \frac{1-13.2\left(\frac{P_0}{E'}\right)L^{0.42}}{1+0.213(1+2.23S^{0.83})L^{0.64}} \quad \text{(3.39)}$$

- P_0 is the maximum Hertzian contact pressure [GPa];
- E' reduced Young's modulus;
- S slide-to-roll ratio given by:

$$S = 2\frac{U_1-U_2}{U_1+U_2} \quad \text{(3.40)}$$

where:

- U_1, U_2 linear velocity of the bodies 1 and 2 in the rolling direction;
- L the thermal load parameter given by:

$$L = \frac{\eta\beta(U_1-U_2)}{c} \quad \text{(3.41)}$$

Where:

- η lubricant's viscosity at the temperature of the surface and local pressure;
- β termoviscosity coefficient;
- c lubricant's specific heat

Measured values of 'Λ' have been found to correlate closely with the limits of EHL and the onset of damage to the contacting surfaces. A common form of surface damage is surface fatigue where spalls or pits develop on the contacting surfaces and prevent smooth rolling or sliding. It is also possible for wear, i.e. surface material uniformly removed from the contacting surface, to occur when EHL is inadequate. The rapidity of pitting and spalling or simple wear is described in terms of a fatigue life which is the number of rolling/sliding contacts till pitting is sufficient to prevent smooth motion between the opposing surfaces. The relationship between 'Λ' and fatigue life is shown in Figure 3.4.

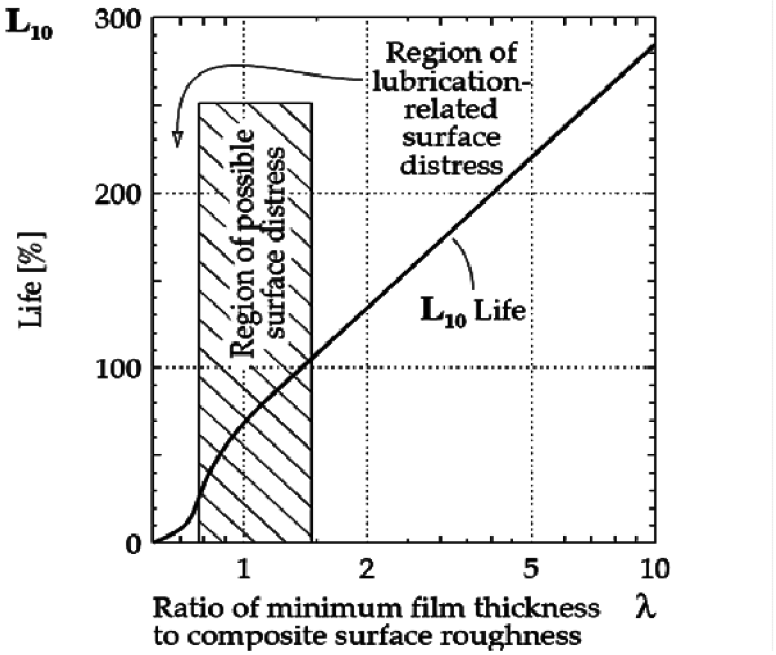

Figure 3.4: Effects of minimum film thickness and composite surface roughness on contact fatigue life, Stachowiak [40].

3.10. Fatigue Design Philosophies and Life Prediction Models.

3.10.1. Fatigue Design Philosophies

The three main approaches in fatigue design philosophy, are Safe-Life, Fail-Safe and Damage-Tolerant.

1. **Safe-Life (**finite lifetime concept):- In the ***Safe-Life*** philosophy products are designed to survive a specific design life with a chosen reserve.
2. **Fail-Safe** (infinite lifetime concept):- Design to keep stress below threshold of fatigue limit, so as to reduce some of this waste of useful fatigue life, and maintain or improve the operating safety of a component in the later stages of its life.

3. **Damage-Tolerant: -** users need to inspect the part periodically for cracks and to replace the part once a crack exceeds a critical length. This approach usually uses the technologies of nondestructive testing and requires an accurate prediction of the rate of

crack-growth between inspections. This is often referred to as damage tolerant design or "retirement-for-cause".

3.10.2. Life Prediction Methods

Once a local stress-time or strain-time history has been established for a point likely to be critical a fatigue analysis method must be chosen. Most FEA based fatigue packages have three main life prediction methods. These are Stress-Life, Strain-Life and Crack-Propagation.

1. **Stress-Life (S-N, or Nominal Stress) Approach**

This is normally used for total life calculation. A stress-time history is estimated for some part of the component judged to be representative. Factors derived from geometry are then applied to turn this into a stress-time history at the point where a crack is likely to start. The S-N method assumes the structure to be fully elastic. It is therefore only applicable to (low load-long life) ***high cycle fatigue*** (HCF) problems. In application to FE models, linear elastic stresses from FE analysis can be used directly to calculate fatigue damage.

2. **Strain-Life (Crack-Initiation or Critical-Location Approach)**

At shorter lives, higher loads, multiplying a nominal stress by a concentration factor will give figures greater than the yield stress at the critical location, so that yielding will occur. Techniques have therefore been developed to use the strain response in the structure for such ***low cycle fatigue*** (LCF) problems. Methods of predicting a strain-life history under reversed yielding were well developed before FEA became a general design tool.

3. **Crack Propagation Models.**

If the crack propagation phase of life, *NP*, is to be taken into account, crack prediction models are needed for two tasks. The first is to predict the rate of growth of a crack in, say, mm/(load application). The second is to predict how long a crack can be before the next peak in the loading

history causes catastrophic propagation. Both of these are handled by Fracture Mechanics, usually Linear Elastic Fracture Mechanics. The role of FEA in Crack-Propagation is therefore similar in some ways to its role in Stress-Life estimates since it replaces existing data banks.

3.10.3. Linking Life Estimation Methods with Design Philosophies

Safe-Life design normally uses Stress-Life analysis, and the usual Damage-Tolerant design uses Crack-Propagation, but these associations are not rigid. Structural deterioration might be measured by a factor other than crack length, and a Safe-Life design could aim to take a component out of service well before a crack could initiate. Strain-Life is the only working method we have at present for predicting so-called life to crack initiation.

3.11. Contact Fatigue Analysis

Buckingham [5], conducted a number of tests relating the fatigue at 10^8 cycles to endurance strength (Hertzian contact pressure). While there is evidence of an endurance limit at about $3(10^7)$ cycles for cast materials, hardened steel rollers showed no endurance limit up to $4(10^8)$ cycles. Subsequent testing on hard steel shows no endurance limit. Hardened steel exhibits such high fatigue strengths that its use in resisting surface fatigue is widespread.

To determine the surface fatigue strength of mating materials, Buckingham designed a simple machine for testing a pair of contacting rolling surfaces in connection with his investigation of the wear of gear teeth. Buckingham gathered large numbers of data from many tests so that considerable design information is now available. To make the results useful for designers, Buckingham defined a *load-stress factor,* also called a *wear factor,* which is derived from the Hertz equations. The maximum contact pressure, (P_{max}) and half width of the contact zone, (b) for contacting cylinders are specified in equations (3.2) and (3.3). If we then designate the length of the cylinders as w (for width of gear) instead of *l* and remove the square root sign, Eq. (3.3) becomes

$$b^2 = \frac{4F}{\pi w}\frac{[1-\nu_1^2]/E_1+[1-\nu_2^2]/E_2}{1/R_1+1/R_2} \quad \text{..... (3.42)}$$

We can define a surface endurance strength S_C using

$$P_{max} = \frac{2F}{\pi bw} \quad \text{..... (3.43)}$$

as

$$S_C = \frac{2F}{\pi bw} \quad \text{..... (3.44)}$$

which may also be called *contact strength,* the *contact fatigue strength,* or the *Hertzian endurance strength*. The strength is the contacting pressure which, after a specified number of cycles, will cause failure of the surface. Such failures are often called *wear* because they occur over a very long time. They should not be confused with abrasive wear, however. By squaring Eq. (3.41), substituting b^2 from Eq. (3. 3), and rearranging, we obtain

$$\frac{F}{w}\left(\frac{1}{r_1}+\frac{1}{r_2}\right) = \pi S_C^2\left[\frac{1-\nu_1^2}{E_1}+\frac{1-\nu_2^2}{E_2}\right] = K_1 \quad \text{..... (3.45)}$$

The left expression consists of parameters a designer may seek to control independently. The central expression consists of material properties that come with the material and condition specification. The third expression is the parameter K_1, Buckingham's load stress factor, determined by a test fixture with values F, w, r_1, r_2 and the number of cycles associated with the first tangible evidence of fatigue. In gear studies a similar K factor is used:

$$K_g = \frac{K_1}{4}sin\varphi \quad \text{..... (3.46)}$$

where φ is the tooth pressure angle, and the term $[(1 - \nu_1^2)/E_1 + (1 - \nu_2^2)/E_2]$ is defined as $1/(\pi C_P^2)$, so that

$$S_C = C_P\sqrt{\frac{F}{w}\left(\frac{1}{r_1}+\frac{1}{r_2}\right)} \text{..... (3.47)}$$

Equation (3.47) can be used in design to find an allowable surface stress by using a design factor. Since this equation is nonlinear in its stress-load transformation, the designer must decide if loss of function denotes inability to carry the load. If so, then to find the allowable stress, one divides the load F by the design factor nd :

$$S_C = C_P\sqrt{\frac{F}{wn_d}\left(\frac{1}{r_1}+\frac{1}{r_2}\right)} = \frac{C_P}{\sqrt{n_d}}\sqrt{\frac{F}{w}\left(\frac{1}{r_1}+\frac{1}{r_2}\right)} = \frac{S_P}{\sqrt{n_d}} \text{..... (3.58)}$$

and $n_d = (S_C/\sigma_C)^2$. If the loss of function is focused on stress, then $n_d = S_C/\sigma_C$.

Buckingham and others reported K_1 for 10^8 cycles and nothing else. This gives only one point on the S_C N curve, Shigley [32]. For cast metals this may be sufficient, but for wrought steels, heat treated, some idea of the slope is useful in meeting design goals of other than 10^8 cycles.

Experiments show that K_1 versus N, K_g versus N, and S_C versus N data are rectified by log-log transformation. This suggests that

$$\left.\begin{aligned} K_1 &= \alpha_1 N^{\beta_1} \\ K_g &= aN^b \\ S_C &= \alpha N^{\beta} \end{aligned}\right\} \text{..... (3.49)}$$

The three exponents are given by

$$\left.\begin{aligned} \beta_1 &= \frac{\log(K_1/K_2)}{\log(N_1/N_2)} \\ b &= \frac{\log(K_{g1}/K_{g2})}{\log(N_1/N_2)} \\ \beta &= \frac{\log(S_{C1}/S_{C2})}{\log(N_1/N_2)} \end{aligned}\right\} \text{..... (3.50)}$$

For applications where little or no pitting is permissible, the American Gear Manufacturers Association (AGMA) uses β=-0.056 between $10^4 < N < 10^{10}$ if the designer has no data to the contrary beyond 10^7 cycles.

AGMA standard, ANSI/AGMA [47] suggests allowable contact-stress numbers (for 10^7 cycles and 0.99 reliability for through hardened steel gears) as high as

$$(S_C)_{10^7} = 2.22H_B + 200\ Mpa \quad \text{..... (3.51)}$$

for grade 1

$$(S_C)_{10^7} = 2.41H_B + 237\ Mpa \quad \text{..... (3.52)}$$

and for grade 2 steel.

Another curve fit to S_C and HB at 10^8 cycles is

$$(S_C)_{10^8} = 2.76H_B - 70\ Mpa \quad \text{..... (3.53)}$$

AGMA strength equation, for allowable contact stress, $\sigma_{c,all}$ given by

$$\sigma_{c,all} = \frac{S_C}{S_H}\frac{Z_N C_H}{K_T K_R} \quad \text{..... (3.54)}$$

Where,

- S_c is the allowable contact stress
- Z_N is the stress cycle life factor
- C_H are the hardness ratio factors for pitting resistance
- K_T are the temperature factors
- K_R are the reliability factors
- S_H is the AGMA factor of safety, a stress ratio

3.11.1. Pitting Load Carrying Capacity According To DIN/ISO

According to ISO 6336-2 the contact stress, σ_H is calculated as follows, ISO 6336-2 [48]:

$$\sigma_H = Z_B \sigma_{H0} \sqrt{K_A K_V K_{H\beta} K_{H\alpha}} \leq \sigma_{HP} \quad \text{(3.55)}$$

$$\sigma_{H0} = Z_H Z_E Z_\epsilon Z_\beta \sqrt{\frac{F_t}{d_1 b} \frac{u+1}{u}} \quad \text{(3.56)}$$

Where:

- Z_B = single pair tooth contact factor
- σ_{HO} = nominal contact stress at the pitch point
- K_A = Application factor
- K_V = Dynamic factor
- $K_{H\beta}$ = Face load distribution factor for contact stress
- $K_{H\alpha}$ = Transverse load distribution factor for contact stress
- σ_{HP} = Permissible contact stress
- Z_H = the zone factor
- Z_E = the elasticity factor
- Z_ϵ = the contact ratio factor
- Z_β = the helix angle factor
- Z_β = the nominal tangential load
- b = the face width
- d_1 = pinion diameter
- u = the gear ratio Z_1/Z_2

The allowable contact stress σ_{HP} can be calculated knowing the endurance limit S_{Hlim} with the following formula:

$$\sigma_{HP} = \frac{\sigma_{Hlim}.Z_{NT}}{S_{Hmin}} . Z_L . Z_V . Z_R . Z_W . Z_X = \frac{\sigma_{HG}}{S_{Hmin}} \quad \text{(3.57)}$$

Z_{NT}= the life factor for contact stress.

σ_{HG} = the pitting stress limit.

S_{Hmin} = the minimum required safety factor for surface durability.

Z_L = the lubricant factor.

Z_V = the speed factor.

Z_R = the roughness factor

Z_W = the work hardening factor.

Z_X = the size factor.

According to DIN/ISO the lubrication conditions in the contact are taken into account by the Z_L, Z_v, and Z_R. The lubricant factor, Z_L accounts for the influence of lubricant viscosity,

$$Z_L = C_{ZL} + \frac{4.(1.0-C_{ZL})}{\left(1.2+\frac{134}{V_{40}}\right)^2} \quad \text{..... (3.58)}$$

the speed factor, Z_v accounts for the influence of pitch line velocity

$$Z_V = C_{ZV} + \frac{2.(1.0-C_{ZV})}{\sqrt{0.8+\frac{32}{V}}} \quad \text{..... (3.59)}$$

and the roughness factor, Z_R accounts for the influence of surface roughness on the surface endurance capacity.

$$Z_R = \left(\frac{3}{R_{Z100}}\right)^{C_{ZR}} \quad \text{..... (3.60)}$$

The material factor, Z_W accounts for the increase of the surface durability of a soft steel gear when meshing with a surface hardened or significantly harder gear with a smooth surface. The size factor Z_X accounts for statistics indicating that the stress levels at which the fatigue damage occurs decrease with an increase of the component size.

3.12. Contact Fatigue Criterion.

Rolling contact fatigue is based on the Lundberg-Palmgren theory, Lundberg [49]. The Lundberg-Palmgren theory postulates that the stress responsible for fatigue damage is the orthogonal shear stress, which can be derived from the Hertzian pressure distribution in the contact surface and the subsurface. The orthogonal shear stress amplitude reaches a maximum simultaneously in two planes, one parallel and one perpendicular to the contact surface. Damage resulting from contact stresses starts as a localized, inelastic cyclic deformation (localized yielding or distortion) followed by the initiation and propagation of a crack. Inelastic deformation theories are based on material deformation occurring when either the maximum shearing stress (Tresca's criterion) or the maximum octahedral shearing stress (von Mises criterion) at any point in a component reaches a critical value that causes slip of the crystal along specific crystallographic planes, Boresi [50]. The maximum shearing stress is given by:

$$\tau_{max} = \frac{1}{2}(\sigma_1 - \sigma_3) \qquad \text{..... (3.61)}$$

where σ_1 and σ_3 are the maximum and minimum values of the principal stresses at a point. The maximum octahedral shearing stress is given by the equation:

$$\tau_{oct} = \frac{1}{3}\sqrt{(\sigma_1 - \sigma_2)^2 + (\sigma_2 - \sigma_3)^2 + (\sigma_3 - \sigma_1)^2} \qquad \text{..... (3.62)}$$

where σ_1 and σ_3 are defined as before and σ_2 is the third principal stress.

If normal forces act alone that is the friction coefficient is zero, the stresses would be, Smith [51]:

$$\sigma_{1\,MAX} = -p_{max}, \sigma_{2\,MAX} = p_{max}, \text{ and } \sigma_{3\,MAX} = -0.5\ p_{max}, \qquad \text{..... (3.63)}$$

Maximum shear stress, $\tau_{max} = 0.30\, p_{max}$ ..... (3.64)

Maximum octahedral shear stress, $\tau_{oct(\max)} = 0.27\ p_{max}$ ..... (3.65)

and these values of τ_{max} and $\tau_{oct(max)}$ occur on the *y*-axis at a certain distance below the contact surface. This distance is a function of only contact geometry.

Chapter Four

4. Finite Element Method in Surface Fatigue Estimation

Mechanical components in the form of simple bars, beams, etc., can be analyzed quite easily by basic methods of mechanics that provide closed-form solutions. Actual components, however, are rarely so simple, and the designer is forced to less effective approximations of closed-form solutions, experimentation, or numerical methods. There are a great many numerical techniques used in engineering applications for which the digital computer is very useful. In mechanical design, where computer-aided design (CAD) software is heavily employed, the analysis method that integrates well with CAD is *finite-element analysis* (FEA). The mathematical theory and applications of the method are vast. There are also a number of commercial FEA software packages that are available, such as ANSYS, NASTRAN, Algor, LSDYNA, etc.

Mechanical component is a continuous elastic structure. FEA divides the structure into small but finite, well-defined, elastic substructures called elements. By using polynomial functions, together with matrix operations, the continuous elastic behavior of each element is developed in terms of the element's material and geometric properties. Loads can be applied within the element, on the surface of the element, or at the *nodes* of the element. The element's nodes are the fundamental governing entities of the element, as it is the node where the element connects to other elements, where elastic properties of the element are eventually established, where boundary conditions are assigned, and where forces (contact or body) are ultimately applied. A node possesses *degrees of freedom*. Degrees of freedom are the independent translational and rotational motions that can exist at a node. At most, a node can possess three translational and three rotational degrees of freedom. Once each element within a structure is defined *locally* in a matrix form, the elements are then *globally* assembled through their common nodes into an overall system matrix. Applied loads and boundary conditions are then specified and through matrix operations the values of all unknown displacement degrees of freedom are determined. Once this is done, it is a simple matter to use these displacements to determine strains and stresses through the constitutive equations of elasticity.

The establishment of the finite element model and the finite element calculation of this thesis work were conducted through the software package, ANSYS. ANSYS is a combined interactive/batch type computer –aided design software package, which contains many mechanical analysis programs developed, commercialized and marked by ANSYS.inc. ANSYS is the name commonly used for ANSYS mechanical, general-purpose finite element analysis (FEA) computer aided engineering software tools. ANSYS mechanical is a self contained analysis tool incorporating pre-processing such as creation of geometry and meshing, solver and post processing modules in a unified graphical user interface.

4.1. Modeling Contact in ANSYS

4.1.1. Contact Classification

ANSYS classifies contact problems into two types: rigid-to-flexible and flexible-to-flexible. In the first case, one contacting surface is treated as rigid, while the other one is flexible. The flexible-to-flexible contact approach is applied when both contacting surfaces are considered deformable. ANSYS further divides contact applications into five models; these are node-to-node, node-to-surface, surface-to-surface, line-to-line, and line-to-surface. Each type of model uses a different set of ANSYS contact elements and is appropriate for specific types of problems.

a) Surface-to-Surface Contact Elements

ANSYS supports both rigid-to-flexible and flexible-to-flexible surface-to-surface contact elements. These contact elements use a "target surface" and a "contact surface" to form a contact pair. These contact elements only support general static and transient analyses, buckling, harmonic, modal or spectrum analyses, or substructure analyses.

b) Node-to-Surface Contact Elements

This contact element supports large sliding, large deformation, and different meshes between the contacting components. Contact occurs when the element penetrates one of the target segment

elements on a specified target surface. It is typically used to model point-to-surface contact applications, such as the corners of snap-fit parts sliding along the mating surface. In this model it is possible to model surface-to-surface contact, if the contacting surface is defined by a group of nodes and multiple elements are generated. The surfaces can be either rigid or deformable. Unlike the node-to-node contact elements, you do not need to know the exact location of the contacting area beforehand, nor do the contacting components need to have a compatible mesh. Large deformation and large relative sliding are allowed, although this capability can also model small sliding. This model does not support 3-D higher-order elements on the contact surface side. The element can fail if the target surface is severely discontinuous. No contour plots are available for contact results.

c) 3-D Line-to-Line Contact

The line-to-line contact element is typically used to model 3-D beam-to-beam contact (crossing beams or beams that are parallel to each other) or a pipe sliding inside another pipe.

d) Line-to-Surface Contact

The line-to-surface contact element can be used to model a 3D beam or shell edge contacting solid or shell elements. It supports both low-order and higher-order elements on the contact surface. The target surface is modeled with 3-D target segment elements. This element is also suitable for large sliding and large displacement applications.

e) Node-to-Node Contact Elements

Node-to-node contact elements are typically used to model point-to-point contact applications. To use node-to-node contact elements, you need to know the location of contact beforehand. These types of contact problems usually involve small relative sliding between contacting surfaces (even in the case of geometric nonlinearities). Node-to-node contact elements can also be used to solve a surface-to-surface problem if the nodes of the two surfaces line up, the relative sliding deformation is negligible, and deflections (rotations) of the two surfaces remain small. These are typically problems with faceted and simple geometry.

4.1.2. Solution approach for contact problems in ANSYS

Various algorithmic procedures have been proposed to solve contact problems in finite element analysis. Most of these procedures are based on penalty and Lagrange multiplier techniques, for enforcing the contact constraints. ANSYS uses four different contact algorithms, these are:

A. Pure penalty method
B. Augmented Lagrangian method
C. Pure Lagrange multiplier method
D. Lagrange multiplier on contact normal and penalty on frictional direction

A. Pure Penalty Method

This method requires both contact normal and tangential stiffness. The main drawback is that the amount penetration between the two surfaces depends on this stiffness. Higher stiffness values decrease the amount of penetration but can lead to ill-conditioning of the global stiffness matrix and to convergence difficulties. Ideally, you want a high enough stiffness that contact penetration is acceptably small, but a low enough stiffness that the problem will be well-behaved in terms of convergence or matrix ill-conditioning.

The contact traction vector is:

$$\begin{Bmatrix} P \\ \tau_1 \\ \tau_2 \end{Bmatrix}$$

where:

- P = normal contact pressure
- τ_1 = frictional stress in direction 1
- τ_2 = frictional stress in direction 2

The contact pressure is:

$$p = \begin{cases} 0 & if \quad U_n > 0 \\ K_n U_n & if \quad U_n \leq 0 \end{cases} \qquad \text{…….. (4.1)}$$

where:

- K_n = contact normal stiffness
- U_n = contact gap size

The frictional stress for isotropic friction is obtained by Coulomb's law:

$$\tau_i = \begin{cases} \tau_i^{n-1} + K_s \Delta U_i & if \quad \|\tau\| = \sqrt{\tau_1^2 + \tau_2^2} - \mu_{iso} P < 0 \ (sticking) \\ \mu_{iso} P \frac{\Delta U_i}{\|\Delta U\|} & if \quad \|\tau\| = \sqrt{\tau_1^2 + \tau_2^2} - \mu_{iso} P = 0 \ (sliding) \end{cases} \quad \text{... (4.2)}$$

where:

- K_s = tangential contact stiffness (input as FKT on **R** command)
- ΔU_i = slip increment in direction i over the current substep
- $\|\Delta U\|$= equivalent slip increment over the current substep
- μ_{iso} = coefficient of friction
- τ_i^{n-1}= frictional stress in direction i = 1,2 at the end of previous substep

For orthotropic friction, slip increment and frictional stress are scaled so that

$$\tau_i' = \begin{cases} \tau_i'^{n-1} + K'_{si} \Delta U'_i & if \quad \|\tau'\| = \sqrt{\tau_1'^2 + \tau_2'^2} - \mu_{eq} P < 0 \ (sticking) \\ \mu_{eq} P \frac{\Delta U'_i}{\|\Delta U'\|} & if \quad \|\tau'\| = \sqrt{\tau_1'^2 + \tau_2'^2} - \mu_{eq} P = 0 \ (sliding) \end{cases} \quad \text{.. (4.3)}$$

where:

- K'_{si}= scaled tangential contact stiffness in principal direction i = 1, 2
- $\Delta U'_i$= slip increment in principal direction i = 1, 2 over the current substep
- $\|\Delta U'\|$ scaled equivalent slip increment over the current substep
- μ_{eq}= equivalent coefficient of friction
- $\tau_i'^{n-1}$= scaled frictional stress in principal direction i = 1, 2 at the end of previous sub step

For consistency between scaled friction stress and scaled slip increment, the scaled tangential contact stiffness in principal direction i = 1, 2 must be defined as:

$$K_{si}' = \left(\frac{\mu_{eq}}{\mu_i}\right)^2 k_s \quad \text{..... (4.4)}$$

B. Augmented Lagrangian Method

The augmented Lagrangian method is an iterative series of penalty updates to find the Lagrange multipliers (i.e., contact tractions). Compared to the penalty method, the augmented Lagrangian method usually leads to better conditioning and is less sensitive to the magnitude of the contact stiffness coefficient. However, in some analyses, the augmented Lagrangian method may require additional iterations, especially if the deformed mesh becomes excessively distorted.
The contact pressure is defined by:

$$p = \begin{cases} 0 & if \quad U_n > 0 \\ K_n U_n + \lambda_{i+1} & if \quad U_n \leq 0 \end{cases} \qquad \text{..... (4.5)}$$

Where

$$\lambda_{i+1} = \begin{cases} \lambda_i + K_n U_n & if \quad |U_n| > \varepsilon \\ \lambda_i & if \quad |U_n| < \varepsilon \end{cases}$$

- ε = compatibility tolerance (input as FTOLN)
- λ_i = Lagrange multiplier component at iteration i

The Lagrange multiplier component λ_i is computed locally (for each element) and iteratively.

C. Pure Lagrange Multiplier Method

The pure Lagrange multiplier method does not require contact stiffness. Instead it requires chattering control parameters. Theoretically, the pure Lagrange multiplier method enforces zero penetration when contact is closed and "zero slip" when sticking contact occurs. However the pure Lagrange multiplier method adds additional degrees of freedom to the model and requires additional iterations to stabilize contact conditions. This will increase the computational cost. This algorithm has chattering problems due to contact status changes between open and closed or between sliding and sticking. The other main drawback of the Lagrange multiplier method is over constraint in the model. The model is over constrained when a contact constraint condition at a node conflicts with a prescribed boundary condition on that degree of freedom at the same node. Over constraints can lead to convergence difficulties and/or inaccurate results. The

Lagrange multiplier method also introduces zero diagonal terms in the stiffness matrix, so that iterative solvers (e.g., PCG) cannot be used. The contact traction components (i.e., Lagrange multiplier parameters) become unknown DOFs for each element. The associated Newton-Raphson load vector is:

$$\{F_{nr}\} = \left\lfloor P, \tau_{1,}\tau_{2,}U_{n,}\Delta U_{1,}\Delta U_{2}\right\rfloor^{T} \quad \text{..... (4.6)}$$

D. Lagrange Multiplier on Contact Normal and Penalty on Frictional Direction

In this method only the contact normal pressure is treated as a Lagrange multiplier. The tangential contact stresses are calculated based on the penalty method. This method allows only a very small amount of slip for a sticking contact condition. It overcomes chattering problems due to contact status change between sliding and sticking which often occurs in the pure Lagrange Multiplier method. Therefore this algorithm treats frictional sliding contact problems much better than the pure Lagrange method.

4.2. Modeling contact problem using parallel cylinders in contact

Whilst the radius of an involute gear tooth will change slightly across the width of contact with a mating tooth it is normal to ignore this and take the contact of spur gear teeth as equivalent to the contact of parallel cylinders with the same radius of curvature at the point of contact. The Hertzian equations can thus be applied to spur gears. Buckingham [5] shows that two contacting parallel cylinders can be used to fair accuracy to study contact stresses of spur gears. Hertz theory assumes that the gear teeth as an equivalent contacting cylinder as shown Fig (4.1).

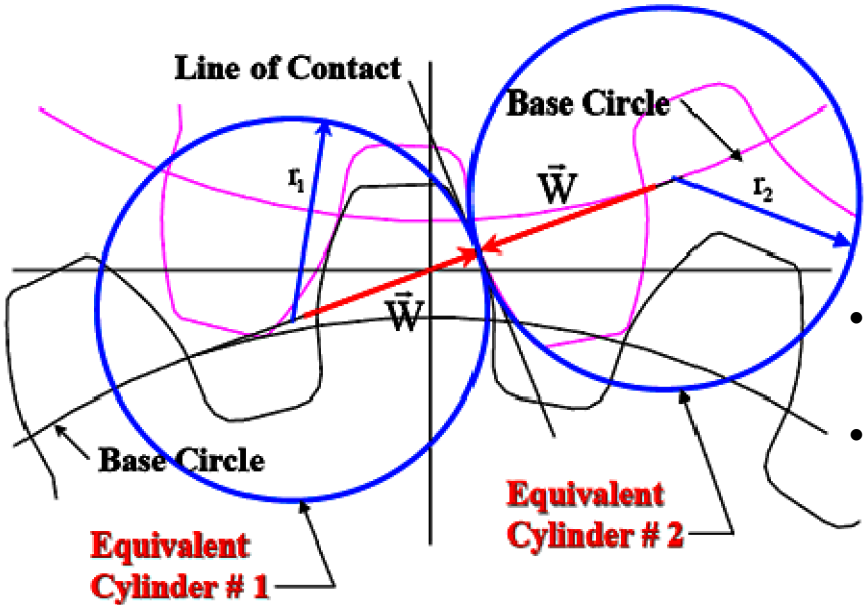

- r_1 and r_2 is the radii of equivalent cylinders,
- $\overrightarrow{W}$ is the normal force

Figure 4.1: Equivalent Contacting Cylinders.

4.3. Numerical Example-1 (Model-1)

Contact Problem of Two Circular Cylinders

To investigate the accuracy of the present method, two circular discs in contact, using 2D & 3D models are analyzed, and comparison with the analytical solutions using Hertz theory is made. In order to reduce computation time and computer memory space, two semi-cylinders with material properties and geometry given in Table (4.1) were analyzed.

Table 4.1: Material Properties & Geometry of Cylinders

Parameter	**Notation(Unit)**	**Cylinder-1**	**Cylinder-1**
Diameter	d (mm)	58	58
Contact length	*l* (mm)	28	28
Material	Chromium-molybdenum alloy steel (SCM 420)		
• **modulus of elasticity**	E (Gpa)	206	206
• **Poisson's ratio**	ν	0.3	0.3

Material Selection Criteria

Many types of gears have been used for various machines, devices, units and other equipment for transmitting power or motions. In automotive industry gears are used for many applications, for example, gears in vehicles are used in steering and transmission systems, differential units and other devices. In the fields of manufacture of automotive vehicles, it is desired to further improve the mechanical strength & manufacturing technology of the gears and other power transmission components, in an attempt to satisfy increasing requirements for enhanced performance, increased horsepower and reduced weight. There is a similar tendency in connection with steels for many mechanical structures. In this thesis work the material under study is SCM 420 alloy steel, since it is commonly used in vehicle technology. SCM 420 steel is an alloy containing chromium and molybdenum. Its symbol is SCM and its specifications comply with Japanese Industrial Standards (JIS). SCM 420 is an improved alloy steel used for manufacture of gears which has improved strength and toughness while exhibiting enhanced machinability. This material suitably used for producing gears for automotive transmissions, it can also be used for gears other than the transmission gears.

A. 2D-Model

A 2D ANSYS contact cylinder model was built with a fine mesh capable of capturing proper stress distribution below contacting surfaces. 2D PLANE82 plane strain elements were used to mesh the geometry. The element shapes used is 4-Node Triangular Structural Planar, in meshing the areas in combination with free area meshing.

To model a contact problem firstly it must identify the parts to be analyzed for their possible interaction. If one of the interactions is at a point, the corresponding component of the model is a node. If one of the interactions is at a surface, the corresponding component of a model is an element: beam, shell, or solid element. The finite element model recognizes possible contact pairs by the presence of specific contact elements. These contact elements are then interpreted with the model exactly where they are being analyzed for interaction. The current contact problem contains two semi-cylinders in contact. Considering this deformable-deformable

(flexible) contact pair is created. In creating the contact pair, the element types used are (TARGE169) as a target surface, and (CONTA 172) as a contacting node.

Boundary conditions are set in all nodes (18533), are constrained in both x and y direction, and using ANSYS APDL language a pilot node is created at the top edge of the model. Then all nodes are coupled to give couple degree of freedom. Then step load was applied to the coupled node. The applied load was incremented from 2000 N to 20000 N in increments of 2000 N.

B. 3D Model with frictionless contact, μ=0

Similar steps are followed as the 2D model. SOLID95 8-node quadrilateral brick elements were used to mesh the geometry. Deformable-deformable (flexible) contact pair is created, using (TARGE1170) as a target surface, and (CONTA 174) as a contacting node. After applying the boundary conditions, step load was applied to the coupled node as of the 2D model.

C. 3D Model with frictional contact, μ=0.42

Friction can be defined as resistance to relative motion of contacting bodies. Commonly encountered types of friction include dry, lubricated, sliding, rolling, dynamic or kinetic, static or starting or limiting, internal or hysteretic, external and viscous. Magnitude of friction is usually expressed as a *coefficient of friction* μ, which is the ratio of the force F required to initiate or sustain relative tangential motion to the normal force (or weight) N which presses the two surfaces together. Thus, $\mu = F/N$. In the early years of technology, the value of F/N was found to be reasonably constant for each class of materials. In modern technology, μ is regarded to be widely variable, depending on operational variables, lubricants, properties of the substrate, and surface films, Ludema [52].

Almost all operating parameters will influence the coefficient of friction. Some of these variables are sliding speed, temperature, starting rate, applied load or contact pressure, wear rate and

surface roughness. Surface roughness usually has little or no consistent effect on the coefficient of friction of clean, dry surfaces. Rough surfaces usually produce higher coefficients of friction in lubricated systems, particularly with soft metals where lubricant films are very thin as compared with asperity height. Surface roughness is highly related with lubrication regime.

In this section, friction is modeled with the same step as that of 3D frictionless contact. The only difference is that, in creating a contact pair in steady of frictionless contact, frictional contact is selected and the value for coefficient of friction, μ is filled in the space provided. In addition asymmetric contact condition is selected. According to Ludema [52], the sliding coefficient of friction, μ for dry contact of hard steel on hard steel is about 0.42 & for lubricated contact it ranges from 0.029-0.1 depending on the lubricant viscosity. Therefore for this model, μ=0.42 is used.

4.4. Three-Dimensional Modeling of Meshed Involute Spur Gear in Contact

4.4.1. Generation of Involute Spur Gears

Consider that a planar curve I is given (Figure. 4.2). Segments M_iN_i (i = 1, 2, . . ., n) represent the curvature radii of curve I at points M_i , where N_i is the curvature center. The locus of curvature centers N_i is the *evolute* E to curve I . The main features of E, evolute to curve I , are as follows:

- The normal M_iN_i at point M_i of curve I is the tangent to the evolute E.
- The evolute to a regular curve I is the *envelope* to the family of normals M_iN_i to I .

Considering E as given, we may determine the involute I for E as the result of development of E. Let us imagine an inextensible thread MN that is wrapped on curve E. Point M of the thread will trace out the involute I while the thread is wound on and off.

Consider the particular case when the evolute E is a circle. The involute I for such a case is the tooth profile for a spur gear. The evolute, the circle of radius r_b (Figure. 4.4), is called the *base circle*. Two branches of an involute curve are shown in Figure. 4.4. They are generated by point

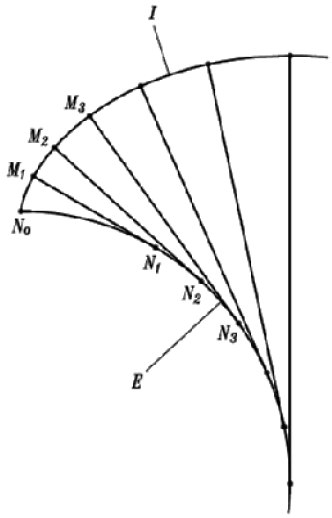

- I is the involute curve
- E is the evolute curve
- $\overline{M_i N_i}$ is curvature radii of curve *I* at points M_i
- N_i is the curvature center of I on E

Figure 4.2: Involute and evolute, Faydor [53].

M_o of the straight line that rolls over the base circle clockwise and counterclockwise, respectively. Each branch represents its respective side of the tooth as seen in figure. 4.3.

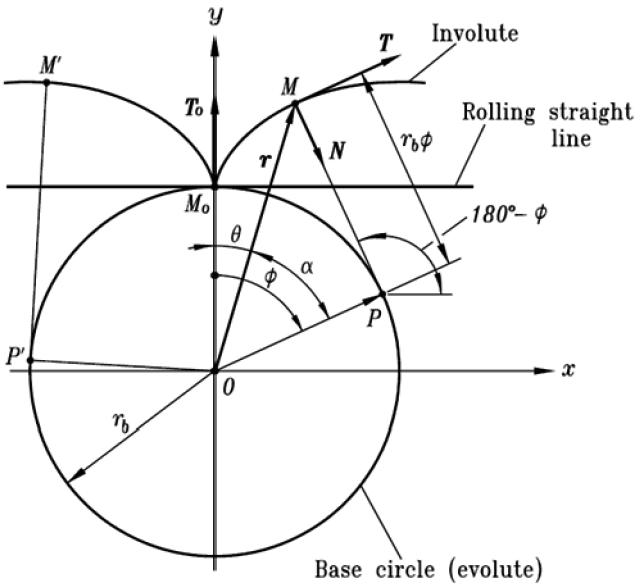

Figure 4.3: Involute curve for spur gear, Faydor [53].

The analytical representation of an involute curve is based on the following considerations (Figure 4.3).

(i) A current point M of the involute curve is determined by the vector equation

$$\overline{OM} = \overline{OP} + \overline{PM} \quad \text{..... (4.7)}$$

where

$$\overline{OP} = r_b[sin\,\varphi\ cos\,\varphi]^T \quad \text{..... (4.8)}$$

$$\overline{PM} = PM\,[-cos\,\varphi\ sin\,\varphi]^T \quad \text{..... (4.9)}$$

(ii) Due to rolling without sliding, we have

$$PM = \widehat{M_oP} = r_b\varphi \quad \text{..... (4.10)}$$

Here, φ is the angle of rotation in rolling motion.

(iii)Equations (4.7) to (4.10) yield

$$x = r_b(sin\,\varphi - \varphi\ cos\,\varphi) \quad \text{..... (4.11)}$$

$$y = r_b(cos\,\varphi + \varphi\ sin\,\varphi) \quad \text{..... (4.12)}$$

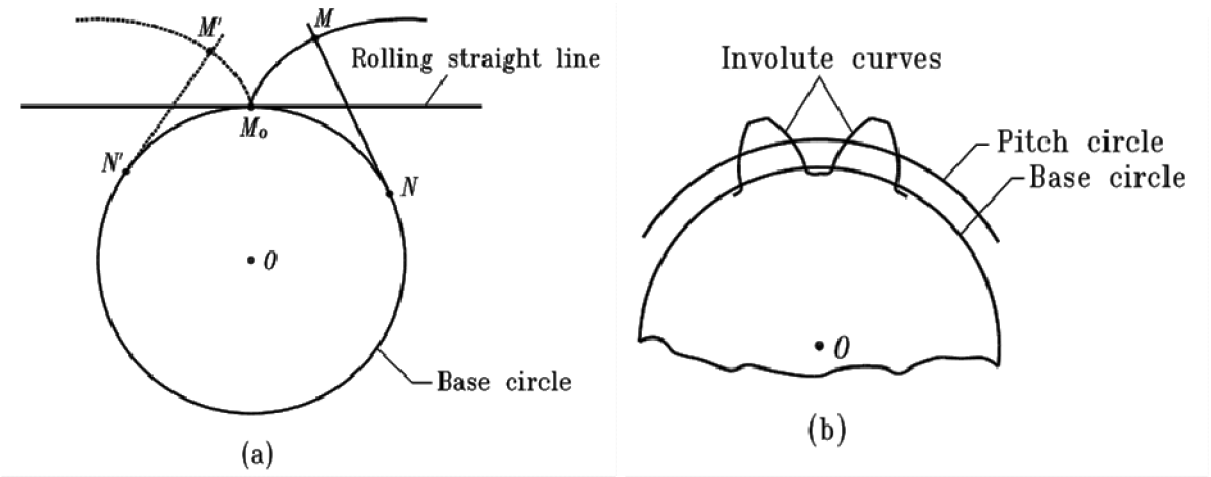

Figure 4.4: Two branches of an involute curve, Faydor [53]

4.5. Application of Finite Element Approach in Gear contact Analysis

Application of finite element analysis allows us to perform; stress analysis, investigation of formation of bearing contact, detection of severe areas of contact stresses inside the cycle of meshing. Such an approach requires, Faydor [53]

(i) Development of the finite element mesh of the gear drive,

(ii) Definition of contacting surfaces,

(iii) Establishment of boundary conditions for loading the gear drive.

In this section finite element approach is used for contact stress analysis in gears. The approach is based on application of ANSYS Workbench version 12.1 computer programs.

Analysis Step

1. The finite element model of meshed gear is generated using the equations of involute profile for spur gear tooth, (for both the pinion and the gear), in CATIA V5R16. Then, one pair of gear tooth is imported in to ANSYS Workbench 12.1as working the model. The involute curve is generated using equations (4.11 & 4.12). Therefore, the loss of accuracy associated with development of solid models using CAD (computer aided design) computer programs is minimized.

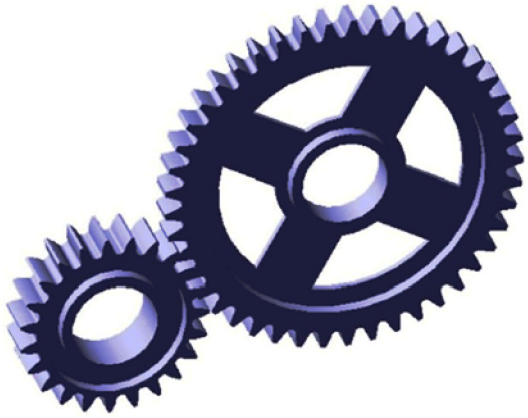

Figure 4.5: Model developed in CATIA

2. Modules for automatic generation of finite element models are integrated into the model in ANSYS Workbench version 12.1, static structural analysis system. Then, the generation of finite element models is accomplished for the cycle of meshing
3. To get the contact stresses the contact wizard is used in ANSYS Workbench. The contact algorithm in ANSYS Workbench computer program requires definition of contacting surface. To define a contact pair completely, contact and target element have to be referred to same characteristic parameters. The contact element CONTA174 and target 170 are used in the present analysis. Then, augmented Lagrangian method contact algorithm, with frictionless contact is used.
4. According to Faydor [53], boundary conditions and loading conditions for gear and pinion is applied as follows:

- Nodes on the sides and bottom part of the rim portion of the gear are considered fixed (Fig. 4.6 (a)).
- Nodes on the two sides and bottom part of the rim portion of the pinion build a rigid surface (Fig. 4.6 (b)).

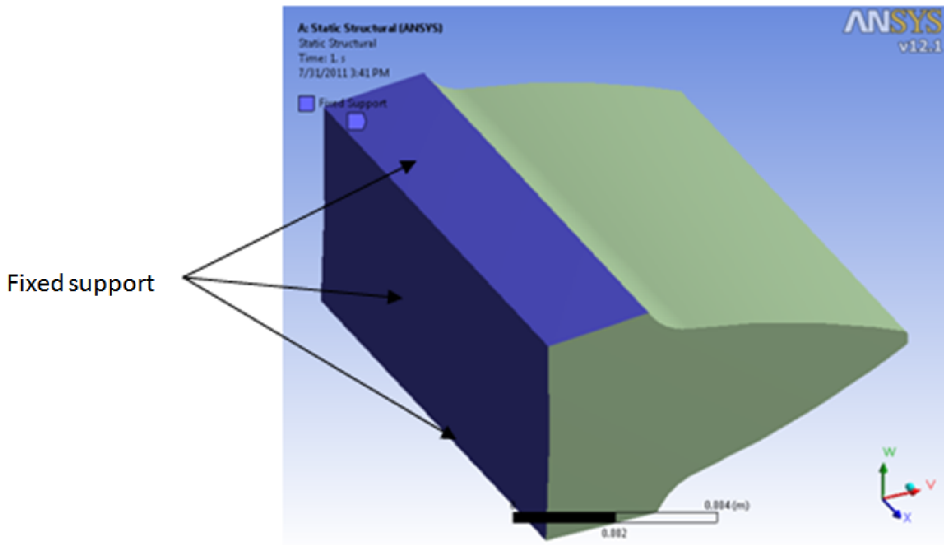

(a). Gear

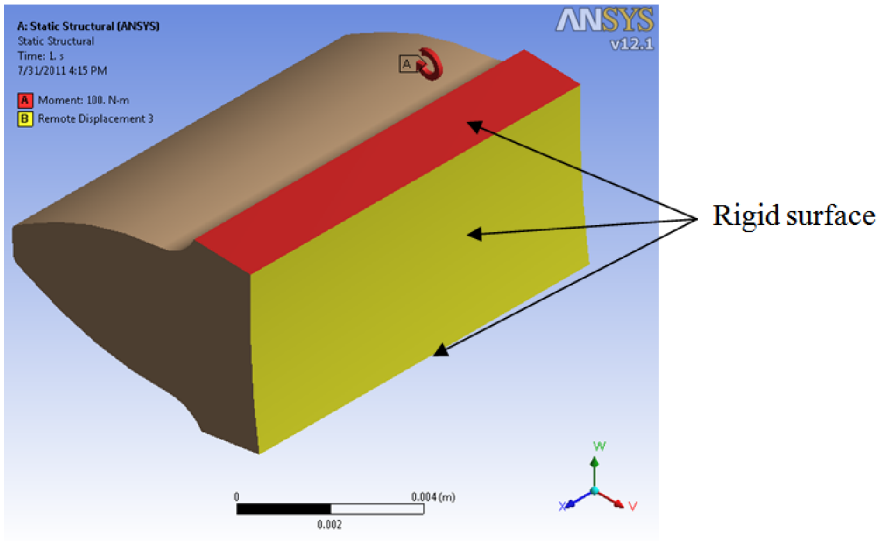

(b). Pinion

Figure 4.6: Boundary Conditions for Gear and Pinion (a). Gear (b). Pinion

Rigid surfaces are three-dimensional geometric structures that cannot be deformed but can perform translation or rotation as rigid bodies. They are also very cost effective because the variables associated with a rigid surface are the translations and rotations of a single node, in ANSYS this node is known as pilot node. The rigid body reference node is located on the pinion axis of rotation with all degrees of freedom fixed to zero, except the rotation around the axis of rotation of the pinion. The torque is applied directly to the remaining degree of freedom of the rigid body reference node.

5. After setting of boundary conditions for gear and pinion initiating the solver to compute the required results.

4.6. Numerical Example-2 (Model-2)

Generation of Spur Gear

The spur gear pair with the properties given in table 4.2 was chosen to model the problem at hand. Using these parameters and the involute curve equations (Eq. 4.11 & 4.12), the solid model is created in CATIA V5R16. In order to generate involute profile in CATIA, 5 key points are created in the range of dedundum and addendum circle radii representing the involute profile using equation (4.11 & 4.12). These points represent radii values in the range of dedundum and addendum circle. All these radii values are connected with spline, in generative shape design workbench. Once the involute shape is generated, by using extrapolation, reflection, and array command the 3D model is developed. To minimize computation time, only a pair of meshed tooth is imported to ANSYS Workbench 12.1 to carry out the analysis.

Table 4.2: Spur gear Parameters.

Parameter	**Pinion**	**Gear**
Module, M (mm)	2.5	2.5
Pressure angle, ϕ (deg)	20°	20°
Number of teeth, N	23	45
Face width, b (mm)	10	10
Pitch circle diameter, D (mm)	57.5	112.5
Gear Material	Chromium-molybdenum alloy steel (SCM 420)	
modulus of elasticity (Gpa)	206	206
Poisson's ratio	0.3	0.3
Applied Torque (NM)	100	

Additional model information

- To investigate the change in contact stress with applied load, the analysis is at five different load, (50 Nm, 112.5 Nm, 175 Nm, 237.5 Nm & 300 Nm)
- To investigate the change in contact stress with material types the analysis is done for four materials. As seen in table 4.3.

Table 4.3: Properties of material under study

Gear Material	modulus of elasticity (Gpa)	Poisson's ratio
Chromium-molybdenum alloy steel (SCM 420)	206	0.3
Grey cast iron GG-20	91	0.25
Grey cast iron GG-25	105	0.25
Grey cast iron GG-30	113	0.25

Generation of Finite Element Model

After the 3D model is generated and imported, the procedure discussed in section (4.5) is deployed to generate the finite element model as seen in figure (4.7). A free and mapped meshing capability of ANSYS Workbench is employed to generate the finite element mesh. Refinement in the contact region is performed using contact sizing option. Then, the meshing (generation of finite elements) is performed.

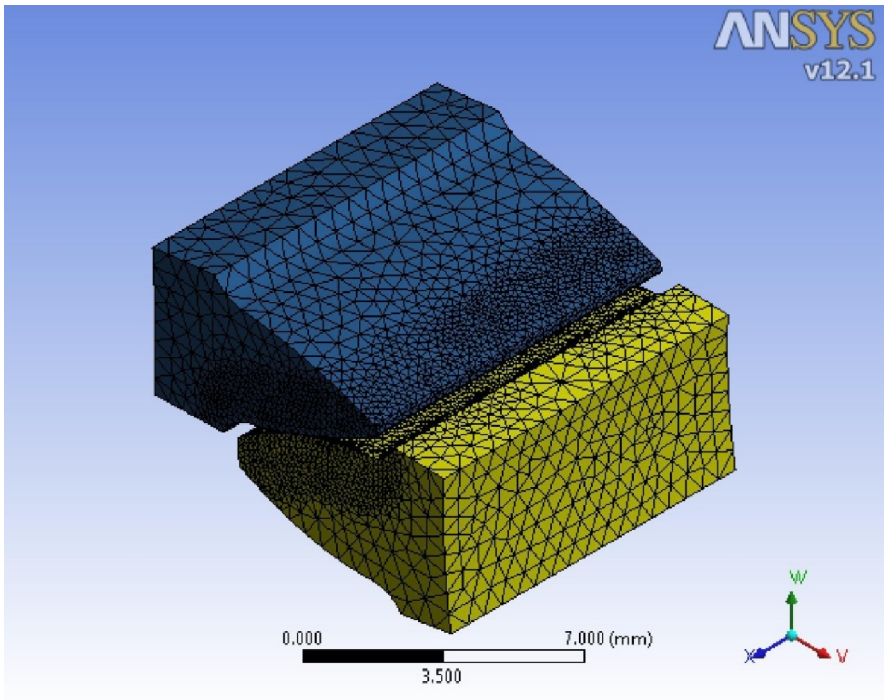

Figure 4.7: Finite Element Mesh of the Model

The finite element mesh is generated in such a way that to fulfill the following criteria so as to reduce computation time and computer memory requirement, within reasonable accuracy.

- Element size decreases at the contact region (maximum stress region)
- The size of the elements increases when moving away from the contact region
- Less number of elements in low stress regions.
- More number of small size elements in the contact region.

Table 4.4: FE Model Summary

Description	Quantity
Total Nodes	283554
Total Elements	172646
Total Body Elements	166408
Total Contact Elements	6238
Element Types	7
Materials	1
Contacts	1
Constraints	1

Table 4.5: Number of Nodes and Elements on the Gear and Pinion

Body Name	Nodes	Elements
Gear	138801	80722
Pinion	144753	85686

The analysis is performed on three dimensional finite element model of a paired meshed tooth. In this work seven types of elements are used, these are listed in table 4.5.

Table 4.6: Element Types Summary

Generic Element Type Name	Mechanical APDL Name
Quadratic Tetrahedron	Solid187
Quadratic Wedge	Solid186
Quadratic Pyramid	Solid186
Quadratic Quadrilateral Contact	Conta174
Quadratic Quadrilateral Target	Targe170
Quadratic Triangular Contact	Conta174
Quadratic Triangular Target	Targe170

4.7. Numerical Example-3 (Model-3)

Modeling Involute Spur Gear with Equivalent Contacting Cylinders

As it is discussed in the preceding sections, two contacting parallel cylinders can be used to fair accuracy to study contact stresses of spur gears. Hertz theory assumes that the gear teeth as an equivalent contacting cylinder. Therefore the model discussed in this section can be modeled by two contacting parallel cylinders to improve the accuracy in estimating the maximum shear and the von Mises stress to a certain level. The model described in table 4.2 can be equivalently modeled by two contacting parallel cylinders with properties described in table 4.7.

Table 4.7: Geometry and material property of equivalent contacting cylinders to model meshed gear of table 4.2.

Parameter	**Cylinder-1**	**Cylinder-2**
Face width, b (mm)	10	10
Diameter, D (mm)(Eq.3.23)	19.66	38.48
Material	Chromium-molybdenum alloy steel (SCM 420)	
5. modulus of elasticity (Gpa)	206	206
6. Poisson's ratio	0.3	0.3
Force (N) (Eq.3.27)	3701.5	

Generation of Finite Element Model

To save computation time and memory to be used, this contact problem can be modeled with half of the full model since it is symmetrical. The following steps are employed, to generate the finite element model.

1. The model is developed in design modeler of ANSYS Workbench 12.1.
2. Modules for automatic generation of finite element models are integrated into the model in ANSYS Workbench version 12.1, static structural analysis system. Then, the generation of finite element models is accomplished for the cycle of meshing.

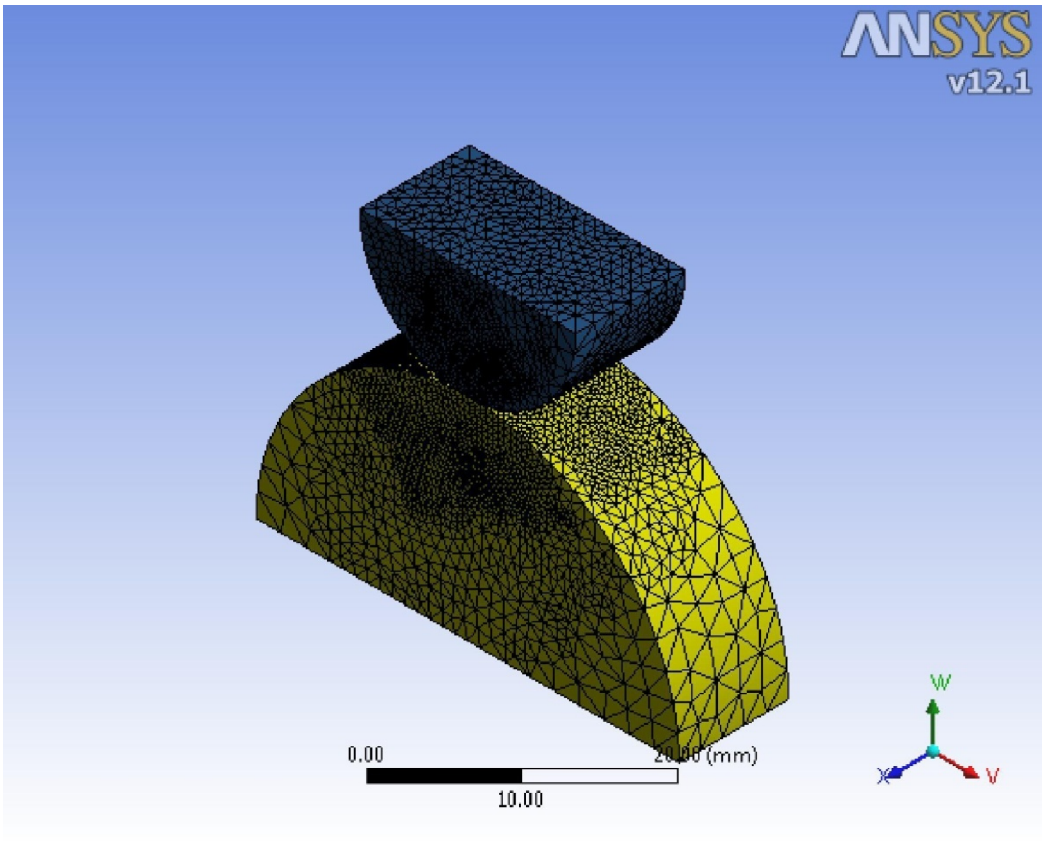

Figure 4.8: Finite Element Mesh of the Model

3. To get the contact stresses the contact wizard is used in ANSYS Workbench. The contact algorithm in ANSYS Workbench computer program requires definition of contacting surface. To define a contact pair completely, contact and target element have to be referred to same characteristic parameters. The contact element CONTA174 and

target 170 are used in the present analysis. Then, augmented Lagrangian method contact algorithm, with frictionless contact is used.

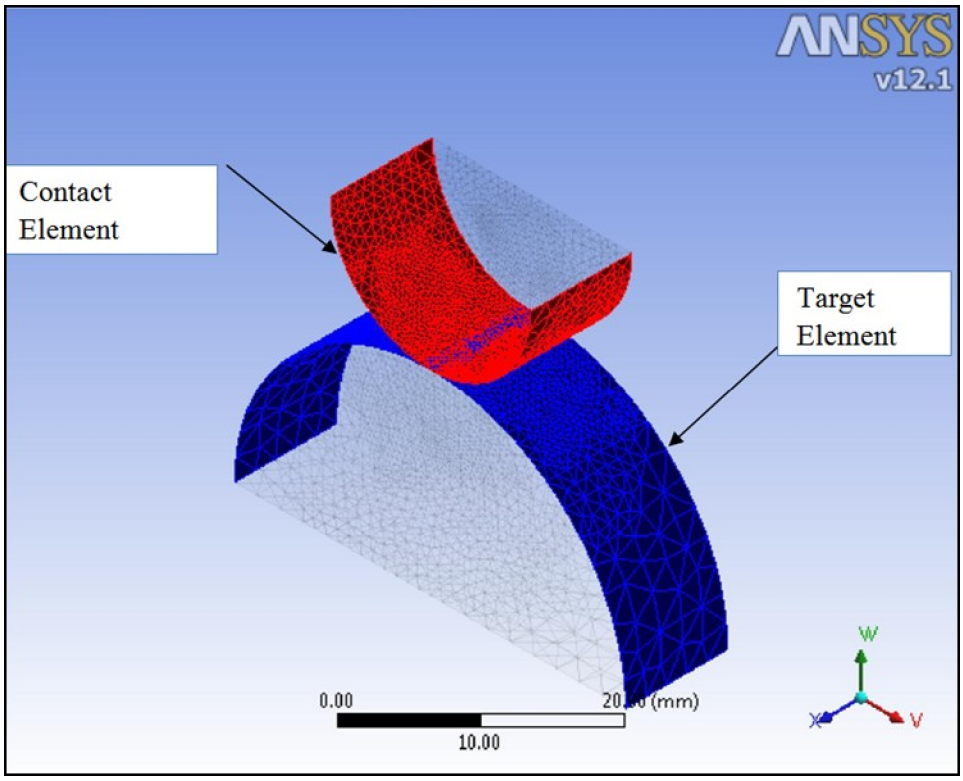

Figure 4.9: Contact and Target Element of the model

4. The setting up of boundary conditions and contact force for the contacting cylinders as follows:

- Nodes on the bottom part of the larger cylinder are considered fixed.
- Nodes on the top portion of the smaller cylinder build a rigid surface.
- Apply the contact force, as seen in Figure 4.10, on the smaller cylinder.

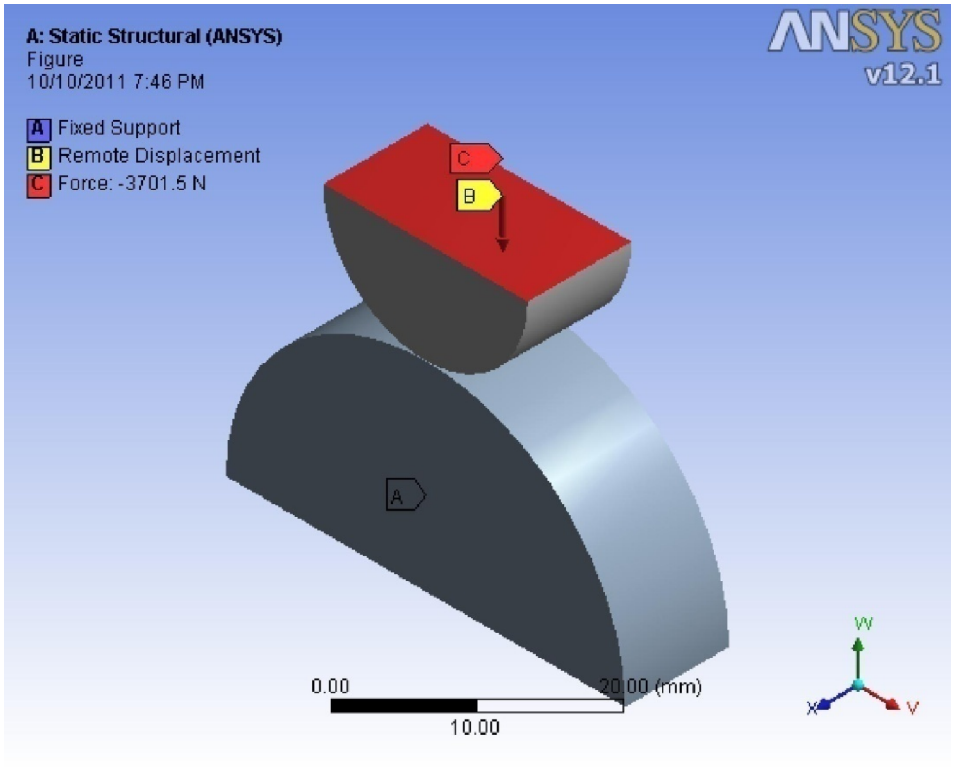

Figure 4.10: Boundary Conditions & Contact Force of the Model.

5. After setting the boundary conditions, for the contacting cylinders, initiating the solver to compute the required results.

Table 4.8: FE Model Summary

Description	Quantity
Total Nodes	91788
Total Elements	63780
Total Body Elements	59607
Total Contact Elements	4173
Element Types	3
Materials	1
Contacts	1

Table 4.9: Number of Nodes and Elements on the cylinders

Body Name	Nodes	Elements
Cylinder-1	44745	29218
Cylinder-2	47043	30389

The analysis is performed on three dimensional finite element models of two contacting cylinders. In this work three types of elements are used, these are listed in table 4.10.

Table 4.10: Element Types Summary

Generic Element Type Name	Mechanical APDL Name
Quadratic Tetrahedron	Mesh200
Quadratic Triangular Contact	Conta174
Quadratic Triangular Target	Targe170

4.8.Overview of fatigue analysis in ANSYS Workbench

A large part of a fatigue analysis requires an accurate description of the fatigue material properties. In ANSYS Workbench, sample fatigue curves are available only for structural steel and aluminum alloy materials. This is because, fatigue analysis is empirical and it becomes very difficult to take in to account all materials type. Therefore in doing fatigue analysis in ANSYS Workbench, users must provide their own fatigue data.

4.8.1. Loading Type

There are essentially five classes of fatigue loading with the fatigue tool in ANSYS Workbench, these are

- Zero-Based
- Fully Reversed

- Ratio
- History Data
- Non-proportional Loading (available only for stress-life applications)

The first three are all constant amplitude, proportional loading types and are illustrated with a graph in the Geometry window.

The fourth type, history data, allows you to navigate to a file containing the data points. This option is a non-constant amplitude proportional loading type. This data is depicted in a graph on the worksheet. You can specify the number of data points this graph will display in the maximum data points to plot field located in the details view of the fatigue tool.

The fifth option is a non-proportional constant amplitude loading type for models that alternate between two completely different stress states (for example, between bending and torsional loading). Problems such as an alternating stress imposed on a static stress can be modeled with this feature. Non-proportional loading is applicable on fatigue tools under Solution Combination where exactly two environments are selected.

4.8.2. Analysis Type

In ANSYS Workbench there are two types of analysis option. These are, stress life and strain life.

1. **Stress Life Analysis**:-This option appears only if Type is set to History Data (non-constant amplitude loading) and defines what life will be used if the stress amplitude is lower than the lowest stress on the SN curve. It may be important in how damaging small stress amplitudes from the rainflow matrix are.

2. **Strain Life Analysis**:-Since the strain-life method is equation based it has no built-in limit, unlike stress-life for which the Fatigue Tool uses a maximum life equal to the last point on the SN curve. Thus to avoid skewed contour plots showing very high lives, you can specify Infinite Life in a strain-life analysis. For example, if you set a value of 1e9 cycles as the Infinite Life, the maximum life reported is 1e9.

- **Mean Stress Theory**

This setting specifies how the mean stress effects should be handled.

1. If analysis type is set to stress life, choose from None, Goodman, Soderberg, Gerber, and Mean Stress Curves. The Goodman, Soderberg, and Gerber options use static material properties along with S-N data to account for any mean stress while Mean Stress Curves use experimental fatigue data to account for mean stress. The default mean stress theory can be defined through the mechanical application fatigue settings in the options dialog box.
2. If Analysis Type is set to Strain Life, choose from None, Morrow, and SWT (Smith-Watson-Topper).

- **Stress Component**

Because stresses are multiaxial but experimental fatigue data is usually uniaxial, the stress must be converted from a multiaxial stress state to a uniaxial one. You can choose from several types, including component stresses, von Mises, and a *signed* von Mises, which takes the sign of the absolute maximum principal stress. The signed von Mises is useful for accounting for any compressive mean stresses.

4.8.3. Reviewing Fatigue Results

In ANSYS Workbench, there are nine results for evaluating fatigue is available for the user. These are,

1. **Life:-**This result contour plot shows the available life for the given fatigue analysis. If loading is of constant amplitude, this represents the number of cycles until the part will fail due to fatigue. If loading is non-constant, this represents the number of loading blocks until failure. Thus if the given load history represents one month of loading and the life was found to be 120, the expected model life would be 120 months. In a constant amplitude analysis, if the alternating stress is lower than the lowest alternating stress defined in the S-N curve, the life at that point will be used.

2. **Damage:-**Fatigue damage is defined as the design life divided by the available life. The default design life may be set through the options dialog box. A damage of greater than 1 indicates the part will fail from fatigue before the design life is reached.
3. **Safety Factor:-** This result is a contour plot of the factor of safety (FS) with respect to a fatigue failure at a given design life. The maximum FS reported is 15.
4. **Biaxiality Indication** This result is a stress biaxiality contour plot over the model that gives a qualitative measure of the stress state throughout the body. A biaxiality of 0 corresponds to uniaxial stress, a value of -1 corresponds to pure shear, and a value of 1 corresponds to a pure biaxial state. For Non-proportional loading, you can choose between average biaxiality and standard deviation of biaxiality in the Details view.
5. **Equivalent Alternating Stress:-**The Equivalent Alternating Stress contour is the stress used to query the S-N curve. This result is not valid if the loading has non-constant amplitude (Loading Type = history data). The result is useful for cases where the design criterion is based on an equivalent alternating stress as specified by the fatigue analyst.
6. **Rainflow Matrix (history data only):-**This graph depicts how many cycle counts each bin contains. This is reported at the point in the specified scope with the greatest damage.
7. **Damage Matrix (history data only):-**Similar to the rainflow matrix, this graph depicts how much relative damage each bin has caused. This result can give you information related to the accumulation of the total damage (such as if the damage occurred though many small stress reversals or several large ones).
8. **Fatigue Sensitivity:-**This plot shows how the fatigue results change as a function of the loading at the critical location on the scoped region. Sensitivity may be found for life, damage, or factory of safety. For instance, if you set the lower and upper fatigue sensitivity limits to 50% and 150% respectively, and your scale factor to 3, this result will plot the data points along a scale ranging from a 1.5 to a 4.5 scale factor. You can specify the number of fill points in the curve, as well as choose from several chart viewing options (such as linear or log-log).
9. **Hysteresis:-**In a strain-life fatigue analysis, although the finite element response may be linear, the local elastic/plastic response may not be linear. The Neuber correction is used to determine the local elastic/plastic response given a linear elastic input. Repeated loading will form close hysteresis loops as a result of this nonlinear local response. In a

constant amplitude analysis a single hysteresis loop is created although numerous loops may be created via rainflow counting in a non-constant amplitude analysis. The Hysteresis result plots the local elastic-plastic response at the critical location of the scoped result (the Hysteresis result can be scoped, similar to all result items). Hysteresis is a good result to help you understand the true local response that may not be easy to infer.

4.9.Numerical Example-4 (Model-4)

Surface fatigue estimation in ANSYS Workbench

The equivalent contacting cylinders with the properties given in table 4.2, is used, with the following additional model information.

Additional model information

- Applied load = 20KN
- To investigate the effect of surface roughness on surface fatigue, the analysis is done for four different surface conditions.
- To investigate the change in fatigue life with applied load, the analysis is done for different loading conditions.

A large part of a fatigue analysis is getting an accurate description of the fatigue material properties. Since fatigue is so empirical, in ANSYS Workbench 12.1, sample fatigue curves are included only for structural steel and aluminum materials. These properties are included as a guide only with intent for the user to provide their own fatigue data for more accurate analysis. Therefore, the fatigue data for contact fatigue strength, Hertzian stress Vs life is inserted in the space provided for the material under study, (SCM420).

Chapter Five

5. Results and discussion

5.1.Contact Stress Analysis in ANSYS for model 1

In this section, results of finite element approach for contact stress estimation in ANSYS and Hertz theory, for the model-1, described in section 4.3 is compared. The result of the analysis summarized as follow. The maximum contact stress value for this model was 7050MPa which obtained by Hertz theory, the well known theoretical calculations method for contact problem. The stress analysis has been done by ANSYS software, where the results have been presented by contours and numerical values. The maximum contact pressure result from ANSYS for the 2D is 7065MPa and for the 3D model is 7372MPa. The error between the theoretical and 2D and 3D model, is about 0.2% and 4.5%. This shows that, the 2D model is more accurate than 3D model in computing contact pressure.

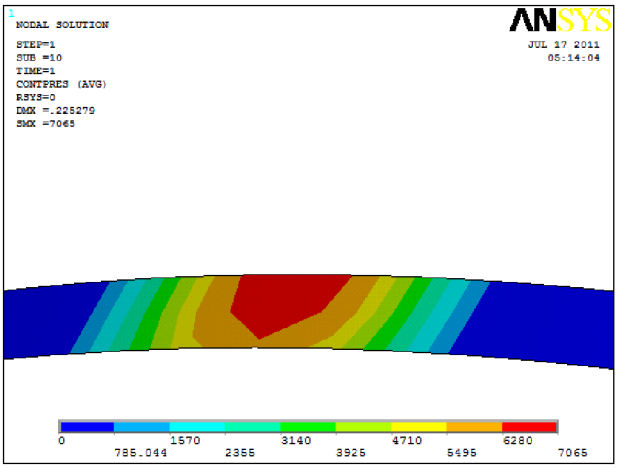

(a)

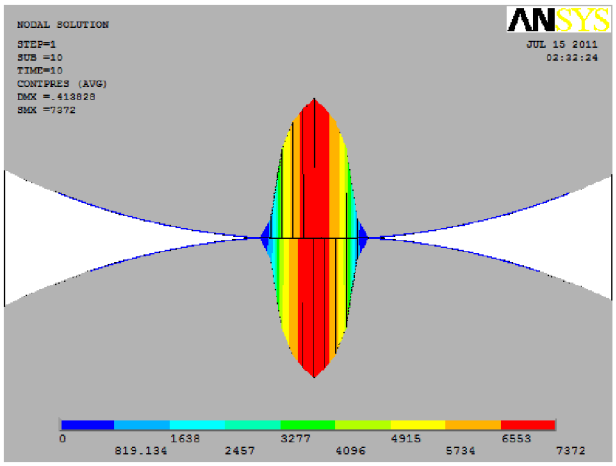

(b)

Figure 5.1: Contact pressure distribution, (a). for 3D model. (b). for 2D model.

Figure 5.2 shows the von Mises stress distribution under the final load step of 20000 N applied to the cylinders. Stress units are MPa and displacement units are mm.

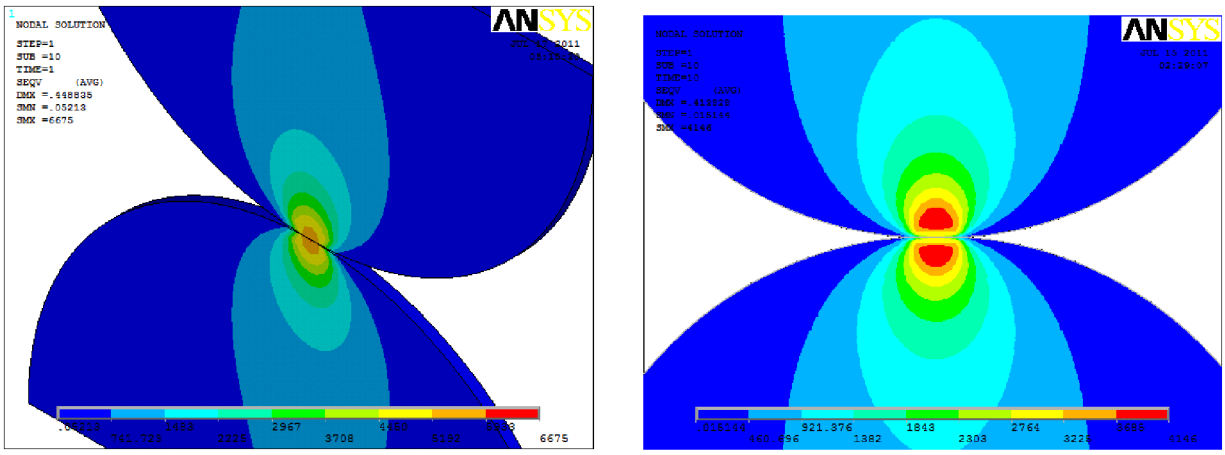

(a) (b)

Figure 5.2: von Mises Stress Distribution, (a). for 3D model, (b). for 2D model.

Figure 5.3 shows the shear stress distribution under the final load step of 20000N applied to the cylinders. Stress units are in Mpa and displacement units are in mm.

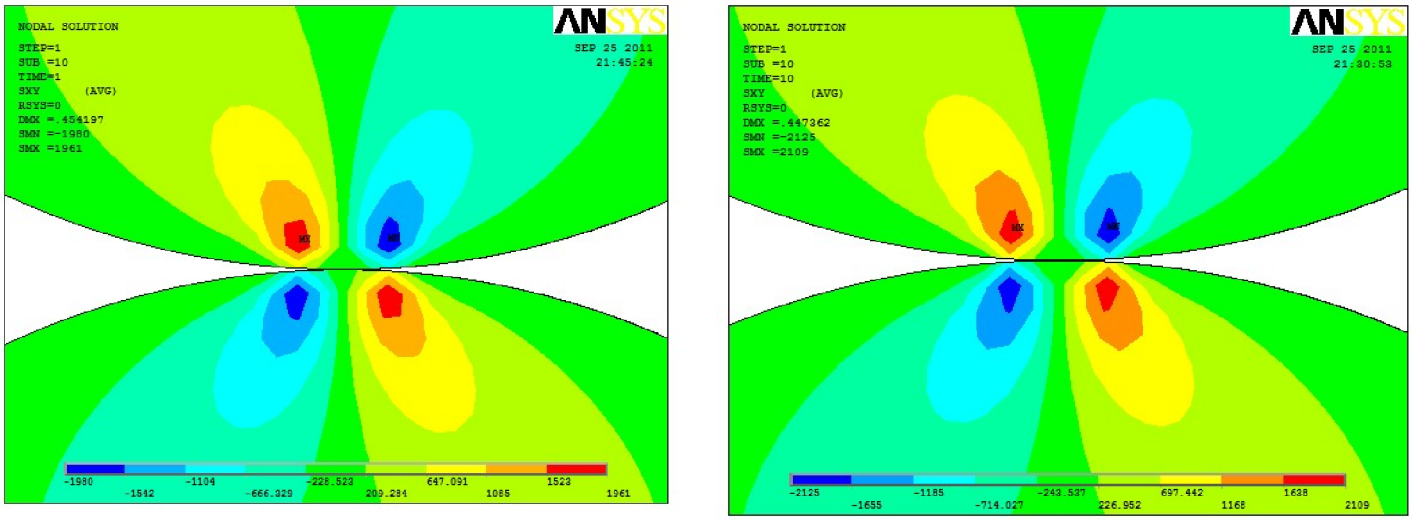

(a) 3D model frictionless **(b) 3D model frictional, μ=0.42**

Figure 5.3: Shear Stress Distribution,

The maximum shear stress value for the 3D frictionless model was 2115MPa which obtained by equation 3.18. The stress analysis has been done by ANSYS software, where the results have been presented by contours and numerical values. The maximum shear stress result from ANSYS for the 3D frictionless model is 1980 MPa and for the frictional 3D model is 2125.5 MPa. The comparison between the theoretical and ANSYS results is done and results are summarized in table 5.1

Table 5.1 Comparison of Theoretical and ANSYS result for frictional contact.

coeff. of friction, **μ**	X (mm)	Y (mm)	ANSYS Result (Mpa)	Theoretical Result (Mpa)	Error (%)
0	1.6453	-0.854	-1980	-2115	6.38
0.42	1.6453	-0.854	2125.5	2310.42388	8.00

The result in the table above shows that, ANSYS can predict maximum shear stress for the 3D frictionless and frictional model with 6.38 and 8.00% error respectively.

The theoretical stress in y and x direction along the y axis is compared to 2D and 3D model. To compare results from ANSYS with the results from the Hertz theory, equations (3.14-3.16) were used and the results are plotted as in figure 5.4 and 5.5. As it is seen in the figure stress in y direction (σ_y), in the 3D model produces non-correlated results near the contact surface this might be due to relatively coarse mesh size and initial adjustments taken to enforce numerical stability at the contact surface.

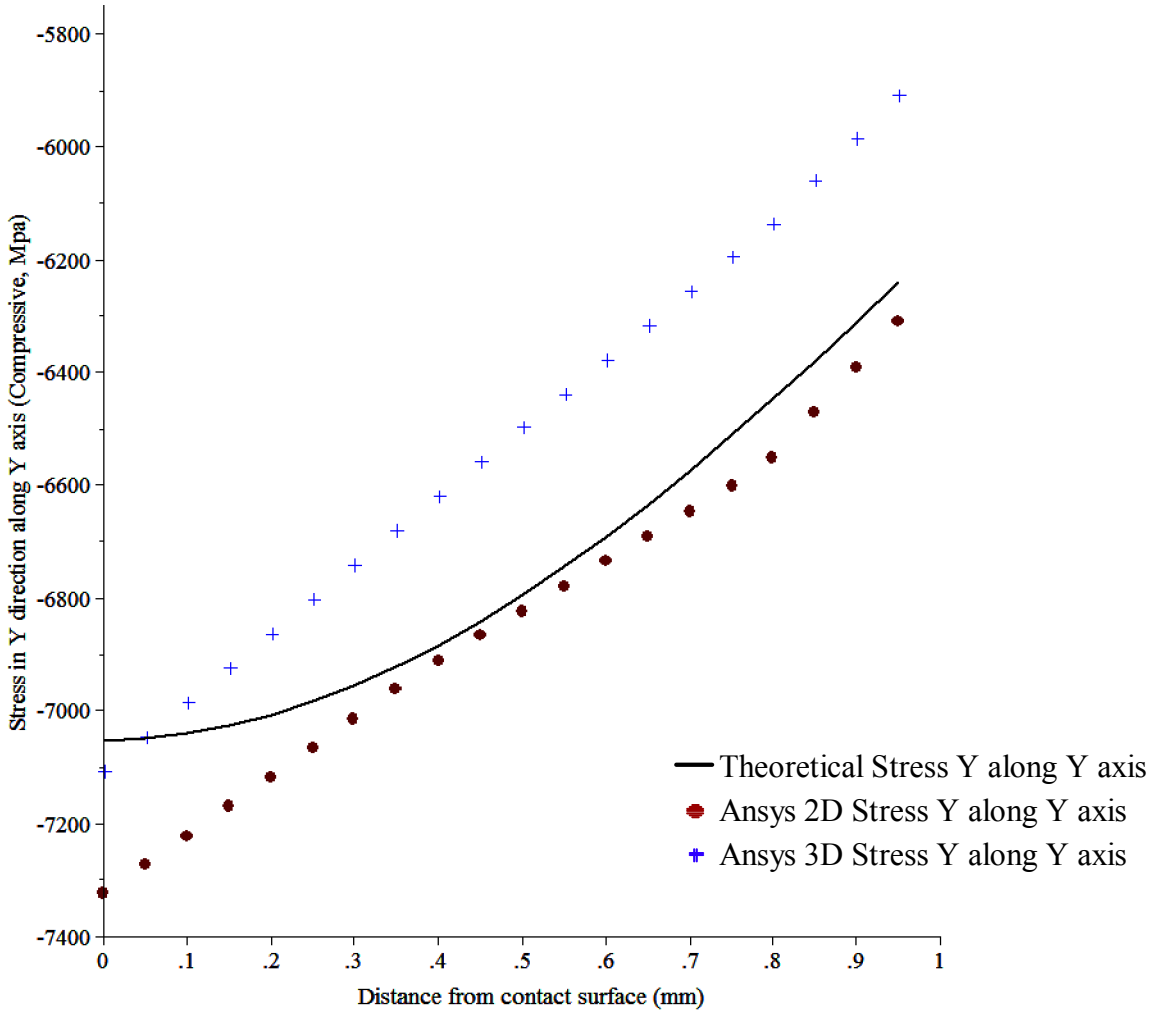

Figure 5.4: Stress in y direction along the y axis

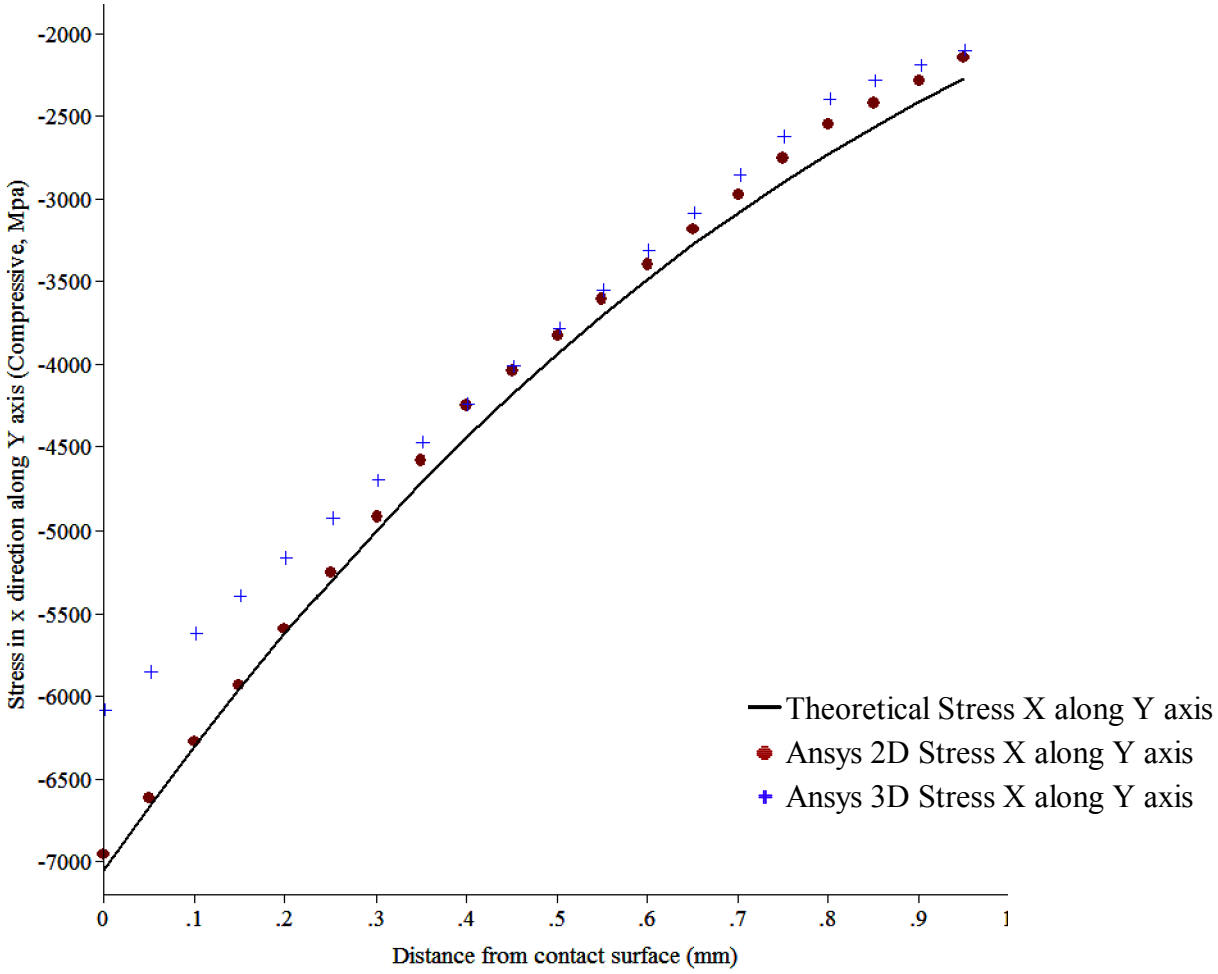

Figure 5.5: Stress in x direction along the y axis

Figure 5.6 shows the comparison of contact pressure distribution obtained from the same 2D model and theoretical calculation. There is a good correlation between the two results. To conclude, a 2D model shows extremely good correlation with theoretical results in estimating stress distribution and contact pressure.

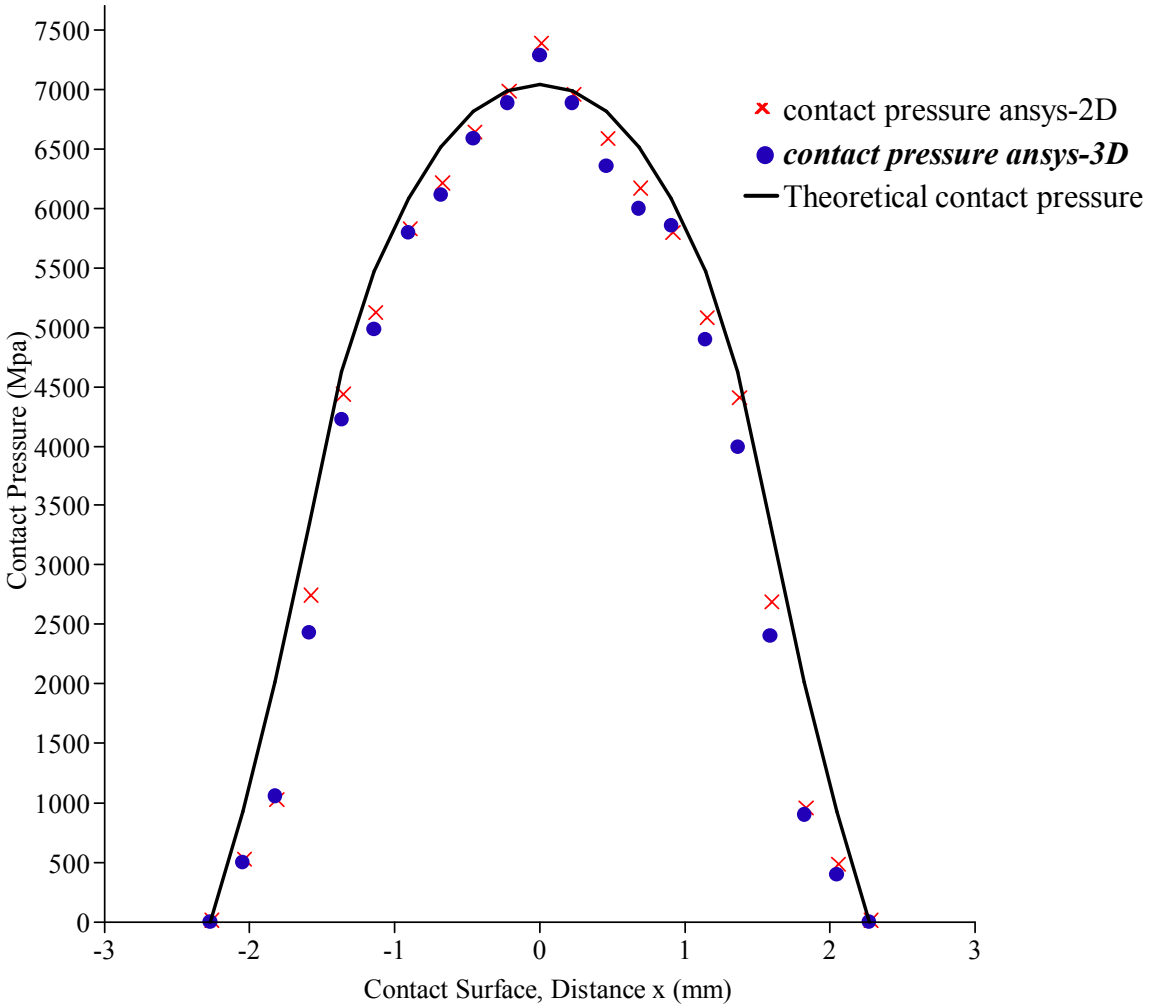

Figure 5.6: Contact pressure distribution for the theoretical and 2D model

As it is seen in this section, when modeling any type of physical problem using finite element analysis, one has to understand the theory behind the phenomenon being modeled. Otherwise, the results obtained could be misleading and potentially dangerous if blindly relied upon. Even though the 3D model showed good correlation with the more refined 2D model in contact pressure estimations, it failed in showing accurate stress distribution below the contacting surfaces. When analyzing parts that come into contact, the area just below the surface is the most critical area as far as the parts failure is concerned. If contact pressure is of interest, the 3D

model developed here is a valid one and can be used to accurately predict. But, the 2D model is legitimate to predict both the surface contact pressure and stress distribution below the contacting surface with certain level of accuracy.

5.2.Contact Stress Analysis in ANSYS Workbench for model 2

In this section, results of finite element approach for contact stress estimation in ANSYS Workbench and Hertz theory, for the model described in section 4.6 (model-2) is compared. The result of the analysis summarized as follow. The maximum contact stress value for this model is 1432.1 Mpa, obtained by Hertz theory (equation 3.28). The stress analysis has been done using ANSYS Workbench v 12.1 software, where the results have been presented by contours and numerical values. The maximum contact pressure result from ANSYS is 1283.3MPa. Comparison with theoretical value was done, and the result agrees with the theoretical result within 10.39% error. The contour plot showing the contact stress distribution of ANSYS Workbench results is shown in figure 5.7.

Figures 5.8 & 5.9 show the von Mises and shear stress distribution for applied torque to the pinion (100 NM), respectively. The maximum shear stress value for this model is 429.63 Mpa, obtained by Hertz theory (Eq. 3.18), and results from ANSYS Workbench is 452.62 Mpa. The von-Mises stress value for this model is 816.3 Mpa, obtained by Hertz theory (Eq. 3.19).

Comparison of shear stress and von-Mises stress results from theoretical relations and ANSYS Workbench shows that, the value from ANSYS 5.4% and 33.5% higher than Hertzian contact stress, this might be because of the involute profile i.e., geometric non-linearity may contribute to the contact non-linearity. Inspite of the higher deviation of shear stress and von-Mieses results of ANSYS with that of Hertzian stress, the contour profile looks interesting, as seen in the figure 5.9, and it is persistent with the usual shear stress and von-Mises contour plot.

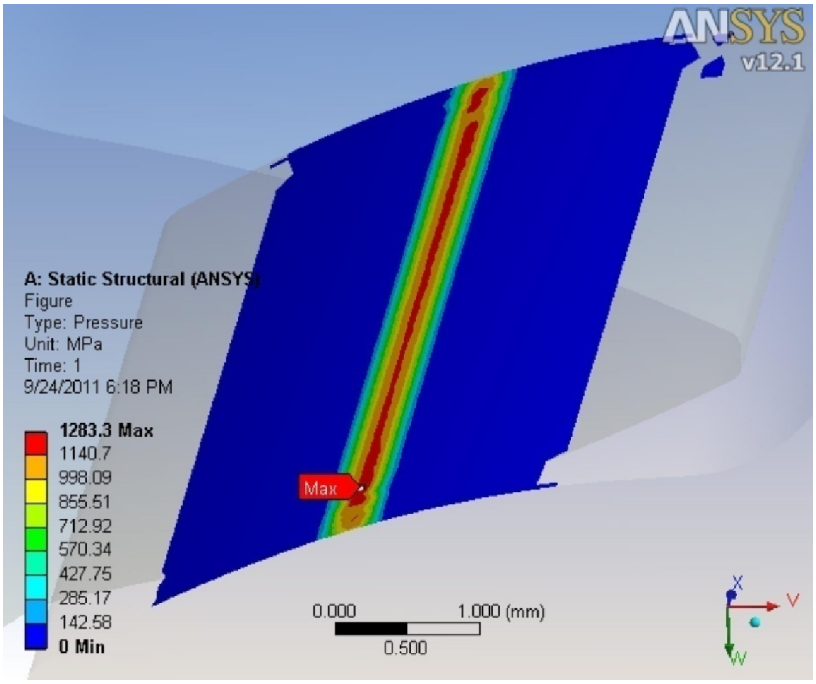

Figure 5.7: Contact Stress Distribution for the model

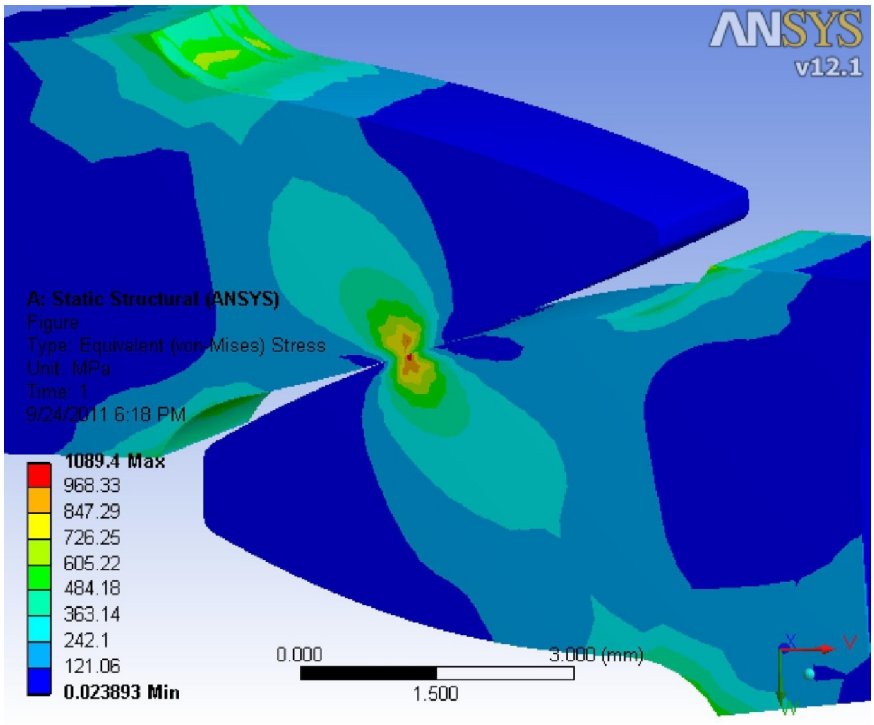

Figure 5.8: von Mises Stress Distribution

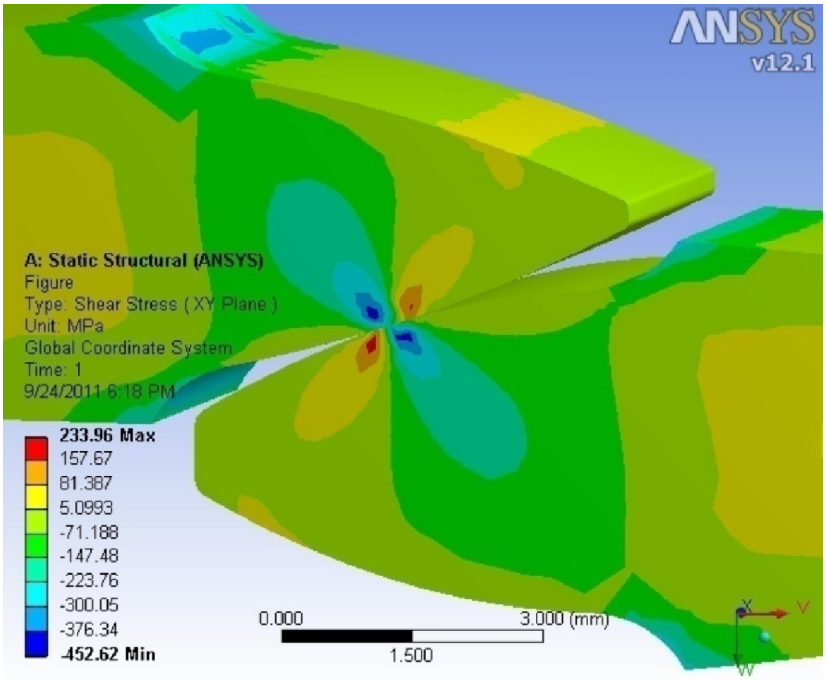

Figure 5.9: Shear Stress Distribution

- **Stress Analysis for Different Loading Condition**

The goal of stress analysis presented in this section is to investigate the change in stress with loading conditions.

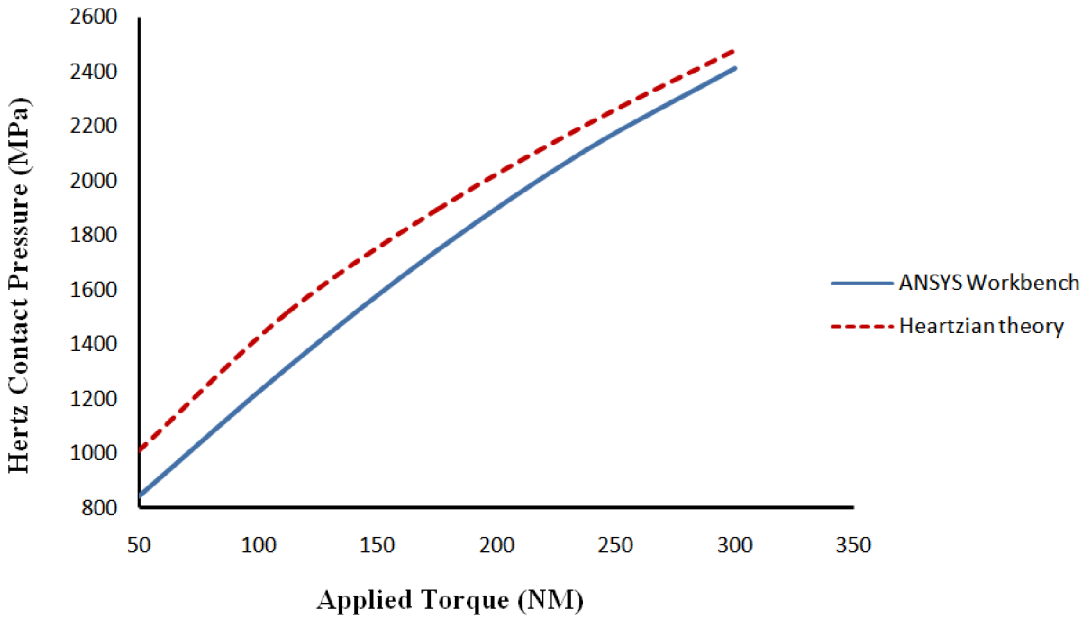

Figure 5.10: Comparison of ANSYS output Hertz theory for different load

Contact pressure results for different loading conditions, using both ANSYS and Hertzian theory are plotted in Figure 5.10. As it is seen in the figure the ANSYS model agrees well for higher load with the theoretical results. The error for all loading condition is computed and shown in table 5.2.

Table 5.2: Comparison of ANSYS Result Hertz Theory for Different Load

Torque (Nm)	ANSYS Contact Pressure (MPa)	Hertzian Contact Pressure (MPa)	Error (%)
50	842.441744	1.01E+03	-16.7983
112.5	1319.878176	1.52E+03	-13.0801
175	1746.274784	1.89E+03	-7.81424
237.5	2112.1328	2.21E+03	-4.2898
300	2413.247616	2.48E+03	-2.69948

As it is seen in table 5.2, at lower loads ANSYS under estimates contact pressure results and the error is higher, as the load increases the error decreases, this is because at higher loads good contact condition is established. As a result for applied torque value greater than 237.5 Nm ANSYS estimates contact pressure within 5% error.

- **Stress Analysis for Different Gear material**

The goal of stress analysis presented in this section is to investigate the change in stress with material types. Maximum contact pressure results for different material, using both ANSYS and Hertzian theory under a constant loading condition of torque 100 Nm are plotted in Figure 5.11. As it is seen in the figure the ANSYS model agrees well with the theoretical results. The error for all loading condition is computed and shown in table 5.3.

Table 5.3: Comparison of Maximum contact pressure for different material

Gear material	ANSYS Max Contact Pressure (Mpa)	Hertzian Max Contact Pressure (Mpa)	Error (%)
Alloy steel (SCM 420)	1298.927904	1432.1	-9.29908
Grey cast iron GG-30	965.612128	1044.87	-7.58543
Grey cast iron GG-25	941.6444	1007.2	-6.5087
Grey cast iron GG-30	889.94632	937.66	-5.08859

From table 5.3 it is verified that, the 3D ANSYS gear model can predict maximum contact pressure within 10% error.

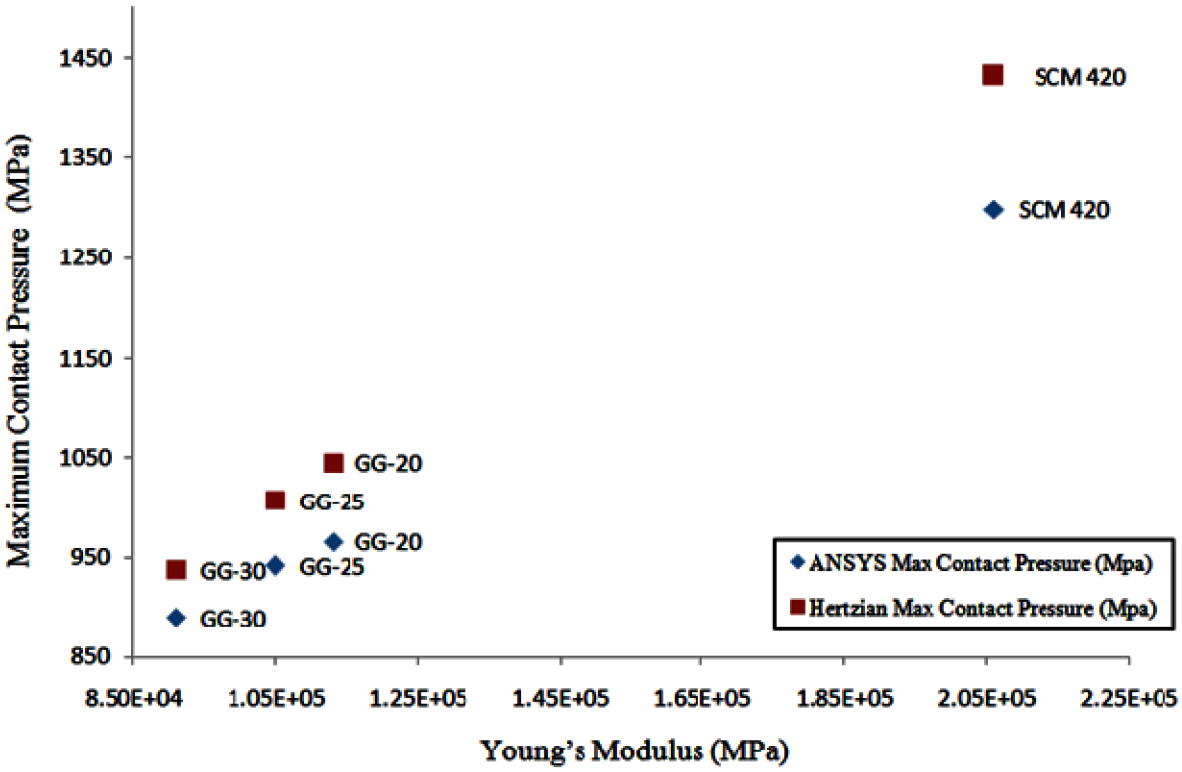

Figure 5.11: Comparison of Maximum contact pressure for different material

- **Correlation Scatter Chart**

The elasticity of the contacting materials becomes important, in studying contact problem of mating surface. To investigate this correlation scatter chart is developed in ANSYS software. Figure 5.12 shows a sample scatter plot of Young's Modulus (Pa) Vs Stress (Pa) results. Two trend lines, linear and quadratic curves, are added to the sample points of the parameter pair. The chart conveys a graphical presentation of the degree of correlation between the parameter pair in linear and quadratic trends. The degree of correlation between Young's Modulus (Pa) and stress results are presented in table 5.4.

Table 5.4: Correlation coefficient for Young's Modulus (Pa) Vs Stress (Pa)

Trend line	correlation coefficient, R2			
	maximum contact pressure	maximum shear stress	minimum shear stress	maximum equivalent stress
linear	R2 = 0.98926	R2 = 0.83853	R2 = 0.94854	R2 = 0.96859
quadratic	R2 = 0.98933	R2 = 0.92599	R2 = 0.98802	R2 = 0.99357

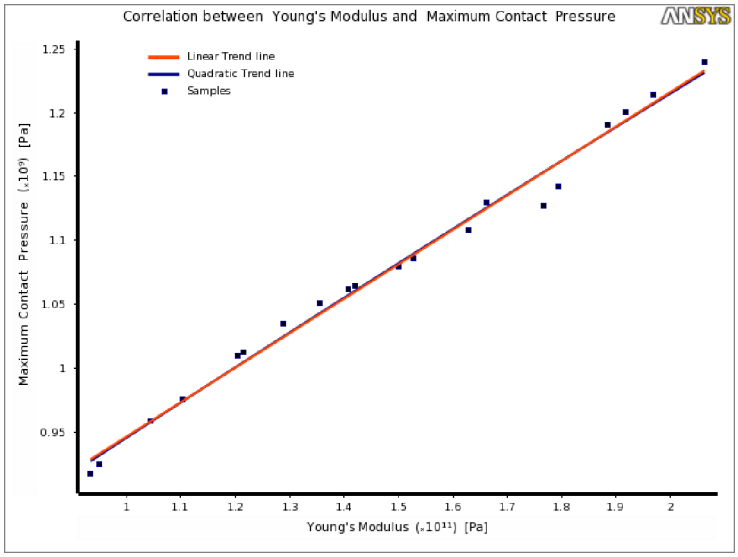

(a)

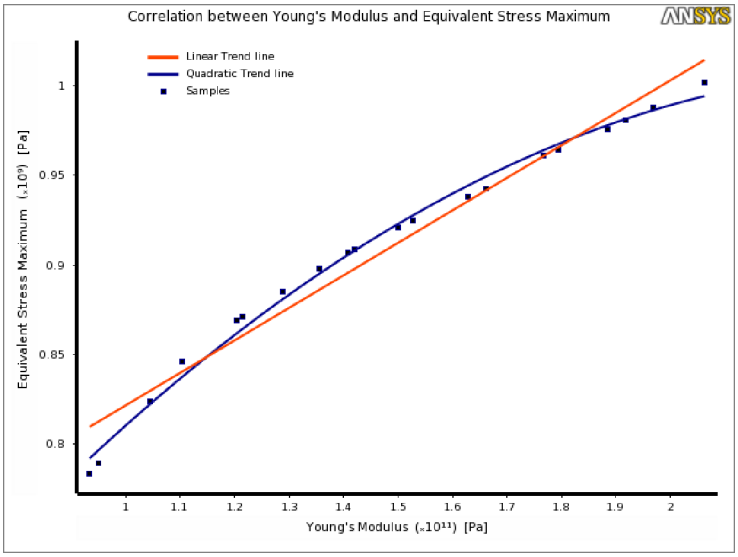

(b)

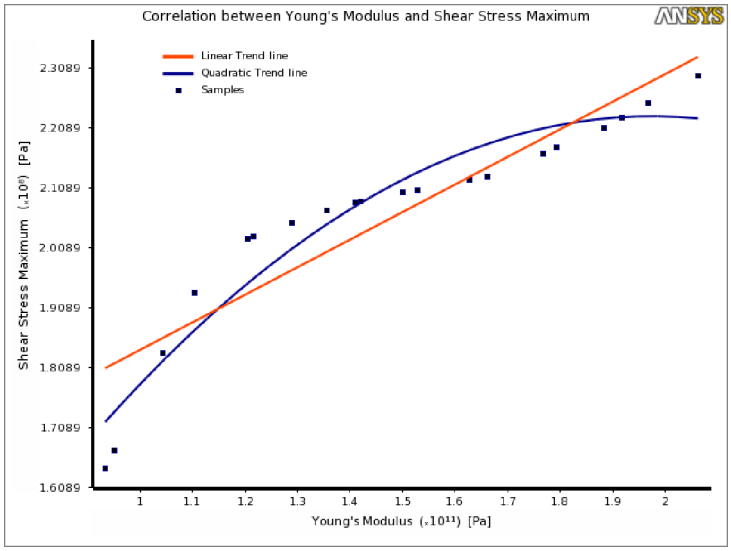

(c)

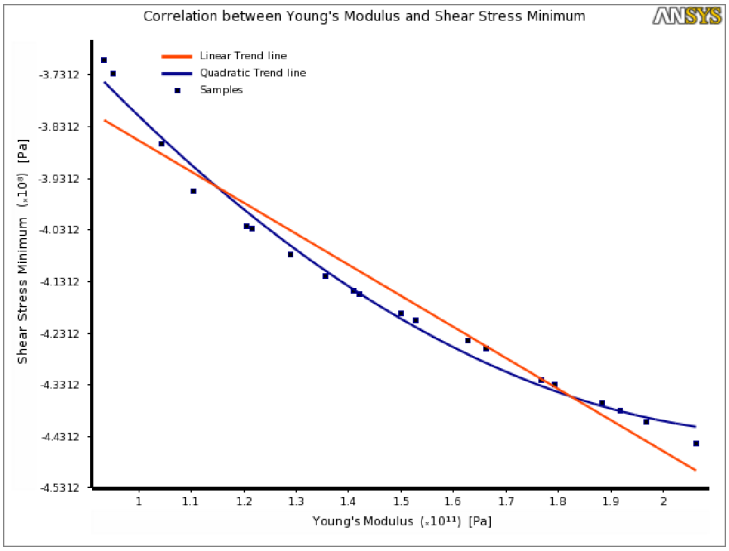

(d)

Figure 5.12: Young's Modulus (Pa) Vs Stress (Pa) results, (a) maximum contact pressure, (b) maximum equivalent stress, (c) tensile shear stress & (d) compressive shear stress.

5.3.Contact Stress Analysis in ANSYS Workbench for model 3

The maximum contact stress value for this model is 1432.1 MPa, obtained by Hertz theory (equation 3.28). The stress analysis has been done using ANSYS Workbench version 12.1 software, where the results have been presented by contours and numerical values. The maximum contact pressure result from ANSYS is 1528.5 MPa. Comparison with theoretical value was done, and the result agrees with the theoretical result within 6.7% error. The contour plot showing the contact stress distribution of ANSYS Workbench results is shown in figure 5.13.

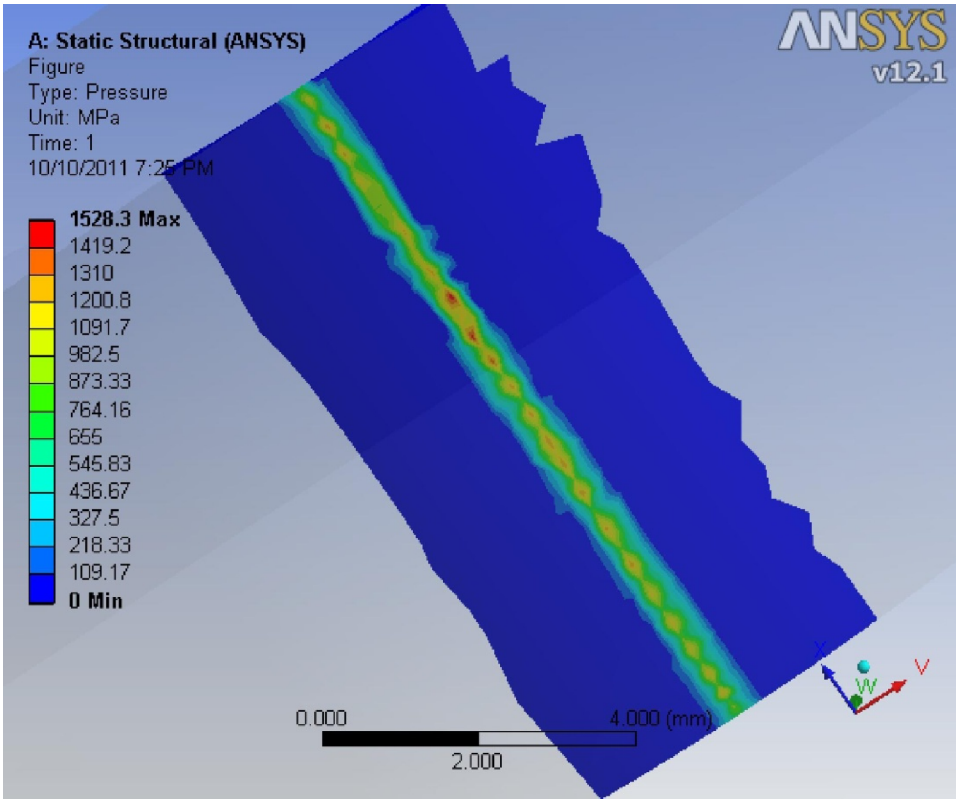

Figure 5.13: Contact Stress Distribution for the model

Figures 5.14 & 5.15 show the von Mises and shear stress distribution respectively for the model described in table 4.11. The maximum shear stress value for this model is 429.63 MPa, obtained by Hertz theory (Eq. 3.18), and a result from ANSYS Workbench is 419.42 MPa. The von-Mises stress value for this model is 816.3 MPa, obtained by Hertz theory (Eq. 3.19), and a result from ANSYS Workbench is 764 MPa.

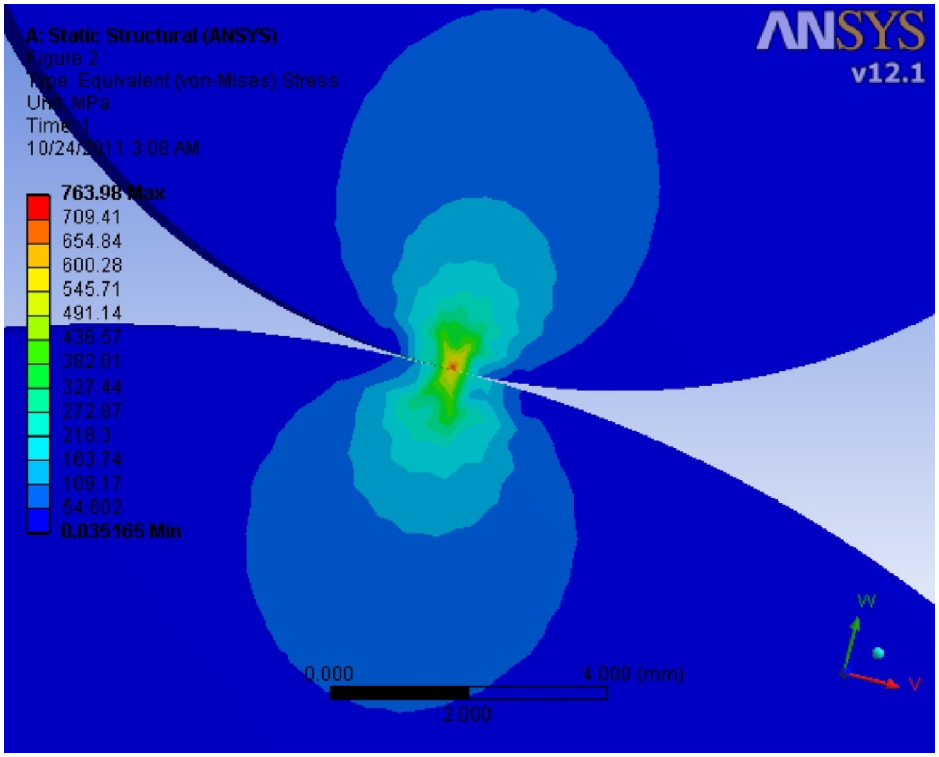

Figure 5.14: von Mises Stress Distribution

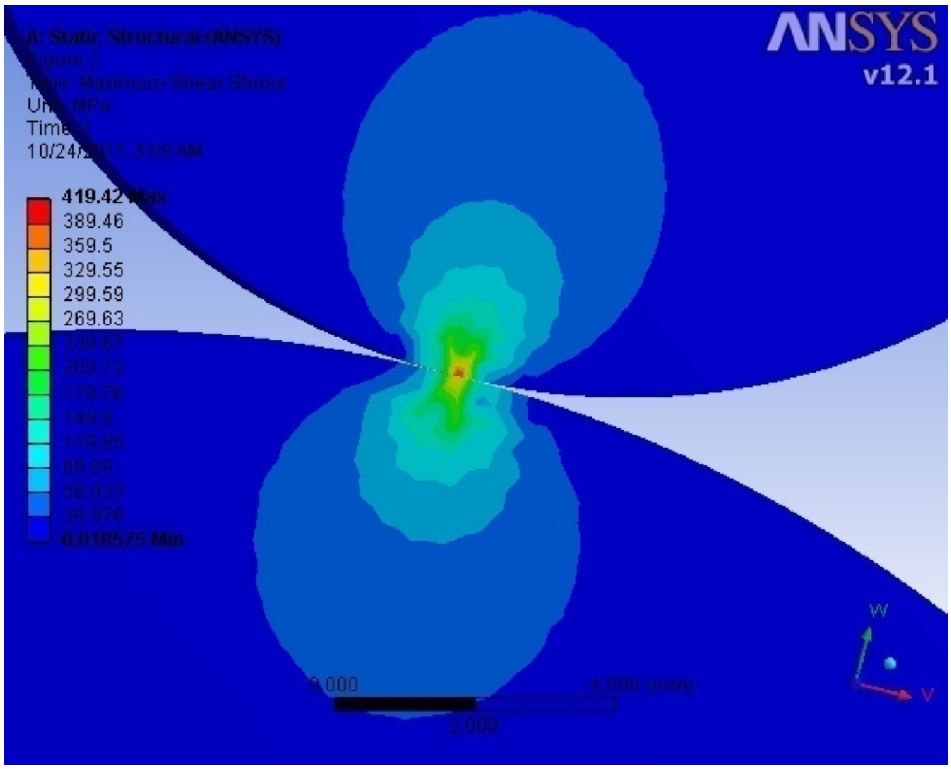

Figure 5.15: Maximum Shear Stress Distribution

Comparison of Maximum shear stress and von-Mises stress results from Hertz theory and ANSYS Workbench shows that, the value from ANSYS 2.38%, and 6.41% lower than Hertzian contact stress.

5.4.Surface Fatigue Estimation in ANSYS Workbench (Model-4)

The dimensioning of a structure or component depends on the type of possible failure. The static strength assessment should be carried out using a stress hypothesis appropriate to the type of failure expected. Researchers are not in complete agreement on the exact mechanism of the pitting; although the subject is quite complicated, they do agree that the Hertz stresses, the number of cycles, the surface finish, the hardness, the degree of lubrication, and the temperature all influence the strength. As it is stated in the chapter 3, when two surfaces are pressed together, a maximum shear stress is developed slightly below the contacting surface. It is postulated by some Researchers that a surface fatigue failure is initiated by this maximum shear stress and then is propagated rapidly to the surface. The other group of experts hypothesizes that, failure of a material subject to contact pressure is typically initiated in the region of maximum subsurface stress, which can be determined using the von Mises yield criterion for a given material. In the next section of this thesis work both methods will be demonstrated.

5.4.1. Influence of Load on Surface Fatigue

- **Contour plot of available life over the model**.

This result shows the available life over the model for the given fatigue analysis. This contour plot represents the number of cycles until the part will fail due to fatigue. Figure 5.16 shows, contour plot of life over the model, for two different types of stress component, with fatigue strength factor, k_f= 1, for standard mirror polished surface finish.

Loading is of constant amplitude because only one set of finite element stress results along with a loading ratio is required to calculate the alternating and mean stress. Loading is proportional since only one set of finite element stress results is needed (principal stress axes do not change over time). Since the loading is proportional, the critical fatigue location can be ascertained by

looking a single set of FEM results. In this type of loading, if the alternating stress is lower than the lowest alternating stress defined in the S-N curve, the life at that point will be used.

As it is seen in the figure 5.16, the minimum fatigue life using the maximum octahedral shearing stress (von Mises criterion) is $8.9297*10^6$ cycles and using the maximum shearing stress (Tresca's criterion) is $4.0396*10^6$ cycles. Theoretically it is known that, maximum shear stress theory is more conservative than the von Mises criterion. This analysis is also in agreement with this formulation.

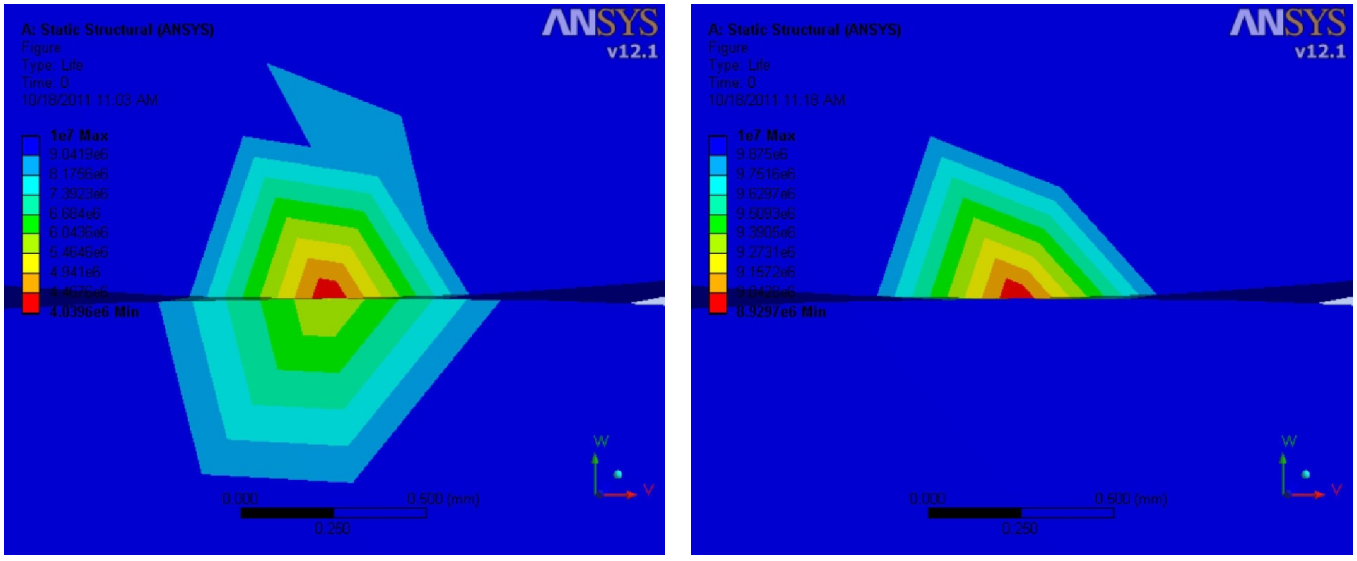

(a) (b)

Figure 5.16: Contour plot of available life for (a) maximum shear stress theory (b) von Mises criterion.

- **Fatigue Sensitivity Chart**

This chart shows how the fatigue results change as a function of the loading at the critical location on the model. Figure 5.17 shows fatigue sensitivity of the model's life if the load was 20% of the current load up to if the loads 140% of the current load, for two different stress

components, in semi-log scale (available life in log scale and load in linear scale, to exclude points with zero fatigue life scale).

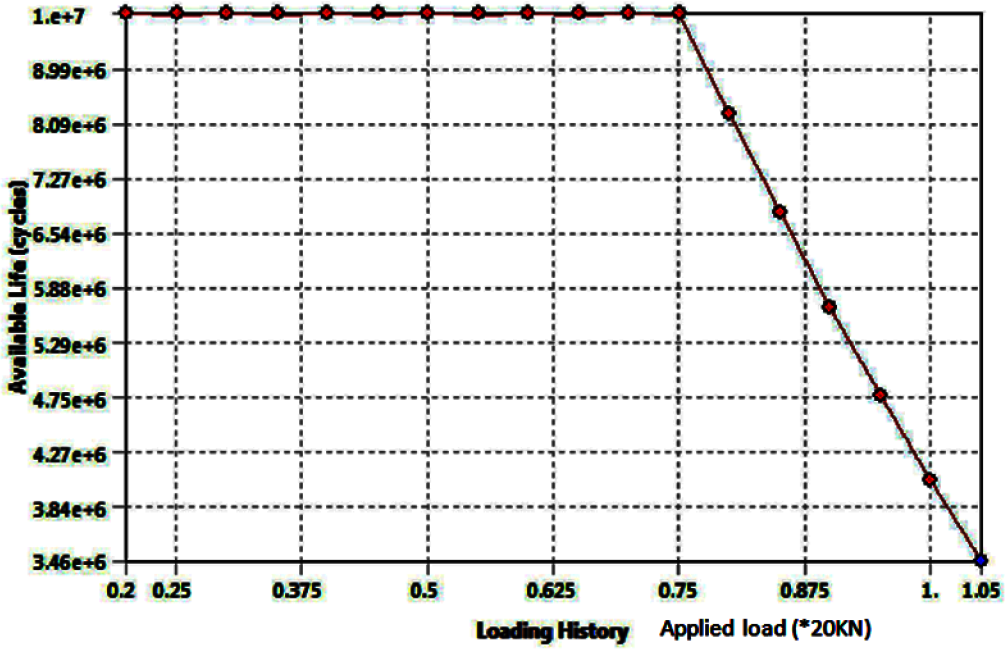

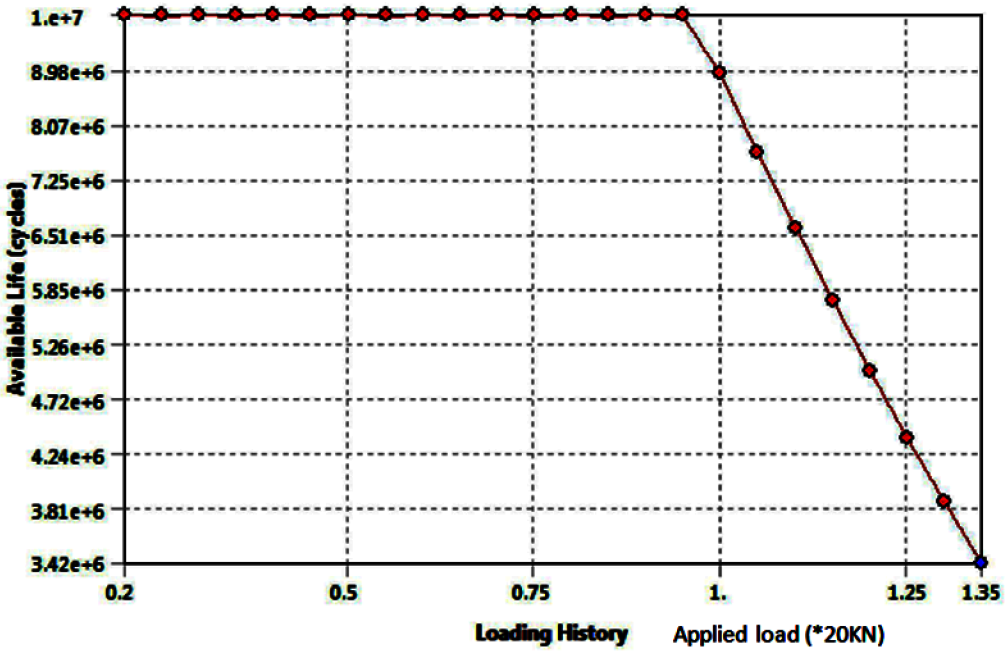

(b)

Figure 5.17: Fatigue sensitivity chart for (a) maximum shear stress theory (b) von Mises criterion.

5.4.2. The Influence of Surface Finish on Surface Fatigue

Surface roughness is recognized as an important factor for the operational behavior of machine elements. This factor is important because it influences the dry or lubricated contacts, friction and wear phenomena or surface failure.

A very high proportion of all fatigue failures nucleate at the surface of components so that surface conditions become an extremely important factor influencing fatigue strength. Various surface conditions are usually judged against the polished laboratory specimen standard. Normally, scratches, pits, machining marks, and so forth, influence fatigue strength by providing additional stress raisers that aid the process of crack nucleation. The diagram below shows that high strength steels are more adversely affected by a rough surface finish than softer steels. For this reason, the surface finish correction factor, $C_{sur} < 1$, is strongly related to tensile strength. Here the surface finish correction factor categorizes finish in qualitative terms such as polished, machined, and forged.

Despite the absence of a clear explanation for micropitting phenomena, it is clear that there are several major factors that contribute to the occurrence (or non-occurrence) of this failure mode. One of these factors is tooth surface finish, which is certainly interrelated with friction and sliding as well as the film thickness. For example, testing conducted by Krantz, et al. [54], found that the micropitting fatigue life of carburized and ground gears was improved quite measurably by superfinishing the gears after grinding. A sampling of the data from that work clearly shows that, fatigue life improvement by super finishing process is significant.

Figure 5.18 is an empirical chart used to determine the surface finishing modifying factor for steels when measurement of the surface roughness is known.

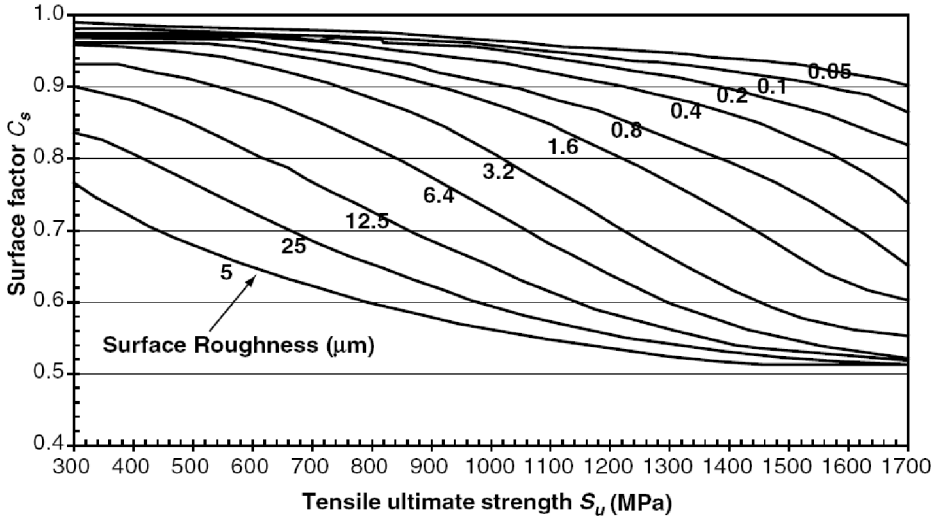

Figure 5.18: Qualitative description of C_s, surface finish factor adapted from Johnson (1973) as cited in [55]

Mechanical processes can introduce residual stresses into a material. For example tensile residual stresses can be generated from machining and compressive residual stresses may be introduced in a material by peening and cold working processing. Figure 5.19 is used to estimate the surface modifying factor based on manufacturing process for steels. In general surface finish is more critical for high strength steel and at high cycle fatigue lives where crack initiation dominates fatigue lives. At shorter lives where crack propagation dominates the fatigue life, the effect of surface finish on fatigue strength is minimal.

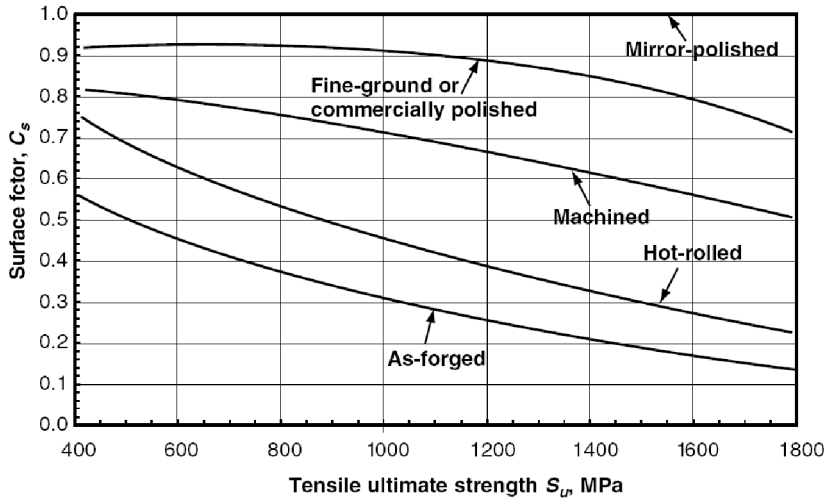

Figure 5.19: Qualitative description of C_s, surface finish factor adapted from Juvinall and Marsher (2000), as cited in [55]

To investigate the effect of surface roughness and manufacturing process on rolling contact fatigue life, the analysis is done on the model developed in the previous section, for the three different surface roughness conditions.

Fatigue Strength Factor (K_f)

This is the fatigue strength reduction factor. In ANSYS Workbench, the stress-life or strain-life curve(s) are adjusted by this factor when the fatigue analysis is run. This setting is used to account for a "real world" environment that may be harsher than a rigidly-controlled laboratory environment in which the data was collected. Common fatigue strength reduction factors to account for such things as surface finish can be found in design handbooks.

Table 5.5: Surface roughness and manufacturing process of contacting surface.

no	Surface roughness (μm)	Manufacturing Process	Surface finish factor
1	0.05	Mirror polished	1
2	12.5	Fine-ground (commercially polished)	0.9
3	25	Machined	0.8
4	50	Hot rolled	0.7

Setting the other surface fatigue reduction factor controlled, (set fatigue strength factor other than surface finish factor to 1), this results in surface finish factor becomes equal with fatigue strength factor. Therefore, by inserting the values in table 5.5 in ANSYS Workbench the analysis is computed. The results are depicted in figure 5.20-5.23, as a contour plot of available life over the model and fatigue sensitivity chart. The result clearly shows that, as the surface becomes rough and rough the minimum fatigue life decreases.

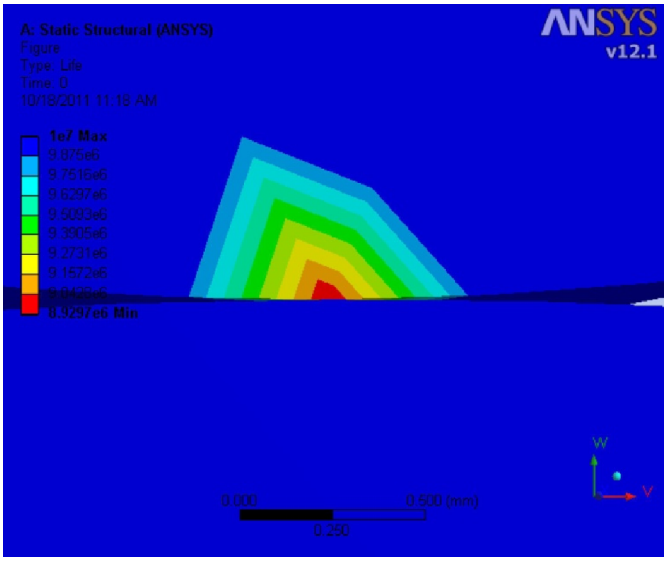

(a)

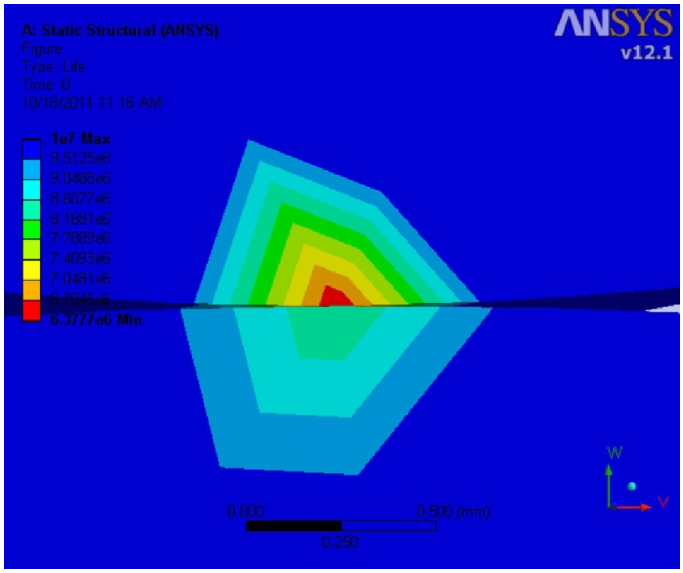

(b)

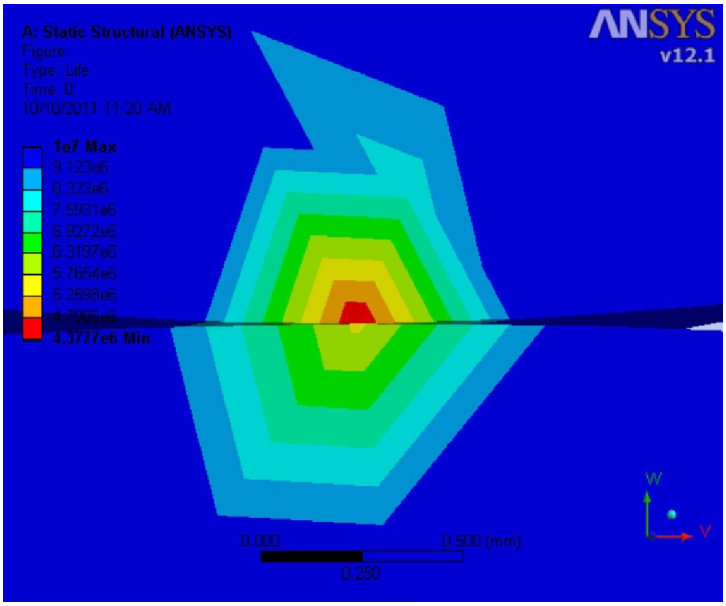

(c)

Figure 5.20: Contour plot of available fatigue life using von Mises criterion for different surface roughness, (a) 0.05µm, (b) 12.5µm & (c) 25µm

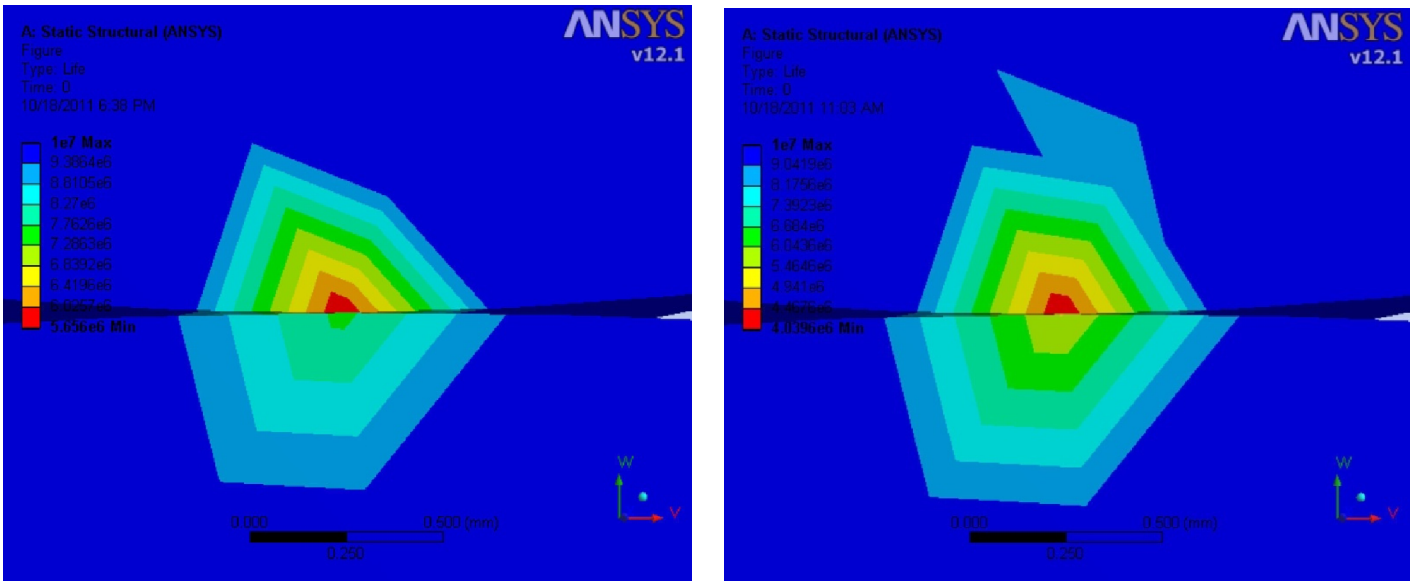

(a) (b)

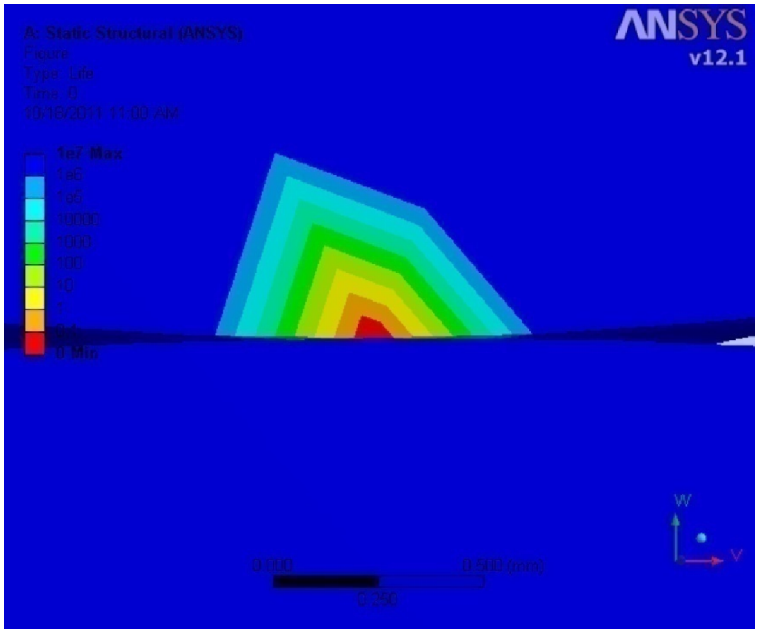

(c)

Figure 5.21: Contour plot of available fatigue life using maximum shear stress criterion for different surface roughness, (a) 0.05µm, (b) 12.5µm & (c) 25µm

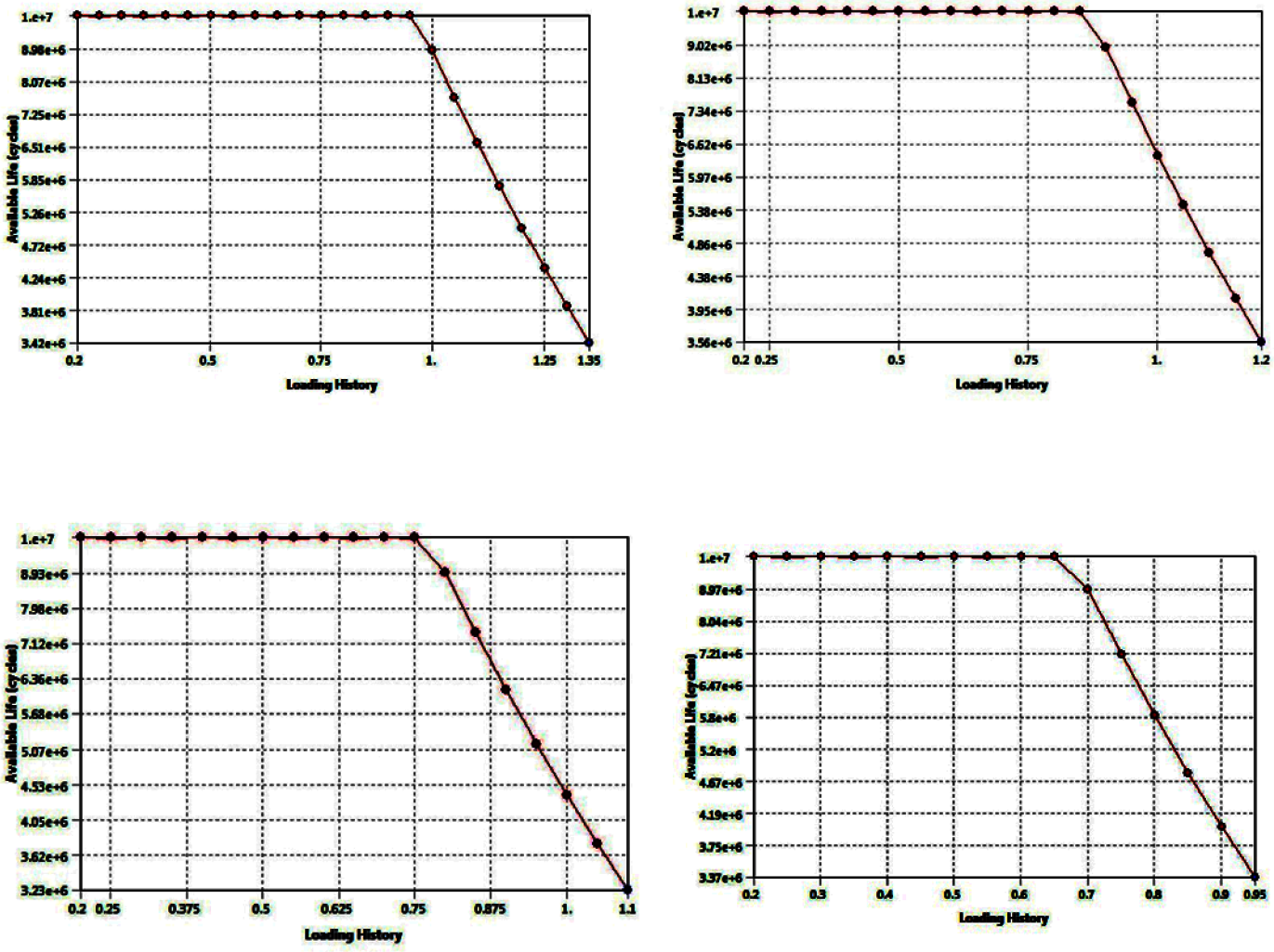

(c)

(d)

Figure 5.22: Fatigue sensitivity chart using von Mises criterion for different surface roughness, (a) 0.05µm, (b) 12.5µm, (c) 25µm & (d) 50µm. (Unit of applied load, *20KN**)**

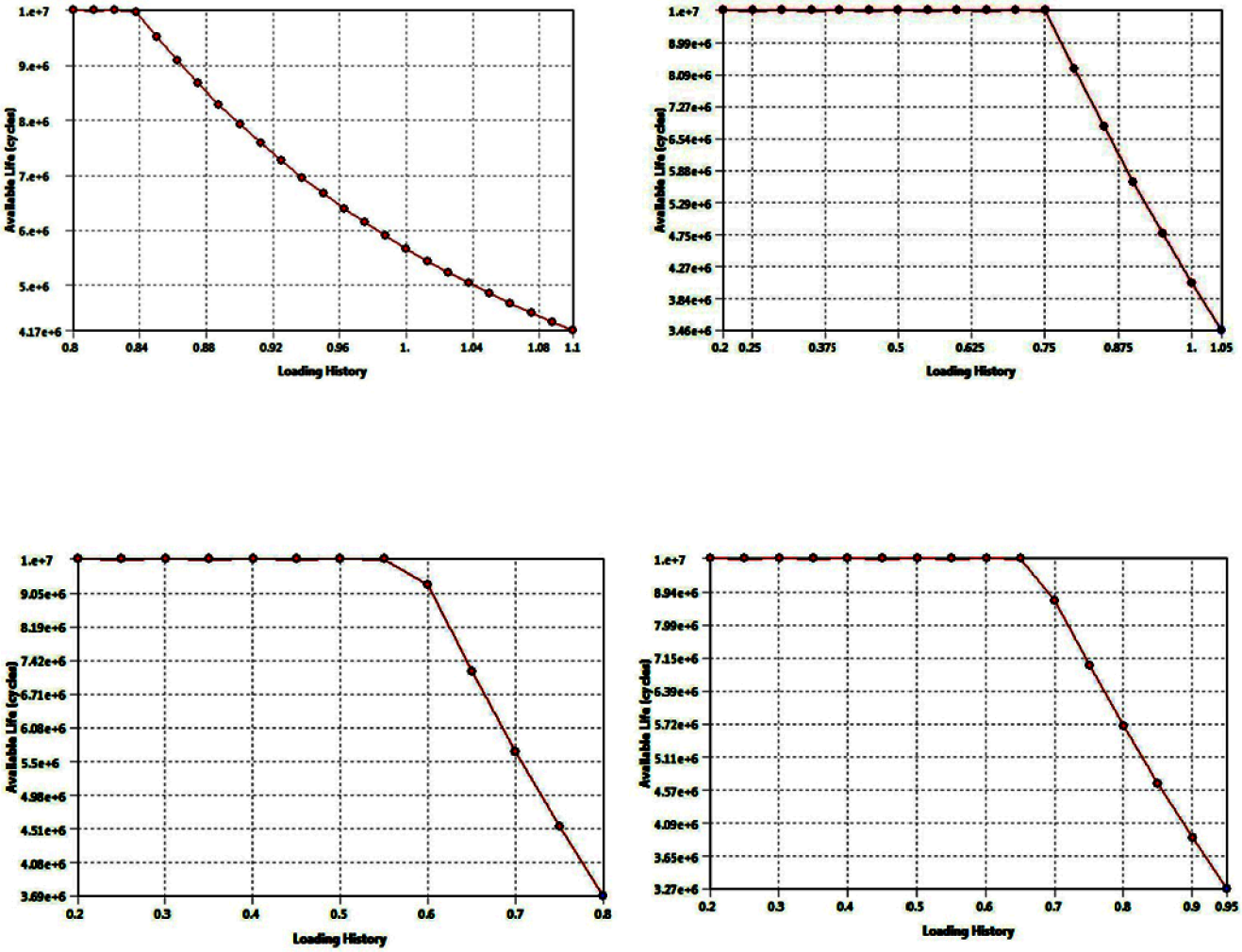

(c) (d)

Figure 5.23: Fatigue sensitivity chart using maximum shear stress criterion for different surface roughness, (a) 0.05µm, (b) 12.5µm, (c) 25µm & (d) 50µm. (Unit of applied load, *20KN**)**

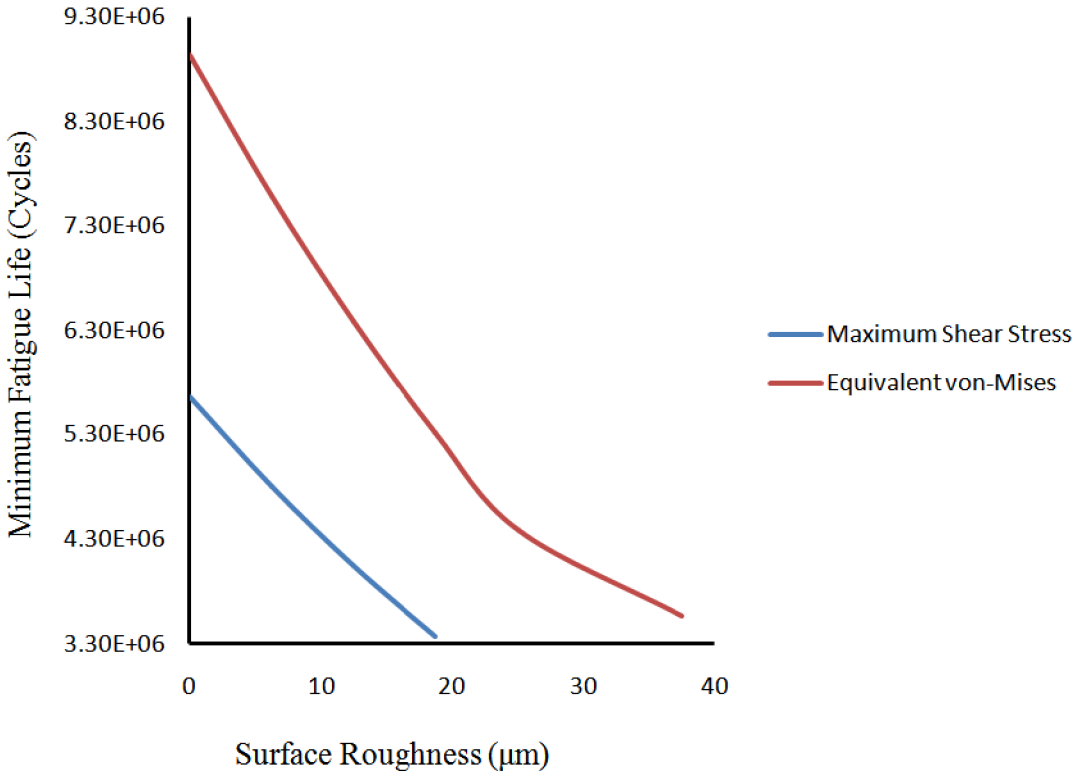

Figure 5.24: Effect of Surface roughness on Minimum Fatigue Life, for two different stress components.

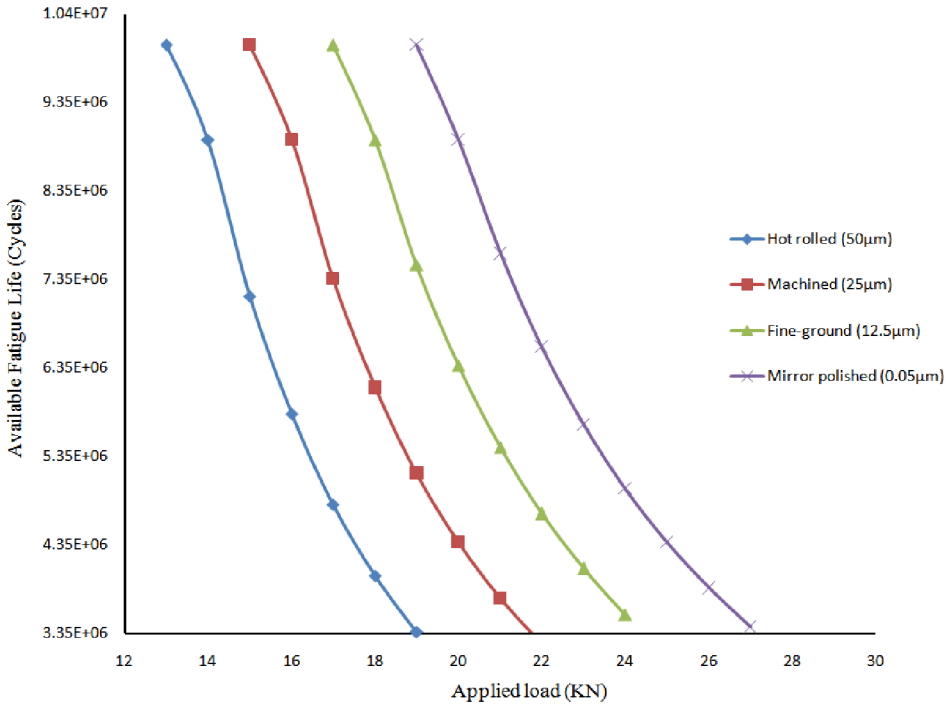

(a)

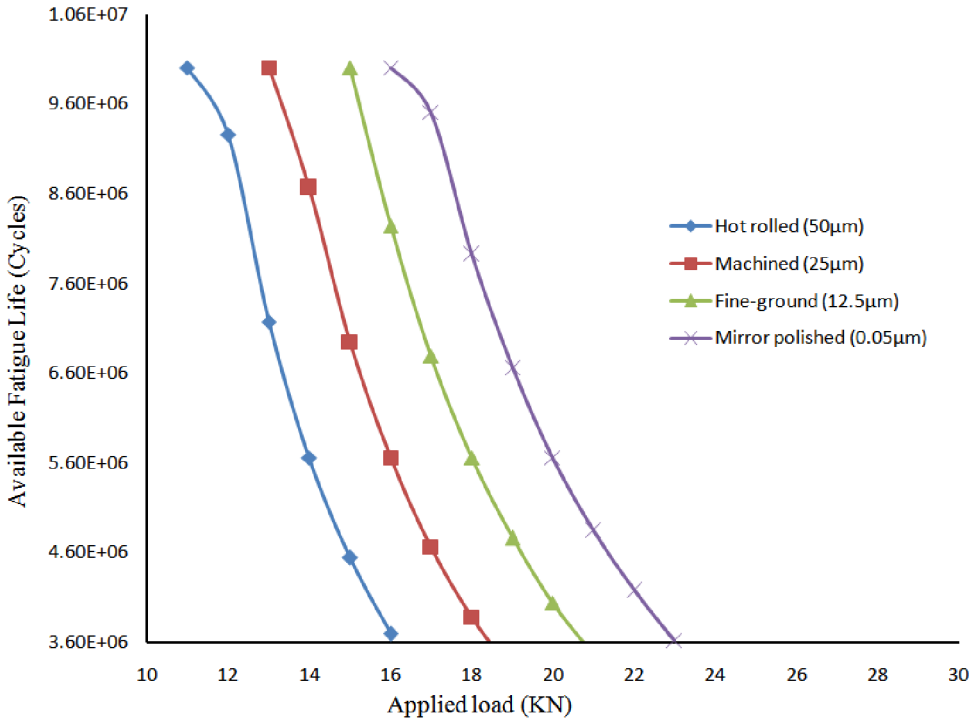

(b)

Figure 5.25: Effect of Applied Load on Fatigue Life for Different Surface Roughness (a) von-Mises criterion (b) maximum shear stress theory.

Generally to summarize, the effect of surface roughness on contact fatigue, results extracted from ANSYS Workbench is plotted in Excel, as figure 5.24 & 5.25. Result of the analysis persistently shows that, the minimum fatigue life decreases as the surface roughness increases, and as the surface roughness increases for a specific fatigue life, the load carrying capacity decreases. Therefore surface conditions affect significantly available fatigue life, irrespective of the other factors. Hence, to improve available fatigue life, smoother surface finish should be used.

5.5. Summary

Even though model-2, (a pair of involute spur gear teeth in contact) showed good correlation with the Hertz theory in contact pressure estimations, it failed in accurate maximum shear and von-Mises stress estimation. In addition, the maximum shear stress criterion and the von-Mises

stress criterion are used to estimate fatigue life of machine components, uses these stress value. Therefore, the results of shear and von-Mises stress obtained from this model could be misleading. If contact pressure is of interest, the model developed here is a valid one and can be used to accurately predict contact pressure.

Model-3, (equivalent contacting cylinders), showed good correlation with the Hertz theory in estimation of contact pressure, maximum shear stress and von-Mises stress. Therefore, the model developed (model-3) is eligible to predict contact pressure, maximum shear stress and von-Mises stress and results obtained from this model can be used to estimate contact pressure, maximum shear stress and von-Mises stress.

It should be evident from the preceding sections that the maximum Hertzian compressive stress is not, in itself, a valid criteria of failure for contacting members although it can be used as a valid design guide provided that more critical stress states which have a more direct influence on failure can be related directly to it. It has been shown, for example, that alternating shear stresses exist beneath the surface which are probably critical to fatigue life but these can be expressed as a simple proportion of the Hertzian pressure, P_o so that P_o can be used as a simple index of contact load severity.

Chapter Six

6. Conclusion and Future Work

6.1.Conclusion

In this thesis work, FEA analysis procedure developed to study contact stress and surface fatigue in involute spur gear. Comparison of FEA result with analytical method is done. The method developed in this thesis work can be used to analyze contact stress and surface fatigue in mating mechanical components. Generally from this thesis work the following can be figured out.

- 2D and 3D contact between two cylinders was used to estimate contact stress using FEA. The result from FEA using ANSYS is agreeable with theoretical formulation with reasonable accuracy. Therefore, users may use FEA using ANSYS to estimate contact stress.
- 3D meshed involute spur gear was modeled to investigate, contact stress, the change in contact pressure with applied torque, the relation between elasticity of material with different stress component and maximum contact pressure for three different materials. FEA results are correlated with theoretical formulation, with tolerable accuracy. But, in this model, the method developed failed to estimate stress below the contacting surface (shear and von-Mises stress) with acceptable accuracy. Therefore, the results of shear and von-Mises stress obtained from this model could be misleading.
- 3D equivalent contacting cylinders was used to model meshed involute spur gear to investigate contact stress. FEA results are correlated with theoretical formulation, with acceptable accuracy. Therefore, the model developed is eligible to predict contact pressure, maximum shear stress and von-Mises stress and results obtained from this model can be used to estimate contact pressure, maximum shear stress and von-Mises stress. In addition results from this FEA model can be used for further analysis, such as fatigue studies
- Rolling contact fatigue analysis is done for the 3D meshed involute spur gear, using ANSYS Workbench. The minimum fatigue life is estimated using von Mises criteria and

maximum shear stress criteria for different surface roughness condition. In addition sensitivity of fatigue life to load is studied.

Finally, the obvious criteria for comparison among FEA, Analytical methods and experimental techniques, are accuracy, cost and time. If sufficient experience on FEA is available, the criteria are in favor of FEA. Therefore users can use FEA using ANSYS to estimate rolling contact fatigue in gears.

6.2. Future Work

In this thesis work contact stress and surface fatigue is studied for different surface roughness condition other influencing factor are not studied. So this work is restricted to the specified cases. However, this paper can be extended to other situation listed below. Further numerical method investigations should be conducted on:

- Effect of temperature in surface fatigue of gears.
- Fracture mechanics approach to study surface fatigue related to initiation and propagation of cracks.
- Contact mechanics in gears under lubricated condition and its effect in surface fatigue.
- Effect of misalignment, sliding speed and friction on surface fatigue.

Reference

1. Van Beek A., ***Advanced engineering design***. 2006, Delft.
2. BS ISO 6336-1 ***Calculation of load capacity of spur and helical gears - Part 1: Basic principles, introduction and general influence factors***, 2008.
3. Suzuki Y., ***Trend of Transmission and Gear Technology***,JSME preprint –mpt2004 symposium (in Japanese), No. 04-17, pp. 1-4.
4. Hertz H., Uber die Beruhrung Fester Elastischer Korper, ***On the Contact of Elastic Solids***, J. Reine und Angewandte Mathematik, Vol. 92, 1881.
5. Buckingham, E. ***Dynamic loads on gear teeth***, ASME Special Committee on Strength of Gear Teeth. New York, 1931
6. Abersek, B., and Flasker, J., ***How Gears Break***, WIT Press, 2004.
7. Dudley, D. W., ***Handbook of Practical Gear Design***, McGraw-Hill, Inc., 1984.
8. Pottinger, M. G., Cohen, R. and Stitz, E. O., "***A Photostress Study of Spur Gear Teeth***", SAE Technical Paper 670503, 1967.
9. Wei Z., ***Stresses and Deformations in Involute Spur Gears by Finite Element Method***, M.Sc thesis, University of Saskatchewan, Canada, October, 2004.
10. Ali R., ***Contact Stress Analysis of Spur Gear Teeth Pair***, World Academy of Science, Engineering and Technology, 2009.
11. Chen, W., and Tsai, P., ***Finite Element Analysis of an Involute Gear Drive Considering Friction Effects***, ASME Journal of Engineering for Industry, vol. 111, pp. 94-100, 1989.
12. Moriwaki, I., Fukuda, T., Watabe, Y., Saito, K., ***Global Local Finite Element Method (GLFEM) in Gear Tooth Stress Analysis***, Journal of Mechanical Design, vol. 115, pp. 1008-1012, 1993.
13. Yi-Cheng Chen and Chung-Biau Tsay, ***Stress Analysis of a Helical Gear Set with Localized Bearing Contact***, Finite Elements in Analysis and Design, vol. 38, pp. 707-723, 2002.
14. Negash A., ***Analysis of Stresses in Helical Gears by Finite Element Method***, Msc., thesis, Addis Ababa University Faculty of Technology, Addis Ababa 2007.
15. Chien-Hsing Li, Hong-Shun Chiou, Chinghua Hung, Yun-Yuan Chang and Cheng-Chung Yen, ***Integration of Finite Element Analysis and Optimum Design on Gear Systems***, Finite Elements in Analysis and Design, vol. 38, pp. 179-192, 2002.

16. Hinojosa J., Hernandez J. and Aceves J., ***Mathematical model to determine the surface stress acting on the tooth of gear*****,** Theoret. Appl. Mech., Vol.37, No.2, pp 97-110, Belgrade 2010
17. Ruben D., Luis J., Miguel A. and Jose A., ***Analysis of Stress Due to Contact between Spur Gears*****,** Advances in Computational Intelligence, Man-Machine Systems and Cybernetics, Venezuela.
18. Way, S., ***Pitting Due to Rolling Contact***, J. Appl. Mech., vol. 2, pp. A49-A58, 1935.
19. Blake, J. W., Draper, C. F., ***Further Development on a Predictive Pitting Model for Gears: Improvements in the Life Prediction Analysis***, Trib. Trans., vol. 37, pp. 237-244, 1994.
20. Bower, A. F., ***The Influence of Crack Face Friction and Trapped Fluid on Surface Initiated Rolling Contact Fatigue Cracks***, Trans. ASME, vol. 110, pp. 704-11, 1988.
21. Tallian, T. E., "Failure Atlas for Hertz Contact Machine Elements", ASME Press, 1992.
22. Alfredsson, B. ***A study on contact fatigue mechanisms***, Doctoral thesis, Department of Solid Mechanics, Royal Institute of Technology, Stockholm, Sweden, 2000.
23. Dimitrov L. & Kovatchev I., ***A Computer Model for Determination of Spur Gear-Teeth Contact Fatigue Life***, International conference power transmission, 2003
24. Hassan H., Ali J., Seyed S., and Ali M., ***Fatigue Analysis of Hydraulic Pump Gears of JD 955 Harvester Combine Through Finite Element Method*****,** Journal of American Science 2010;6(7)
25. Lin A.D. & J. H. Kuang, ***On the Bending and Surface Fatigues of an Engaging Spur Gear Pair*****,** 12th IFToMM World Congress, Besançon (France), June18-21, 2007
26. Ferreira B., ***Gear Micropitting Prediction Using the Dang Van High-Cycle Fatigue Criterion***, MSc thesis, Portugal Porto, 2007.
27. Batista & A.C. A.M. Dias, ***Contact Fatigue of Carbonitrided and Shot-Peened Gears***;
28. Johansson P., Sven Bengtsson and Senad Dizdar, ***RCF-Testing of Selectively Densified Rollers of Power Metallurgy Materials for Gear Applications***, Höganäs AB, Sweden
29. Gang D. and Tsutomu N., ***Evaluation of Surface Fatigue Strength Based on Surface Temperature; Surface Temperature Calculation for Rolling-Sliding Contact,*** JSME International Journal Series C, Vol. 44, No. 1, pp 217-222, 2001.

30. Tsutomu N., Daniel T. & Gang D., ***Influences of surface texture and lubricating oil temperature on surface failure of rolling sliding contact in the case of case-carburized alloy steels***. JSME International conference on motion and power transmissions, 2009, Matsushima Isles report, Japan
31. Susumu M., Yuko Y., Yusuke T., Toshihiko Y. & Takeshi Y., ***Pitting at contact end changing in contact and lubricating condition due to plastic deformation***. JSME International conference on motion and power transmissions, 2009, Matsushima Isles report, Japan
32. J. Shigley, ***Mechanical Engineering Design, Eighth Edition***, McGraw−Hill, USA, 2006.
33. V. Bhargava, G.T. Hahn, and C.A. Rubin, ***Rolling Contact Deformation and Microstructural Changes in High Strength Bearing Steel***, *Wear,* Vol 133, 1989.
34. T.E. Tallian, ***Failure Atlas for Hertz Contact,*** Asme, 1992
35. ***ASM Metals Handbook Volume 19-Fatigue and Fracture,*** USA, 1997.
36. H. Hertz, *Miscellaneous Papers by H. Hertz*, Jones & Schott (eds), Macmillan, London, 1986.
37. Manuel, V. ***Investigations on Surface Damage by Rolling Contact Fatigue in Elastohydrodynamic Contacts Using Artificial Dents***, MSc thesis, Department of Mechanical Engineering University of Porto, Portugal, 2005
38. Smith J. O. and Liu C. K., ***Stresses Due to Tangential and Normal Loads on Elastic Solid with Application to Some Contact Problems***. *Journal of Applied Mechanics*, Vol. 20, pp. 157-166, 1953.
39. ***Standard Handbook of Machine Design***, the Mcgraw-Hill Companies, 2004.
40. Stachowiak, G. W., Batchelor, A. W., ***Engineering Tribology***, Butterworth-Heinemann Publishers, 2001.
41. Hamrock, Dowson, ***Ball Bearing Lubrication the Elastohydrodynamics of Elliptical Contacts,*** John Willey & Sons, 1981.
42. W.E. Littmann, ***The Mechanism Of Contact Fatigue***, Conf. Proc., An Interdisciplinary Approach To The Lubrication Of Concentrated Contacts, National Aeronautics And Space Administration, 1969.

43. E.V. Zaretsky And W.J. Anderson, ***Material Properties And Processing Variables And Their Effect On Rolling-Element Fatigue***, National Aeronautics And Space Administration, 1966.
44. D. Scott, ***The Effect Of Material Properties, Lubricant, And Environment On Rolling Contact Fatigue***, *Inst. Mech. Eng.,* Vol 181, 1966.
45. X. Hogbin, C. Qing, S. Eryu, W. Dengzhen, C. Zhaohong, And W. Zhengle, ***The Effect Of Shot Peening On Rolling Contact Fatigue Behavior And Its Crack Initiation And Propagation In Carburized Steel***, *Wear,* Vol 151, 1991
46. Fan, H., Keer, L. M., Cheng, W., Cheng H. S., ***Competition Between Fatigue Crack Propagation and Wear***, J. Trib., vol. 115, pp. 141-147, 1993.
47. *ANSI/AGMA 2001-D04 and 2101-D04*
48. ISO 6336-2: ***Calculation of load capacity of spur and helical gears***. ISO, 1996.
49. G. Lundberg And A. ***Palmgren, Dynamic Capacity of Rolling Bearings***, *Acta Polytech.,* Vol 1 (No. 3), 1947
50. A.P. Boresi And O.M. Sidebottom, ***Advanced Mechanics Of Materials,*** John Wiley & Sons, 1985
51. J.O. Smith and C.K. Liu, ***Stresses Due to Tangential and Normal Loads on an Elastic Solid with Application to Some Contact Stress Problems***, *J. Applied Mech.,* 1953
52. K. C. Ludema, ***Hand book of lubrication theory and practice of tribology*** , CRC press, 1983
53. Faydor L. Litvin and Alfonso Fuentes, ***Gear Geometry and Applied Theory, Second Edition***, Cambridge University Press, New York, USA, 2004.
54. Krantz T., L.Alanou, M P. Evans, H P and Snidle, RW., ***Surface fatigue lives of case carburized gears with an improved surface finish***, Trans ASME, Journal of Tribology vol 123, pp709-716, 2001
55. Yung-Li Lee, Jwo Pan, Richard B. Hathaway, Mark E. ***Barkey Fatigue Testing and Analysis, Theory and Analysis*** Elsevier Butterworth-Heinemann Elsevier Inc Burlington USA, 2005.